光線力学療法用光増感剤としての糖連結ポルフィリン誘導体の合成と機能評価

光線力学療法用光増感剤としての糖連結ポルフィリン誘導体の合成と機能評価

(Synthesis and Functional Evaluation of Glycoconjugated Porphyrin Derivatives toward Photodynamic Therapy)

奈良女子大学
大学院人間文化研究科
機能性物質科学講座

廣原志保

平成17年1月

Synthesis and Functional Evaluation of Glycoconjugated Porphyrin Derivatives toward Photodynamic Therapy

A Disseratation for the Degree of Doctor of Science

Shiho Hirohara

Devision of Material Science,
Graduate School of Humanities and Sciences,
Nara Women's University
January, 2005

Abbreviations

AcOH,	acetic acid
ALA,	5-aminolevulinic acid
ATR,	attenuated total reflection
BOPP,	boronated protoporphyrin
BSA,	bovine serum albumin
COSY,	correlated spectroscopy
CH_2Cl_2,	dichloromethane
$CHCl_3$,	chloroform
CLSM,	confocal laser scanning microscope
DMSO,	dimethyl sulfoxide
DMEM,	Dulbecco's modified Eagle's medium
DPBF,	1,3-diphenylisobenzofuran
ESI-TOF mass,	electron-spray ionization time-of-flight mass
Et_2O,	diethyl ether
FAB mass,	fast atom bombardment mass
FCS,	fetal calf serum
Foscan™,	*meta*-tetrahydroxyphenylchlorin
$^3O_2$,	ground state molecular oxygen
HBr,	hydrobromic acid
H_2O,	water
HCl,	hydrochloric acid
HOMO,	highest occupied molecular orbital
Hp,	hematoporphyrin
HpD,	hematoporphyrin derivatives
HPLC,	high-performance liquid chromatography
HRMS,	high resolution mass spectrometry
IR spectra,	infra-red absorption spectra
ISC,	intersystem crossing
LD_{50},	the lethal dose to 50 % of the population

Log *P*,	partition coefficient
Lutrin®,	Antrin®, motexafin lutetium
MeOH,	methanol
NaOH,	sodium hydroxide
Na_2SO_4,	sodium sulfate
NaOMe,	sodium methoxide
$NaHCO_3$,	sodium hydrogen carbonate
NMR,	nuclear magnetic resonance
NPe6,	mono-L-aspartyl chlorin e6
PBS,	phosphate buffered saline
Pc,	phthalocyanines
PDT,	photodynamic therapy
Photochlor®,	hexyl ether of pyropheophoribide-*a*
Photosens,	chloro-aluminum sulfonated phthalocyanine
PpIX,	protoporphyrin
Purlytin™,	tin ethyl etiopurpurin
$^1O_2$,	singlet oxygen
QOL,	quality of life
RP-TLC,	reversed phase thin layer chromatography
m-THPC,	5,10,15,20-tetrakis(3-hydroxyphenyl)chlorin
m-THPP,	5,10,15,20-tetrakis(3-hydroxyphenyl)porphyrin
THF,	tetrahydronfuran
TPPS,	tetraphenylporphyrin tetrasulfonic acid
TPPS4,	tetrasodium tetraphenyl porphine sulfonate
TPPs,	tetrapheynylporphyrins
TPCs,	tetrapheynylchlorins
Visudyne™,	benzoporphyrin derivative-monoacid ring A
Xcytrin®,	motexafin gadolinium
$Zn(OAc)_2 \cdot 2H_2O$,	zinc acetate dihydorate
$BF_3 \cdot OEt_2$,	boron trifluoride dimetyl ether complex

Contents

Chapter 1

Photodynamic Therapy

1-1. Cancer treatments

Medical science is progressing by leaps and bounds, however one in three is said to be death by cancer in mortality rate. While early cancer diagnostic technology or surgical treatment has been progressed in recent years, the effective treatment for cancer has been not found yet [**1-6**]. The cancer treatments can be classified into operative treatment, endoscope treatment, radiotherapy, laser treatment, thermotherapy, chemotherapy, endocrinetherapy and immunotherapy (Table 1-1) [**6**]. In addition, the combined treatment is also performed. Chemotherapy, endocrinetherapy and immunotherapy are applied for the medical treatment of metastatic tumor. Operative treatment, endoscope treatment, radiotherapy, laser treatment and thermotherapy are used for the medical treatment for early cancer [**6**]. In photodynamic therapy (PDT), photosensitizers generate reactive singlet oxygen ($^1O_2$) which are able to damage tumor cells. Because photosensitizers tend to accumulate in tumor tissues rather than in normal tissues, PDT can potentially destroy unwanted tissue selectively [**1-4,7**]. Photosensitizer, which is administrated to the patient usually by injection, is harmless and has no effect on either healthy or abnormal tissue. When light (often from a laser) is directed onto tissue containing photosensitizers, however, the photosensitizers are activated and the tissue is rapidly destroyed. Then PDT can destroy the abnormal tissue selectively by careful irradiation of light. This treatment is excellent also from the point of quality of life (QOL).

1-2. Photodynamic therapy (PDT)

1-2-1. History [1-4,8-12]

Phototherapy is generally considered to have originated to Finsen who treated lupus vulgaris, a tubercular condition of the skin with irradiation using a carbon arc lamp equipped with heat-filter in 1890's. The history of PDT was old and Raab found out the fatality-effect to *paramecium candatum ehrenberg* by combination use of acridine dye and light in 1900. Tappeiner and others reported eosin dye, sunlight and lamp light have made tumor necroses in 1903. Policard discovered the affinity of porphyrin to cancer cells in 1924. He discovered that the cancer of human and laboratory animals emitted fluorescence by irradiation with Wood light. He pointed out that the endogenous porphyrin produced by bacteria infection accumulated in cancer cells and emits red fluorescence. Figge et al. reported the affinity of hematoporphyrin (Hp) in various mouse cancer cells in 1948. However, the cancer diagnosis using these porphyrin derivatives did not attract much attention. The technology of endoscope diagnosis progressed in the 1960's. Consequently, people came to have the concern about

Table 1-1 Cancer treatment

treatment	tumors
1. operative treatment	brain tumor, tongue cancer, pharyngeal cancer, esophageal cancer, stomach cancer, colon cancer, liver cancer, biliary tract carcinoma, spleen cancer, lung cancer, malignant tumor, eosinophilic granuloma of soft tissue, skin cancer, lymphoma, breast cancer, cervical cancer, cancer of uterine body, ovarian cancer, prostate gland cancer, thyroid gland cancer, endocrine gland tumor
2. endoscop treatment	esophageal cancer, stomach cancer, bladder carcinoma, adrenal tumor
3. radiotherapy	brain tumor, pharyngeal cancer, nasal cavity cancer, esophageal cancer, colon cancer, spleen cancer, lung cancer, skin cancer, Hodgkin disease, cervical cancer, cancer of uterine body, testicular tumor, bladder carcinoma, thyroid gland cancer, tongue cancer
4. laser treatment	brain tumor, oral pharyngeal tumor, cervical cancer (early cancer)
5. thermotherapy	brain tumor, oral pharyngeal tumor, eosinophilic granuloma of soft tissue, cervical-cancer (early cancer)
6. chemotherapy	brain tumor, nasal cavity cancer, esophageal cancer, spleen cancer, lung cancer, malignant tumor, eosinophilic granuloma of soft tissue, skin cancer, Hodgkin-disease, leukemia, breast cancer, cervical cancer, cancer of uterine body, ovarian cancer, prostate gland cancer, testicular tumor, bladder carcinoma, renal cancer, thyroid gland cancer, infantile cancer
7. endocrinetherapy	breast cancer, cancer of uterine body, prostate gland cancer
8. immunotherapy	renal cancer, malignant melanoma, lymphoma, leukemia

fluorescence diagnosis of cancer. Lipson and Baldes reported hematoporphyrin derivatives (HpD) which were prepared by the treatment of Hp with H_2SO_4 in acetic acid at room temperature. These HpD were a mixture containing hydroxyethyl(vinyl)deuteroporphyrin as a main ingredient. Hydroxyethyl(vinyl)-deuteroporphyrin showed photocytotoxicity higher than HpD. Lipson et al. performed local diagnosis for human bronchus cancer and esophagus cancer by HpD in 1961. This experiment was the first application to the diagnosis and medical treatment of cancer by HpD. However, it was not effective to diagnose early cancer, because fluorescence from dye was hardly distinguish from private fluorescence and excitation light. In 1966, Lipson et al. firstly demonstrated the modern "photodynamic therapy" by use of HpD, in which cancer cells were destructed by irradiation with light. Dougherty et al. performed PDT treatment using Xenon lamp after injection of HpD in 1975. They reported that only cancer cells could be disappeared selectively without destroying normal cells. The clinical test using porphyrin derivatives and white light was extensively studied by many researchers. In 1980's, totally new light source, i.e., "light amplification by stimulated emission of radiation (Laser)" was developed. A lot of study on photodynamic therapy using HpD and laser had been performed. On the other hand, novel photosensitizers were also synthesized to improve the PDT treatment. Several first generation photosensitizers including rose bengal (Royster et al., 1988; Huang et al., 1989; Corrent et al., 1989) and dihematoporphyrin ether/ester (Packer et al., 1984, Obana et al., 1996) were developed. However they were inappropriate for the clinical use because of either prolonged cutaneous photosensitivity resulting from slow-rate excretion or low photodynamic activity. Recently, Sakata et al. synthesized a water-soluble photosensitizer ATX-S10 with a longer absorption wavelength, greater absorption coefficient, lower skin photosensitivity, stronger photooxygenation activities and a lower value of LD_{50} (Nakajima et al., 1992, 1995) as compared to the first generation photosensitizers. The agents possessing these advantages are classified as second generation photosensitizers. The second generation photosensitizers under clinical trial are 5,10,15,20-tetra(*p*-hydroxyphenyl)porphyrin (berenbaum et al., 1986), chloro-aluminium sulfonated phthalocyanine (Miller et al., 1991; Pallikaris et al., 1993; Kliman et al., 1994; Tsilimbaris et al., 1994), benzoporphyrin derivative (Schmidt-Erfurth et al., 1995; Miller et al., 1995; Kramer et al., 1996; Husain et al., 1996), tin ethyl etiopurpurin (Bauma et al., 1996; Soliman et al., 1997; Peyman et al., 1997), mono-L-aspartyl chlorin e6 (Mori et al., 1997), 5,10,15,20-tetra(*m*-hydroxyphenyl)chlorin (Bonnet et al., 1989, 1995, and 1999), 5-aminolevulinic acid (Kennedy et al., 1990, 1992 and 1996), hexyl ether of pyropheophorbide-*a* (Potter et al., 1999, Henderson et al., 1997,

Pandy et al., 1996), boronated protoporphyrin (Tibbitts et al., 1999, Kahl et al., 1990, Spizzirri et al., 1996), motexafin luteium (Young et al., 1996, Woodburn et al., 1998, Rockson et al., 1999, Grossweiner et al., 1999). Now, photosensitizers to have high tumor selectivity have been developed as third generation photosensitizers. Photofrin® is an only photosensitizer approved in Japan in 1994. The research and development of laser equipment (light source) and photosensitizer (drug) have been actively made in every country in the world.

1-2-2. Mechanisms of photodynamic therapy **[1-3,9-16]**

The PDT treatment is carried out in the following steps (Scheme 1-1). At first, the solution of photosensitizers injects to the diseased part of patient. The tumor cells are allowed to accumulate photosensitizers. In some case, the concentration of photosensitizers in the tumor cells become higher than that in normal cells in 24 ~ 72 h after injection. The diseased part is irradiated with an appropriate dose of visible light (600 ~ 800 nm). In the tumor cells, the activation of the photosensitizers and subsequent photoreactions occurs within few hours (2 ~ 3 h) after irradiation. The PDT action at deeper cells occurs within 12 to 18 h. After 2 ~ 3 weeks necrosis of the tumor cells takes place.

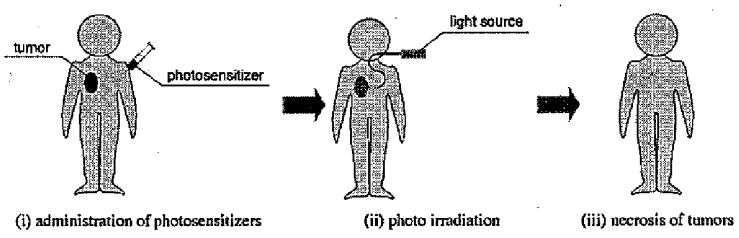

Scheme 1-1

1-2-3. Photochemistry of photodynamic therapy **[1-3,9-16]**

In photodynamic therapy (PDT), photosensitizer generates reactive singlet oxygen ($^1O_2$) which are able to damage tumor cells. The photochemical reaction that generates $^1O_2$ from ground state oxygen is shown by the Jablonski diagram (Figure 1-1). The photosensitizer is irradiated by light of the proper wavelength (i.e., 600 ~ 800 nm) to excited singlet states (S_1) (A). The photosensitizer can relax back to the ground state by emitting a fluorescent photon (B) or to excited triplet states by way of intersystem

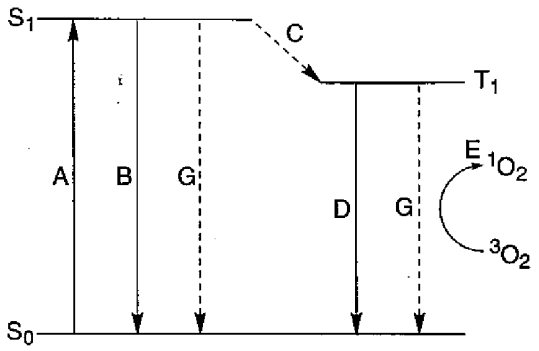

Figure 1-1 Jablonski diagram showing the various modes of excitation and relaxation in a photosensitizer (e.g., porphyrin derivatives): (A) excitation; (B) fluorescence; (C) intersystem crossing; (D) phosphorescence; (E) non-radiative transfer of energy to $^1O_2$; (G) internal conversion.

crossing (ISC) ($S_1 \rightarrow T_1$) (C). From triplet excited states (T_1) the photosensitizer can relax back to the ground state by emitting a phosphorescent photon (D) or transferring energy to another molecule by way of a radiationless transition (G). As one of the radiationless transition, in addition, the photosensitizer can also lose energy though the collisions with other molecules (E). In oxygenated environments the chromophore readily transfers its energy to ground state molecular oxygen ($^3O_2$) to produce singlet oxygen ($^1O_2$) which can reacts with organic substrates. The triplet state of photosensitizer easily interact with $^3O_2$ because $^3O_2$ has a unique, triplet ground state and low-lying excited states. The transition between triplet to singlet states in $^3O_2$ requires 92 kcal·mol^{-1}, which corresponds to a wavelength of 1274 nm. Thus relatively low energy is needed to produce $^1O_2$. There are two mechanisms by which the triplet state

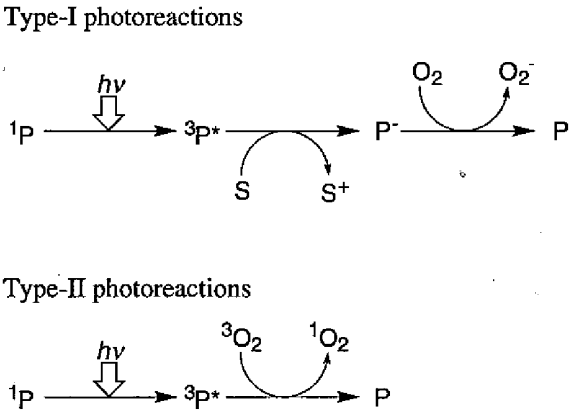

Figure 1-2 Type I and Type II photoreactions. photosensitizer (^1P) is in a singlet ground state; $^3P^*$ is in a triplet excited state; S is a substrate molecule, P^- is reduced photosensitizer molecule; S^+ is an oxidized substrate molecule; oxygen molecule ($^3O_2$) is triplet ground state, O_2^- is the superoxide anion, P^- is the oxidized photosensitizer, $^3O_2$ is triplet ground state O_2, $^1O_2$ is O_2 in a singlet excited state.

photosensitizer can react with biomolecules; these are known as the Type I and Type II reactions (Figure 1-2). In Type I reactions, the excited photosensitizers ($^3P^*$) can react directly with organic compounds (S) by electron exchange to produce an oxidized compound (S^+) and reduced photosensitizer (P^-) in hypoxic environments. The reduced P^- can react with O_2 to produce superoxide anions (O_2^-) which can then form the highly reactive hydroxyl radical ($OH^\cdot$). The $^3P^*$ can also produce superoxide anions (O_2^-) which can then create hydroxyl radical ($OH^\cdot$). These radicals attack tumor cells as described below. On the other hand, it is well-known that Type II photoreactions dominate in PDT action. This reaction produces the electronically excited and highly reactive state of oxygen known as $^1O_2$. Direct interaction of the $^3P^*$ with molecular $^3O_2$ results in the deactivation of photosensitizer and the formation of $^1O_2$. The photodynamic effect depends on the $^1O_2$ quantum yield (denoted as ϕ_Δ) of photosensitizers. If $^1O_2$ generates only from triplet state of the photosensitizers, ϕ_Δ must be less than triplet quantum yield (ϕ_T). Oxygen molecules are very efficient quenchers for triplet states, hence, ϕ_Δ values are often not far from ϕ_T. The ϕ_Δ values for some organic and some porphyrinoids are listed in Table 1-2. PDT treatment usually requires

Table 1-2 $^1O_2$ quantum yields (ϕ_Δ) values of photosensitizers

groups	photosensitizers	solvent	ϕ_Δ
General	acridine	benzene	0.83
	benzophenone	benzene	0.35
	eosin Y	H_2O	0.61
	8-methoxypsoralen	D_2O	0.009
	methylene blue	MeOH	0.51
	rose bengal	MeOH	0.87
	rose bengal	H_2O	0.76
Porphyrins	porphyrins	CCl_4	0.75
	hematoporphyrins	MeOH	0.52
	TPP	benzene	0.66
	Zn complex	benzene	0.72
Phthalocyanines (Pc)	Mg Pc complex	C_6H_5N	0.40
	sulphonate Pc of -		
	Cl Al complex	H_2O	0.34
	Cu complex	H_2O	0.0
	Zn complex	H_2O	0.45

the ϕ_Δ values over 0.3. The values listed in Table 1-2 are satisfactory for PDT treatment in almost compounds quoted. The aluminium and zinc phthalocyanine derivatives listed have appreciable ϕ_Δ values (*ca.* 0.4), the corresponding copper (II) complex has a ϕ_Δ value of zero.

1-2-5. Photosensitizers **[1-4, 9-10, 12-18]**

In PDT treatment, photosensitizers should meet several criteria: (1) chemical purity (2) tumor selectivity (3) fast accumulation in target tissues and rapid clearance (4) activation at wavelengths which reaches deeper cells (600 ~ 800 nm) (5) high photocytotoxicity and (6) no dark toxicity. Porphyrins, purpurins, benzoporphyrins, chlorins and bacteriochlorins are the most useful photosensitizers for PDT treatments, although other classes of porphyrinoides such as phthalocyanines, naphtalocyanines, and texaphyrins are also used. Porphyrin skeletons (i.e., porphyrins, purpurins, benzoporphyrins, chlorins and bacteriochlorins) have Q_1 band of absorption maxima in the red region of the electronic absorption spectrum and generate $^1O_2$ efficiently. Red absorption maxima (600 ~ 800 nm) allow activating light to reach deeper tumor cells (Figure 1-3). Porphyrin skeleton is generally planar-aromatic structure composed of four symmetrically arranged pyrrol units linked by methine bridges. On the other hand, texaphyrins have three pyrrol units and phthalocyanines and naphtalocyanines are linked by azone bridges, while these photosensitizers are planar-aromatic molecules and have similar photophysical properties as porphyrin skeleton compounds. Porphyrins, chlorins and bacteriochlorins are all fully conjugated, but chlorins have one pyrrolic double bond reduced (i.e., dihydro-porphyrins) and bacteriochlorins have two

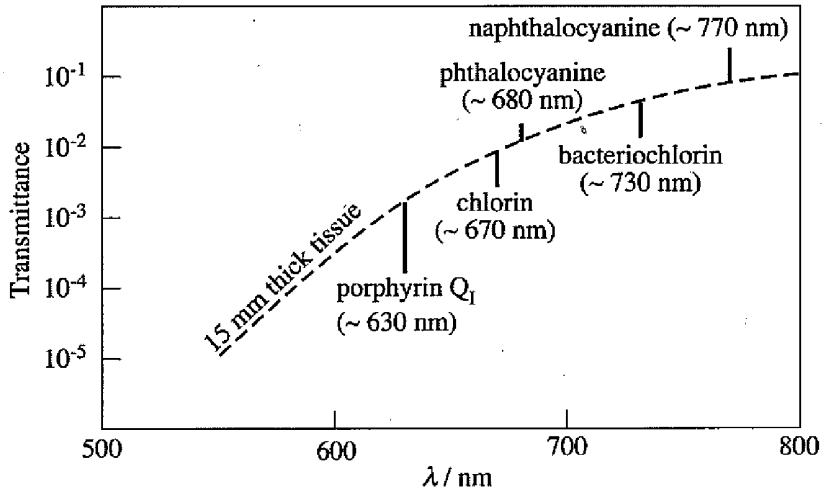

Figure 1-3 Photochemical propeties of photosensitizers and transmission of light in tissues.

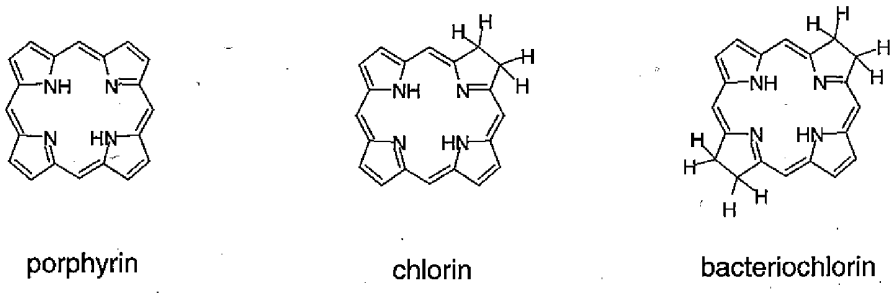

Figure 1-4 Structure of porphyrin ring, chlorin ring and bacteriochlorin ring.

pyrrolic double bonds reduced (i.e., tetrahydro-porphyrins) (Figure 1-4). Hence, porphyrins, chlorins, and bacteriochlorins have 22-, 20-, and 18-π electrons in their porphyrin skeletons, in which similar ring current effect occurs. All porphyrin skeleton groups (i.e., porphyrin, chlorin, and bacteriochlorin) have a strong absorption band ($\varepsilon \sim 2 \times 10^5\ M^{-1}\cdot cm^{-1}$) about at 400 nm called the Soret band. However Soret band is not useful for PDT treatment since blue light can not reach the deeper tumor cells. Hence the Q_1 band between 600 ~ 800 nm is used for PDT treatment, although the band has relatively weak absorption. Porphyrins exhibit Q_1 band with maximum absorption wavelength (λ_{max}) of about 630 nm, while chlorins and bacteriochlorins have Q_1 bands with λ_{max} of about 650 nm and 710 nm, respectively. Chlorins and bacteriochlorins have stronger Q_1 band than that of porphyrins. The difference in Q_1 band of electronic absorption spectra can be explained by unstablization of highest occupied molecular orbital (HOMO) due to reduction of pyrrole units in the porphyrin skeleton [2]. Most porphyrinoides exhibits highly efficient $^1O_2$ producing ability. The porphyrinoides which is approved or under clinical trial is briefly reviewed as follows (Figure 1-5):

(1) Hematoporphyrin derivatives (HpD, Photofrin®, Photosan®)

The absorption maximum wavelength of Photofrin® is 630 nm in PBS. The PDT treatment is applied via intravenous injection of 2 mg/kg followed by a subsequent irradiation with light (630± 3 nm) at the light dose (200 ~ 300 J/cm²) in 48 h after injection. The residual photosensitivity usually lasts for 30 days after injection. The photosensitizer has been investigated for use against esophageal cancer and endobroncheal cancer. The purified oligohematoporphyrin derivative (Photosan®) has also been used for PDT treatment. This photosensitizer shows a very excellent PDT effect to skin cancer.

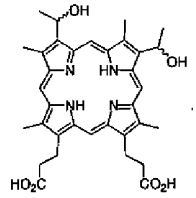

(1) Hematoporphyrin IX

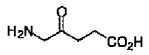

(2) 5-Aminolevulinic acid (Levulan®)

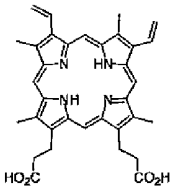

Protoporphyrin IX (PpIX)

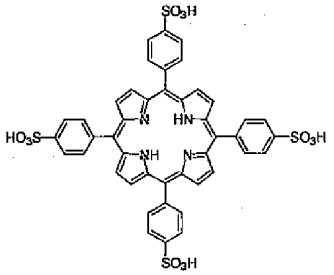

(3) Tetrasodium tetraphenyl porphine sulfonate (TPPS4)

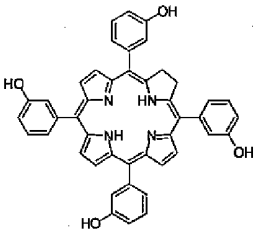

(4) *meta*-Tetrahydroxyphenylchlorin
(*m*-THPC, Foscan™, Temoporfin)

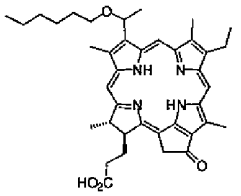

(5) Hexyl ether of pyropheophorbide-*a*
(HPPH, Photochlor®)

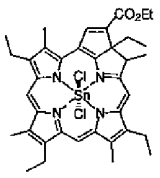

(6) Tin ethyl etiopurpurin
(SnET2, Purlytin™)

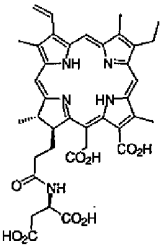

(7) mono-L-aspartyl chlorin e6
(NPe6)

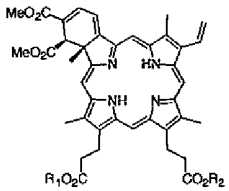

(8) Benzoporphyrin derivative-monoacid ring A
(BPD-MA, verteporfin, Visudyne™)

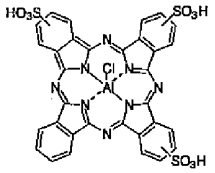

(9) Chloro-aluminum sulfonated phthalocyanine
(CASPc, Photosens)

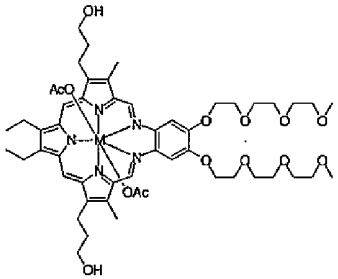

(10) Texaphyrin groups
(Lu-Tex Motexafin lutetium, Antrin® / Lutrin Optrin™ (M = Lu), and motexafin gadolinium, Xcytrin® (M = Gd))

Figure 1-5 The porphyrinoides which are approved or under clinical trial.

(2) 5-Aminolevulinic acid (Levulan®)

5-Aminolevulinic acid (ALA) is not photosensitizers, is a precursor for endogenous protoporphyrin IX (PpIX) in biosynthesis. So that the PDT treatment using Levulan® is conceptionally different from the conventional treatment. In the treatment, this product (i.e., PpIX) shows an excellent effect as a photosensitizer. The PDT treatment is applied via intravenous injection of 30 mg/kg, while the oral drug is 60 mg/kg followed by a subsequent irradiation with Wood's light (635 nm) in 24 h after injection. The photosensitizer has been investigated for use against bladder cancer photodiagnosis, acne and hair removal.

(3) Tetrasodium tetraphenyl porphine sulfonate (TPPS4)

Tetrasodium tetraphenyl porphine sulfonate (TPPS4) is a synthetic pophyrin with high potency of photosensitization. Even though early reports indicated its neurotoxicity, further study revealed that its neurotoxicity comes form imperfect purification procedures. The PDT treatment is applied via intravenous injection of 75 μg/mL of PBS followed by a subsequent irradiation with light (630 nm) in 24 h after injection. However, the low potency of photosensitizer were found.

(4) *meta*-Tetrahydroxyphenylchlorin (*m*-THPC, Foscan™, Temoporfin)

meta-Tetrahydroxyphenylchlorin (Foscan™) exerts efficacious PDT treatment with very low drug (as little as 0.1 $mgkg^{-1}$) and low light doses (as low as 10 $J \cdot cm^{-2}$), which means 100-fold more active than Photofrin®. The photosensitizer has been investigated for use in esophageal, lung, laryngeal, thoracic and skin cancers. Phase III clinical trials of Foscan™ have begun in Europe and the US against head and neck cancers. The absorption maximum wavelength of Foscan™ is 652 nm in mixture of water, polyethylene glycol 400 and ethanol (5 : 3 : 2). The time between intravenous injection and irradiation is 96 hours. Foscan™ has short clearance time of 20 days after injection. The reasons behind this exceptionally high activity are not fully understand.

(5) Hexyl ether of pyropheophorbide-*a* (HPPH, Photochlor®)

The absorption maximum wavelength of Photochlor® is 665 nm. The photosensitizer has been investigated for use in obstructive esophageal tumors, early stage esophageal cancer, skin cancer, and locally recurring breast cancer on the chest wall following mastectomy. The use of the photosensitizers can avoid the long-lasting photosensitivity such as Photofrin®. Under typical condition, the PDT treatment

is applied via intravenous injection of 0.3 mg/kg with a subsequent irradiation with monochromatic laser light (660 nm) at the light dose of 2 J/cm^2. The residual photosensitivity usually lasts for 28 days after injection.

(6) Tin ethyl etiopurpurin, (SnET2, Purlytin™)

The PDT treatment is applied via intravenous injection of 0.8 ~ 1.6 mg/kg followed by a subsequent irradiation with monochromatic laser light (660 nm) in 24 h after injection. The residual photosensitivity usually lasts for 30 days after injection. The photosensitizer has been investigated for application in many different fields including oncology, dermatology, ophthalmology and cardiology.

(7) mono-L-aspartyl chlorin e6 (NPe6)

The PDT treatment is applied via intravenous injection of 0.5 ~ 3.5 mg/kg followed by a subsequent irradiation with monochromatic laser light (664 nm) in 4 h after injection. The photosensitizer has been investigated for use against adenocarcinoma of the breast, basal cell carcinoma and squamous cell carcinoma.

(8) Benzoporphyrin derivative-monoacid ring A (BPD-MA, verteporfin, Visudyne™)

The PDT treatment is applied via intravenous injection of 0.2 ~ 0.5 mg/kg followed by a subsequent irradiation with monochromatic laser light (690 nm) in 30 ~ 150 min after injection. The photosensitizer has been investigated for use against age-related macular degeneration, skin cancer, psoriasis, arterial restenosis, rheumatoid arthritis and autoimmune disorders.

(9) Phthalocyanine groups (Photosens etc)

Chloro-aluminum sulfonated phthalocyanine (CASPc, Photosens) and silicon-based phthalocyanines (Pc4, Pc10, Pc12 and Pc18) are a new group of synthetic photosensitizers which are still under investigation. These substances are activated about 700 nm light which penetrates deeper into tissues than 630 nm light. Irradiation times can use within several minutes (in ophthalmology) up to 3 h (in oncology). In the case of Photosens, The PDT treatment is applied via intravenous injection of 0.5 ~ 1.5 mg/kg followed by a subsequent irradiation with monochromatic laser light (675 nm) at the light dose of 150 ~ 600 J/cm^2. The photosensitizer has been investigated for use against skin cancer, breast cancer and oropharyngeal

cancer.

(10) Texaphyrin groups (Lu-Tex Motexafin lutetium, Antrin® / Lutrin Optrin™ and Motexafin gadolinium, Xcytrin®)

Texaphyrins has been investigated for use against breast cancer. This photosensitizer can be excited by longer wavelength light (720 ~ 760 nm) to irradiate deeper tumor cells. Motexafin lutetium (Lutrin®, Antrin®) and motexafin gadolinium (Xcytrin®) are still under clinical research. Lutrin® has a broad peak between 720 and 760 nm (centred at 732 nm) in the electronic absorption spectrum. The PDT treatment is applied via intravenous injection of 0.6 ~ 7.2 mg/kg followed by a subsequent irradiation in 2 ~ 4 h after injection. It is expected that these photosensitizers can be applicable to atherosclerosis, subcutaneous metastases of malignant melanoma, Kaposi's sarcoma and epithelial skin cancer.

Today, several next generation photosensitizers have been actively developed to enable them to accumulate in targeted tumor tissue selectively. BOPP (boronated protoporphyrin), ATX-S10, chlorophyll derivatives, porphycens, antracens, purpurins, hypericin, hypocrellin and brominated rhodamines are examined on phase I/II clinical trials of PDT treatment.

1-2-6. Glycoconjugated porphyrin derivatives [(1)-(38)]

Even though second generation photosensitizers exerts high photocytotoxicity for PDT treatment, they must be improved the tumor selectivity to avoid side effect such as photosensitivitiy [2-4]. For this reason, the development of third generation photosensitizers which have high accumulation in tumor tissue is challenging field in PDT study. One of the promising strategies is conjugation of molecular recognition elements such as sugar unit. Hence, the glycoconjugated porphyrin derivatives have been synthesized as third generation photosensitizers not only to improve water-solubility but also to take advantage of the biological activity of the sugar unit. Synthesis of glycoconjugated porphyrin derivatives and evaluation of its photocytotoxicity has been reported since 1990 (Figure 1-6) [(1)]. Most glycoconjugated porphyrins has either structure of tetraphenylporphyrin [(1)-(4),(7)-(13),(15)-(17),(19),(21),(23)-(28),(30)-(32),(34)] or protoporphyrin IX [(5)-(6),(14),(20),(32),(35)]. As very rare examples, glycoconjugated porphyrins with structure of tetraphenylporphyrin dimer has been also synthesized [(21),(25)]. These glycoconjugated porphyrins are combined with most monosaccaharaides

(e.g., D-glucose, D-galactose and D-glucosamine), disaccaraides (e.g., maltose and lactose) [(8),(10)-(12),(14),(21),(23),(26)] and oligosaccaraide groups [(30),(31)]. In addition, the glycoconjugated porphyrins having not only sugar units but also alkyl chain with various length has been synthesized to give it amphiphilic properties [(2),(7),(11),(12),(14),(15),(21),(23),(25),(26),(30)-(32)].

Glycoconjugated chlorins and bacteriochlorins have been also reported since 1997 [(14)]. These photosensitizer are generally synthesized by means of diimide reduction [(18),(37),(38)] or 1,3-dipolar cycloadition [(33)]. Zheng et al. reported to synthesis of glycoconjugated purpurinimides [(29)]. Although a lot of glycoconjugated porphyrin derivatives have been synthesized, the sugar unit effect on their pharmaceutical nature and photocytotoxicity for PDT treatment is not studied systematically and it is still not fully understood.

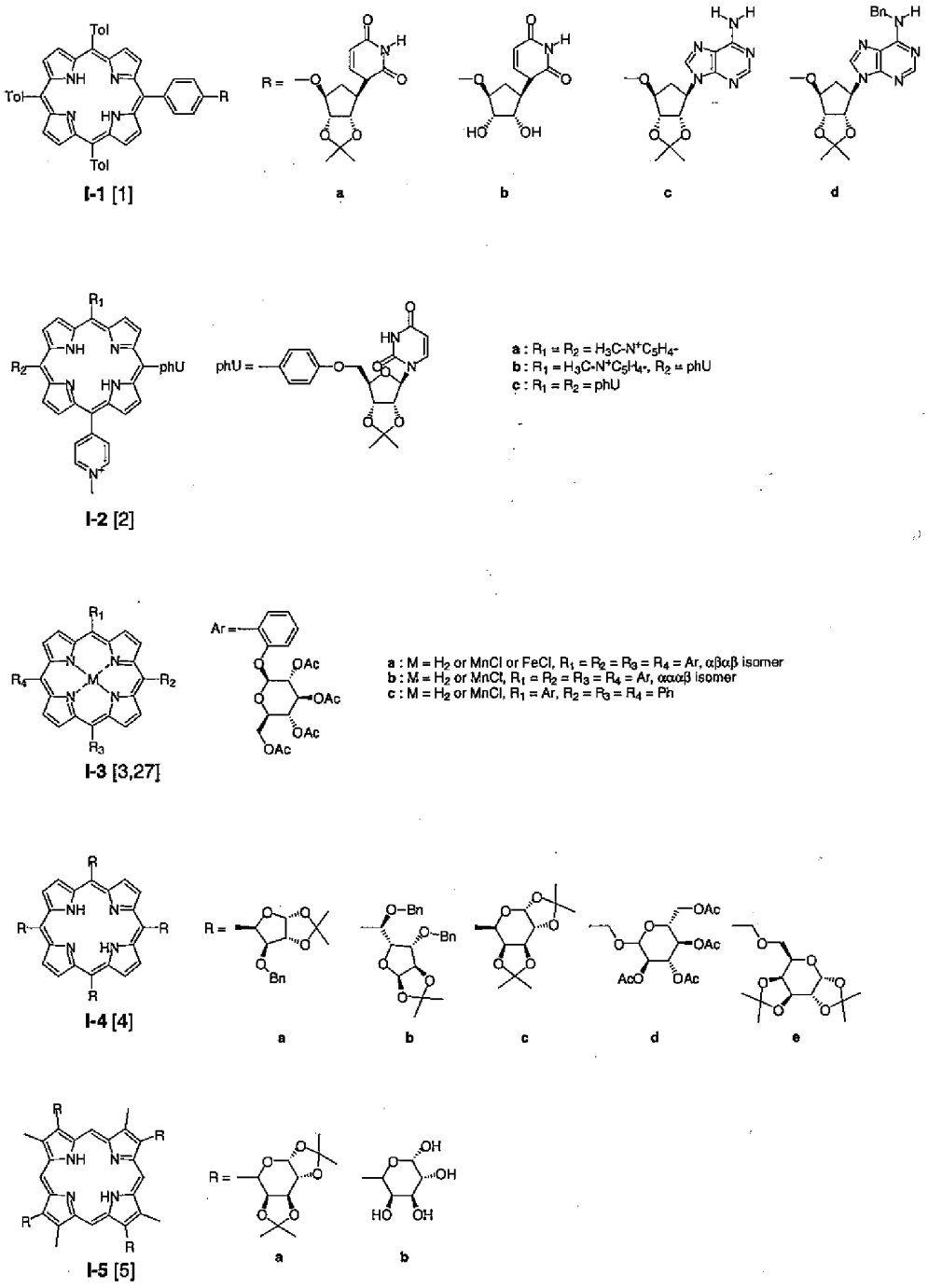

Figure 1-6 Structure of glycoconjugated porphyrins

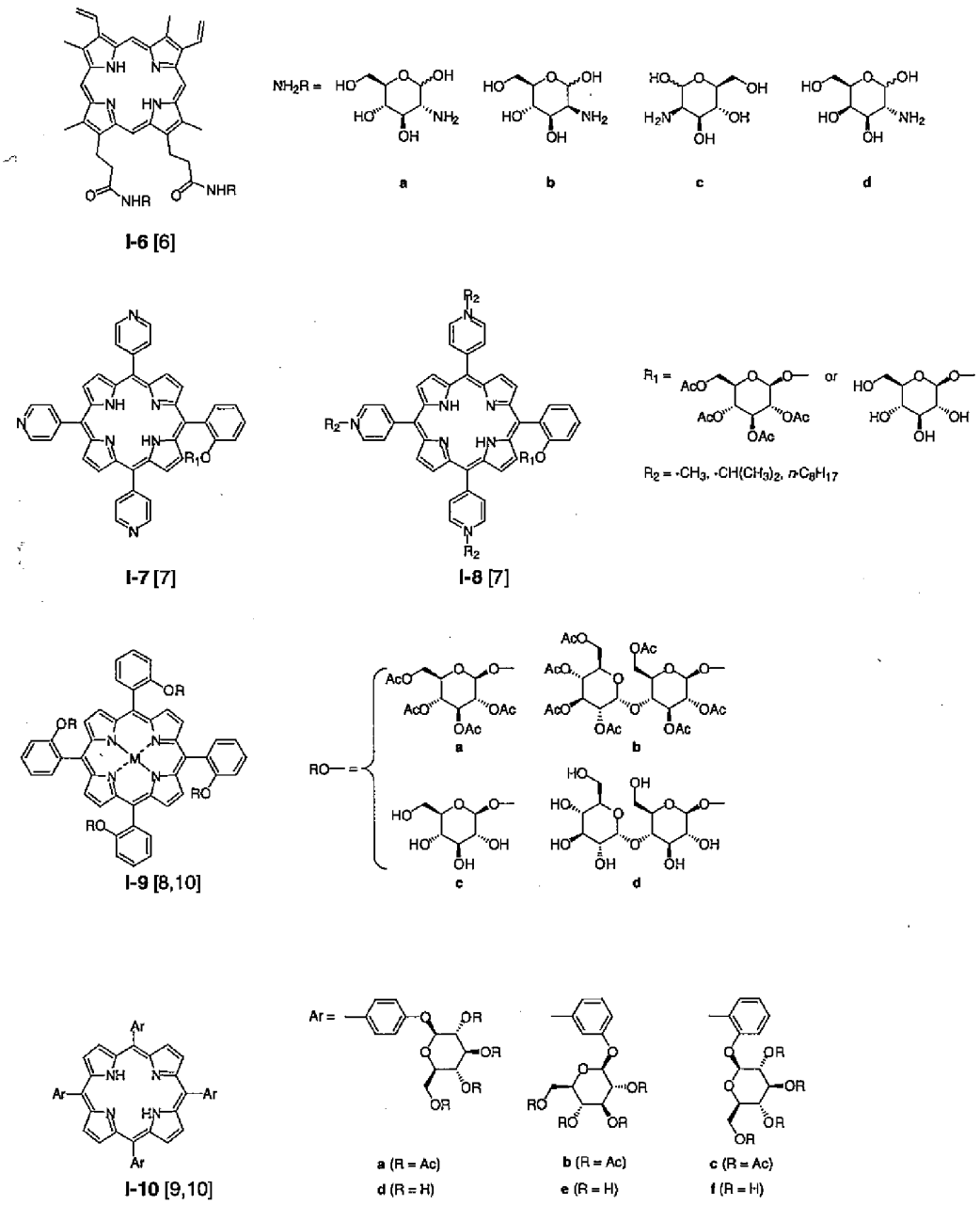

Figure 1-6 Structure of glycoconjugated porphyrins (continued)

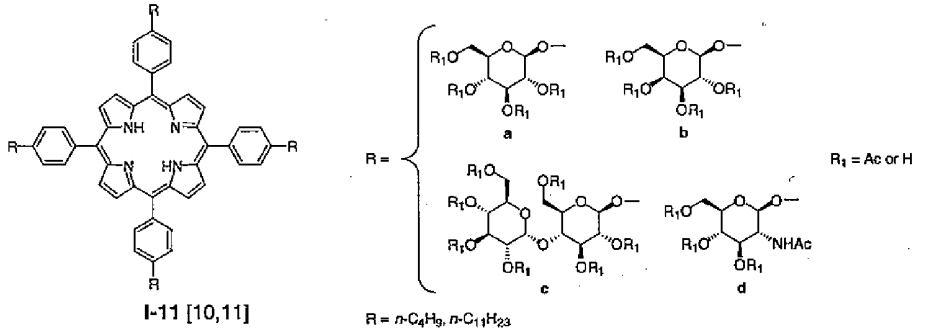

I-11 [10,11]

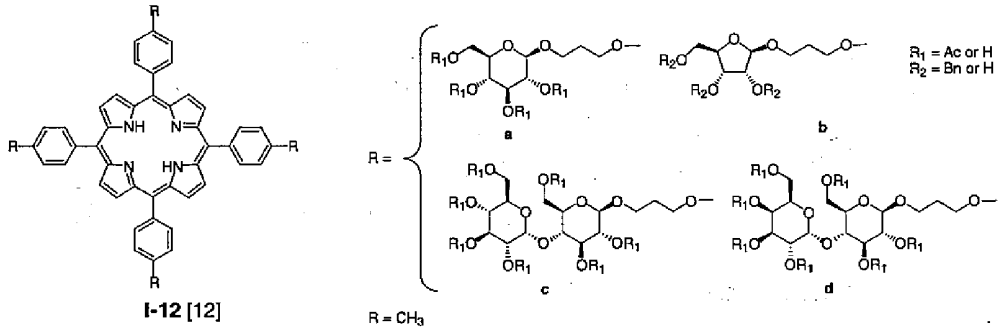

I-12 [12]

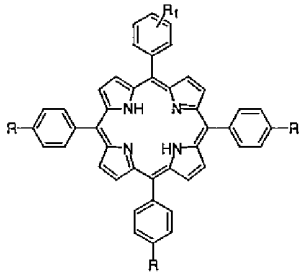

I-13 [13]

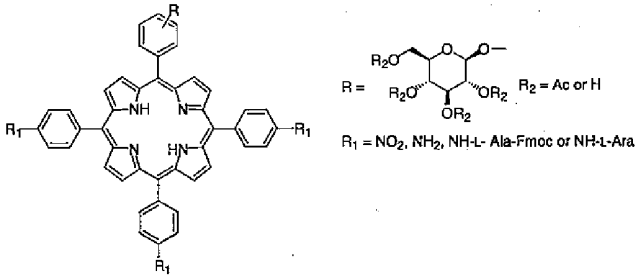

I-14 [13]

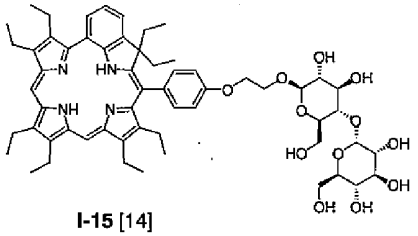

I-15 [14]

Figure 1-6 Structure of glycoconjugated porphyrins (continued)

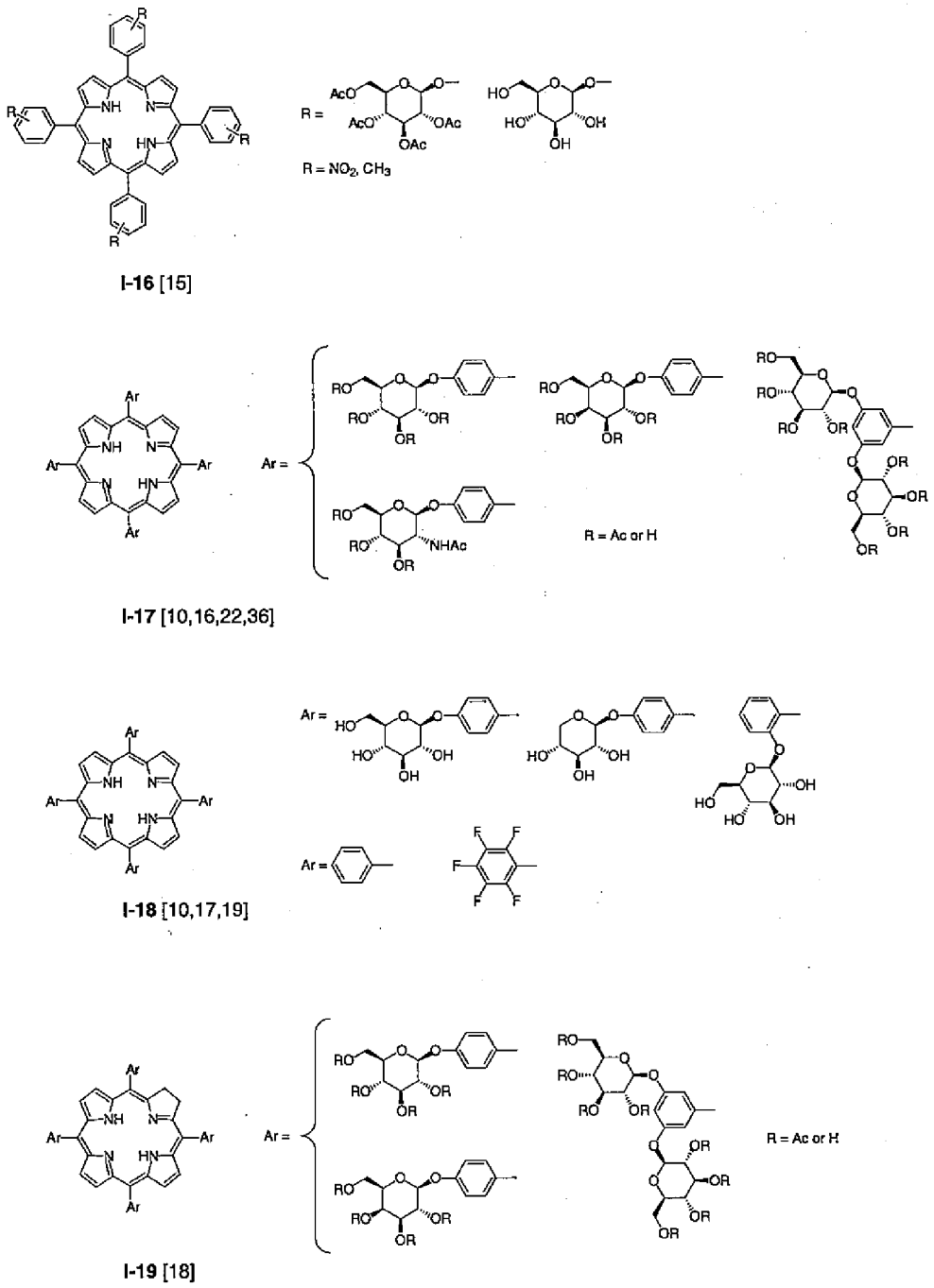

Figure 1-6 Structure of glycoconjugated porphyrins (continued)

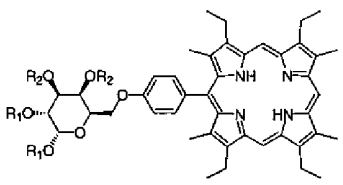

I-20 [20]

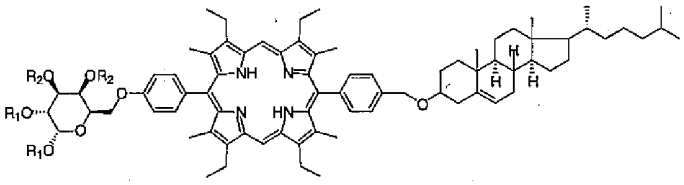

I-21 [20]

R_1, R_1 = isopropyridene or 2H
R_2, R_2 = isopropyridene or 2H

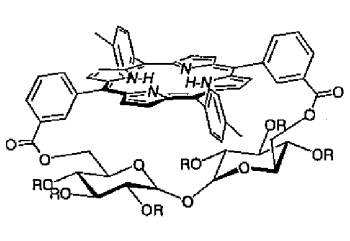

I-22 [21]

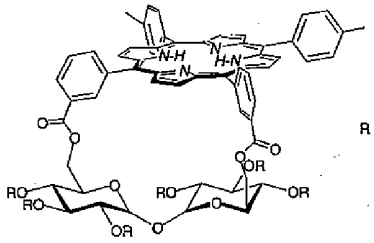

I-23 [21]

R = $SiMe_3$ or H

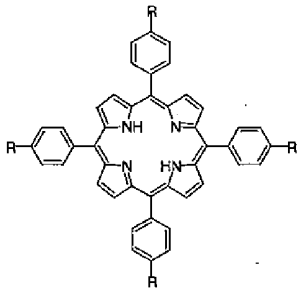

I-24 [23]

R = 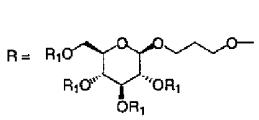

a

R = CH_3

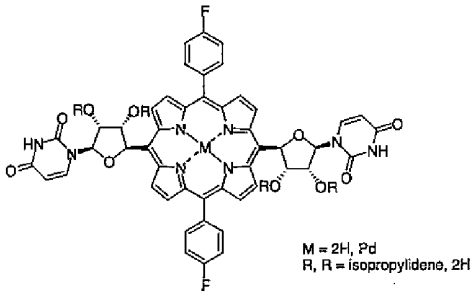

M = 2H, Pd
R, R = isopropylidene, 2H

I-25 [24]

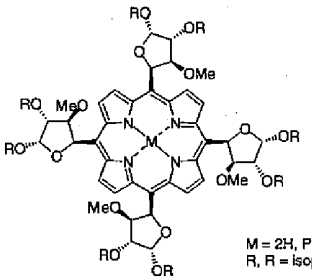

M = 2H, Pd, Zn, Ni
R, R = isopropylidene, 2H

I-26 [24]

Figure 1-6 Structure of glycoconjugated porphyrins (continued)

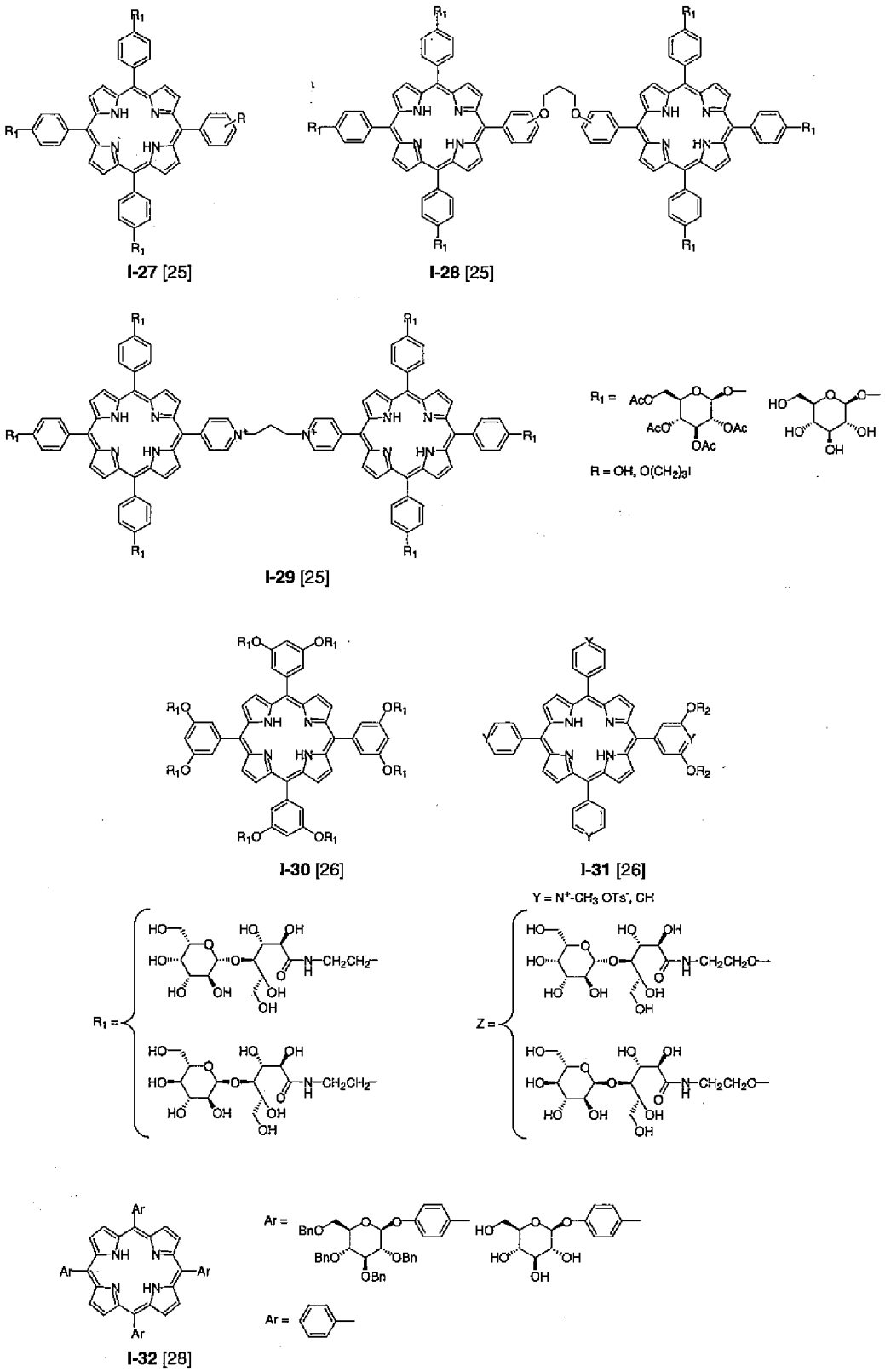

Figure 1-6 Structure of glycoconjugated porphyrins (continued)

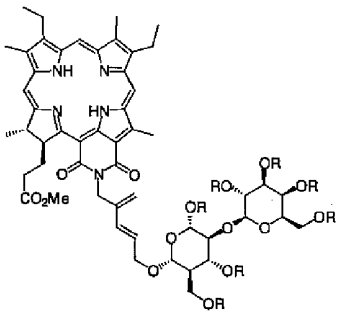

I-33 [29]

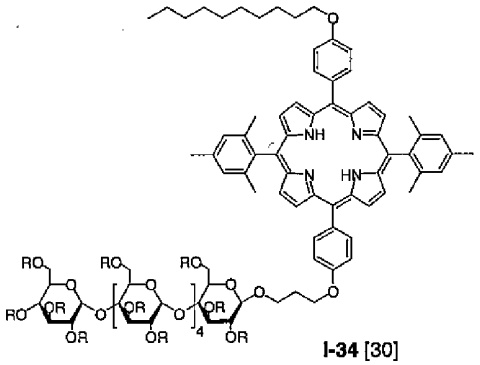

I-34 [30]

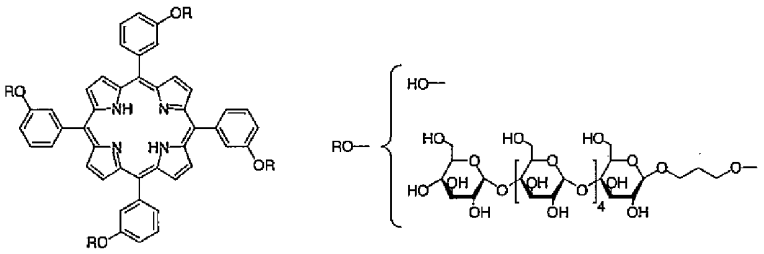

I-35 [31]

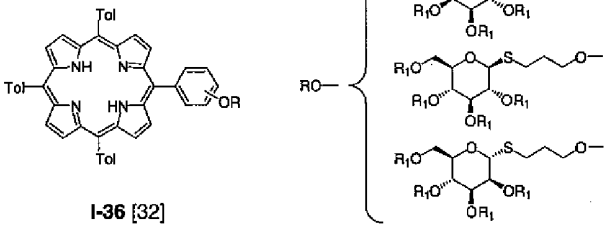

I-36 [32]

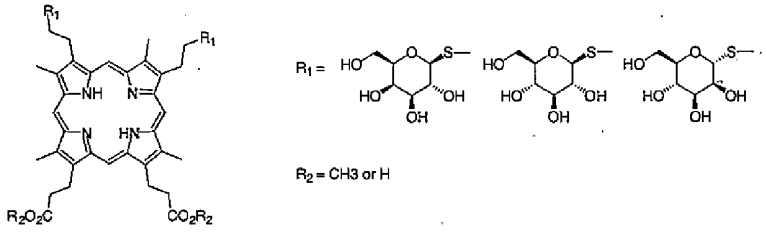

I-37 [32]

Figure 1-6 Structure of glycoconjugated porphyrins (continued)

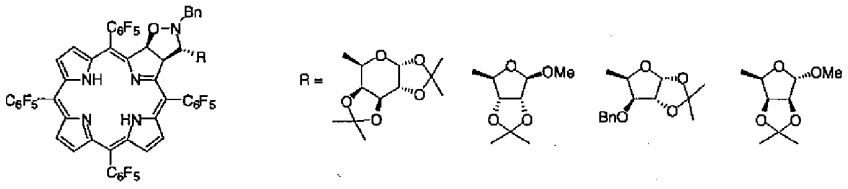

I-38 [33]

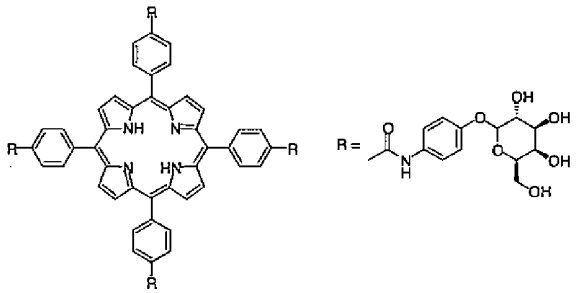

I-39 [34]

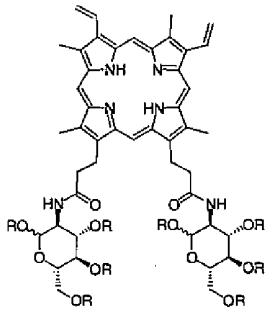

I-40 [35]

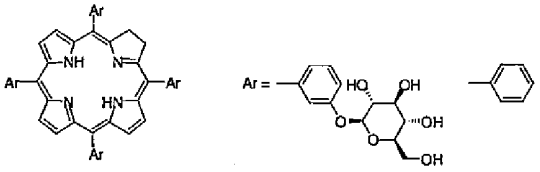

I-41 [37,38]

Figure 1-6 Structure of glycoconjugated porphyrins (continued)

1-3. Object and outline of the thesis

In this study, glycoconjugated tetrapheynylporphyrins (TPPs) and tetrapheynylchlorins (TPCs) were synthesized, and the sugar unit effect on pharmaceutical nature and photocytotoxicity by HeLa cells were investigated for these photosensitizers. The outline of the thesis is as follows:

In chapter 2, glycoconjugated porphyrins were synthesized by a modification of Lindsey method in the presence of $Zn(OAc)_2 \cdot 2H_2O$ as a template. The resulting zinc porphyrins readily afford the corresponding free-base porphyrins in moderate yield upon treatment with HCl, even in the case of *meta*-substituted glycoconjugated porphyrins. The versatility of this method for the synthesis of *para*- and *meta*-substituted glycoconjugated porphyrins was examined with D-glucose, D-galactose, D-xylose and D-arabinose. All of glycoconjugated porphyrins have been characterized by ^1H and ^{13}C NMR, electronic absorption, IR, ESI-TOF and FAB mass spectra.

In chapter 3, the hydrophobicity parameters of glycoconjugated porphyrins were estimated by Shake-Flask method and reversed phase high performance liquid chromatography (RP-HPLC). In addition, binding equilibrium of some glycoconjugated porphyrins to bovine serum albumin (BSA) were also studied by fluorometric titration. These glycoconjugated porphyrins were subjected to test the cellular uptake by HeLa cells and the photocytotoxicity *in vitro*. These cellular uptake behavior and photocytotoxity were discussed on the basis of hydrophobicity, binding properties to BSA and photochemical study in aqueous media such as cytoplasm for these photosensitizers.

In chapter 4, glycoconjugated chlorins were synthesized by means of the Whitlock method with diimide reduction and purified by reversed phase thin layer chromatography (RP-TLC). The versatility of this method for the synthesis of *para*- and *meta*-substituted glycoconjugated chlorins was examined with D-glucose, D-galactose, D-xylose and D-arabinose. All of glycoconjugated chlorins have been characterized by ^1H NMR, electronic absorption, IR and ESI-TOF mass spectra.

In chapter 5, the hydrophobicity parameters of glycoconjugated chlorins were estimated by Shake-Flask method and reversed phase high performance liquid chromatography (RP-HPLC). These glycoconjugated chlorins were subjected to test the cellular uptake by HeLa cells and the photocytotoxicity *in vitro*. These cellular uptake behavior and photocytotoxicity were discussed on the basis of hydrophobicity, and photochemical study in cytoplasm and aqueous media for these photosensitizers.

Finally, chapter 6 summarized the results of the systematic study of glycoconjugated porphyrins and chlorins for PDT photosensitizers.

1-4. References

1. R. Bonnett, Photosensitizers of the Porphyrin and Phthalocyanine Series for Photodynamic Therapy. Chem. Soc. Rev. 24 (1995) 19-33.
2. R. Bonnett, Chemical Aspects of Photodynamic Therapy. Taylor & Francis, London. (2000).
3. I. Okura, Photosensitization of Porphyrins and Phthalocyanines. Kodansha. Tokyo. (2000).
4. J. G. Moser, PHOTODYNAMIC TUMOR THERAPY. harwood academic publishers. Amsterdam. (1998).
5. 加藤 治文, 奥中 哲弥, PDT ハンドブック. 医学書院. (2002).
6. 垣添 忠生, これだけは知っておきたいがんの情報、がんの治療. 日本放送出版. (2002) 16-180.
7. ポルフィリン研究会, ポルフィリン・ヘムの生命化学 遺伝病・がん・工学応用などへの展開, 東京化学同人, (1995).
8. Y. Gohto, A. Obana, K. Kaneda, T. Miki, Photodynamic Effect of a New Photosensitizer ATX-S10 on Corneal Neovascularization. Exp. Eye Res. 67 (1998) 313-322.
9. R. Bonnet, G. Martínez, Photobleaching of sensitizers used in photodynamic therapy, Tetrahedron. 57 (2001) 9513-9547.
10. I.J. Macdonald, T.J. Dougherty, Basic principles of photodynamic therapy. J. Porphyrins. Phthalocyanines. 5 (2001) 105-129.
11. E.S. Nyman, P.H. Hynnine, Research advances in the use of tetrapyrrolic photosensitizers for photodynamic therapy. J. Photochem. Photobiol. B: Biol. 73 (2004) 1-28.
12. W.M. Sharman, C.M. Allen, J.E. Lier, Photodynamic therapeutics: basic principles and clinical applications. DDT. 4 (1999) 507-517.
13. M.C. DeRosa, R.J. Crutchley, Photosensitized singlet oxygen and its applications, Cood. Chem. Rev. 233-234 (2002) 351-371.
14. A.S. Soboleva, D.A. Jansc, A.A. Rosenkranza, Targeted intracellular delivery of photosensitizers, Progress in Biophys. Mol. Biol. 73 (2000) 51-90.
15. A.C.E. Moor, Signaling pathways in cell death and survival after photodynamic therapy. J. Photochem. Photobiol. B: Biol. 57 (2000) 1-13.
16. R.D. Almedia, B.J. Manadas, A.P. Carvalho, C.B. Duarte, Intracellular signaling mechanisms in photodynamic therapy. Biochem. Biophys. Acta. 1704 (2004) 59-86.

17. T.D. Mody, Pharmaceutical development and medical applications of porphyrin-type macrocycles. J. Porphyrins. Phthalocyanines. 4 (2000) 362-367.

18. R.K. Pandy, Recent advances in photodynamic therapy. J. Porphyrins. Phthalocyanines. 4 (2000) 368-373.

Glycoconjugated porphyrin derivatives

(1) P. Kus, G. Knerr, L. Czuchajowski, FIRST REPRESENTATIVES OF PORPHYRINYL-NUCLEOSIDES. Tetrahedron Lett. 31 (1990) 5133-5134.

(2) L. Czuchajowski, J. Habdas, H. Niedbala, V. Wandrekar, Porphyrinyl-uridines as the First Water Soluble Porphyrinyl-nucleosides. Tetrahedron Lett. 32 (1991) 7511-7522.

(3) Ph. Maillard, J.L. Guerquin-Kern, M. Momenteau, Catalytic Properties of Iron and Manganese Glycoconjugated porphyrins. Tetrahedron Lett. 32 (1991) 4901-4904.

(4) Ph. Maillard, C. Huel, M. Momentueau, Synthesis of New Meso -Tetrakis (Glycosylated) Pophyrins. Tetrahedron Lett. 33 (1992) 8081-8084.

(5) N. Ono, M. Bougauchi, K. Maruyama, Water-Soluble Porphyrins with Four Sugar Molecules. Tetrahedron Lett. 33 (1992) 1629-1632.

(6) J-H Fuhrhop, C. Boettcher, J. Köning, U. Siggel, Chiral Micellar Porphyrin Fibers with 2-Aminoglycosamide. J. Am. Chem. Soc. 114 (1992) 4159-4165.

(7) K. Driaf, P. Krausz, B. Verneuil, Glycosylated Cationic Porphyrins as Potential Agents in Cancer Phototherapy. Tetrahedron Lett. 34 (1993) 1027-1030.

(8) P. Maillard, J-L. Guerquin-Kern, C. Huel, M. Momenteau, Glycoconjugated Porphyrins. 2. Synthesis of Sterically Constrained Polyglycosylated Compounds Derived from Tetraphenylporphyrins. J. Org. Chem. 58 (1993) 2774-2780.

(9) K. Kohata, H. Higashio, Y. Yamauchi, M. Koketsu, T. Odashima, Synthesis and Characterization of New Style of Water-Soluble Glycosylated Porphyrins as a Spectrophotometric Reagent for Metal Ions. Bull. Chem. Soc. Jpn. 67 (1994) 668-679.

(10) M. Momenteau, D. Oulmi, Ph. Maillard, A. Croisy, Photodynamic Therapy of cancer II. SPIE. 2325 (1994) 13-23.

(11) D. Oulmi, P. Maillard, J-L. Guerquin-Kern, C. Huel, M. Momenteau, Glycoconjugated Porphyrins. 3. Synthesis of Flat Amphiphilic Mixed *meso*-(Glycoconjugated aryl)arylporphyrins and Mixed

meso-(Glycosylated aryl)alkylporphyrins Bearing Some Mono- and Disaccharide Groups. J. Org. Chem. 60 (1995) 1554-1564.

(12) O. Gaud, R. Granet, M. Kaouadji, P. Krausz, J. Claude, Synthése analyse structurale de nouvelles méso-arylporphyrins glycosylées en vue de l'application en photothérapie des cancers. Can. J. Chem, 74 (1996) 481-499.

(13) V. Sol, J.C. Blais, G. Bolbach, V. Carré, R. Granet, M. Guilloton, M. Spiro, P. Krausz, Toward Glycosylated Peptidic Porphyrins: a New Strategy for PDT?. Tetrahedron Lett. 38 (1997) 6391-6394.

(14) M. Philippe, H. Clotide, M. Michel, Synthesis, Characterization and photocytotoxicity of a Glycoconjugated meso-monoarylbenzochlorin. Tetrahedron Lett. 38 (1997) 3731-3734.

(15) V. Sol, P. Branland, R. Granet, C. Kaldapa, B. Verneuil, P. Krausz, Nitroglycosylated meso-arylporphyrins as Photoinhibitors of Gram positive Bacteria. Bioorg. Med. Chem Lett. 8 (1998) 3007-3010.

(16) Y. Mikata, Y. Onchi, K. Tabata, S. Ogura, I. Okura, H. Ono, S. Yano, SUGAR-DEPENDENT PHOTOCYTOTOXIC PROPERTY OF TETRA- AND OCTA-GLYCOCONJUGATED TETRAPHENYLPORPHYRINS. Tetrahedron Lett. 39 (1998) 4505-4508.

(17) G. Csík, E. Balog, I. Voszka, F. Tölgyesi, D. Oulmi, Ph. Maillard, M. Momenteau, Glycosylated derivatives of tetraphyenyl porphyrin: photophysical characterization, self-aggregation and membrane binding. J. Photochem. Photobiol B: Biology 44 (1998) 216-224.

(18) Y. Mikata, Y. Onchi, M. Shibata, T. Kakuchi, H. Ono, S. Ogura, I. Okura, S. Yano, Synthesis and Phototoxic Property of Tetra- and Octa-Glycoconjugated Tetraphenylchlorins. Bioorg. Med. Chem. Lett. 8 (1998) 3543-3548.

(19) D. Oulmi, P. Maillard, G. Verer-Bizet, M. Mometeau, D. Brault, Glycosylated Porphyrins: Characterization of Association in Aqueous Solution by absorptionand Fluorescence Spectroscopies and Determination of Singlet Oxygen Yield in Organic Media. Photochem. Photobiol. 67 (1998) 511-518.

(20) C. Schell, H.K. Hombrecher, Synthesis and Investigation of Glycosylated Mono- and Diarylporphyrins for Photodynamic Therapy. Bioorg. Med. Chem. 7 (1999) 1857-1865.

(21) E. Davoust, R. Greanet, P. Krausz, Synthesis of Glycosyl Strapped Porphyrins. Tetrahedron Lett. 40 (1999) 2513-2516.

(22) I. Voszka, R. Galántai, P. Maillard, G. Csík, Interaction of glycosylated tetra phenyl porphyrins with model lipid membranes of different compositions. J. Photochem. Photobiol.B: Biology. 52 (1999) 92-98.

(23) V. Carré, O. Gaud, I. Sylvain, O. Boundon, M. Spiro, J. Blais, R. Granet, P. Krausz, M. Guilloton, Fungicidal properties of *meso*-arylglycosylporphyrins: influence of sugar substituents on photoinduced damage in the yeast *Sacharomyces cerevisia*. J. Photochem. Photobiol.B: Biology. 48 (1999) 57-62.

(24) M. Cornia, M. Menozzi, E. Ragg, S. Mazzini, A. Scarafoni, F. Zanardi, G. Casiraghi, Synthesis and Utility of Novel *C-meso*-Glycosylated metalloporphyrins. Tetrahedron 56 (2000) 3977-3983.

(25) C. Kaldapa, J.C. Blais, V. Carré, R. Granet, V. Sol, M. Guilloton, M. Spiro, P. Krausz, Synthesis of new glycosylated neutral and cationic porphyrin dimers. Tetrahedron Lett. 41 (2000) 331-335.

(26) K. Fujimoto, T. Miyata, Y. Aoyama, Saccharide-Directed Recognition and Molecular Delivery Using Macrocyclic Saccharide Clusters: Masking of Hydrophobicity to Enhance the Saccharide Specificity. J. Am. Chem. Soc. 122 (2000) 3558-3559.

(27) X.B. Zhang, C-C. Guo, J-B. Xu, R-Q Yu, Synthesis of acetylglycosylated metalloporphyrins and their catalysis for cyclohexane oxidation with PhIO under mild conditions, J. Mol. Catlysis A: Chemical. 154 (2000) 31-38.

(28) P. Pasetto, X. Chen, C. Michael, R.W. Franck, Synthesis of hydrolytically stable porphyrin C- and S-glycoconjugates in high yeilds. Chem.Commun. (2001) 81-82.

(29) G. Zheng, A. Graham, M. Shibata, J. R. Missert, A.R. Oseroff, T.J. Dougherty, R. Pandey, Synthesis of β-Galactose-Conjugated Chlorins Derived by Enyne Methathesis as Galectin-Specific Photosensitizers for Photodynamic Therapy. J. Org. Chem. 66 (2001) 8709-8716.

(30) A. Hamazawa, I. Kinoshita, B. Breedlove, K. Isobe, M. Shibata, T. Kakuchi, S. Hirohara, M. Obata, Y. Mikata, S. Yano, meso-Tetraphenylporphyrin Having Hexa-maltosyl and Decyl Chain as an Amphiphilic Photosensitizer toward Photodynamic Therapy. Chem. Lett. 3(2002) 388-389.

(31) Y. Arima, S. Akimoto, T. Yamazaki, M. Shibata, S. Hirohara, S. Yano, T. Kakuchi, I. Yamazaki, Excitation relaxation dynamics and molecular dispersion of malto hexaose-linked tetra phenyl porphyrins in aqueous solution. Chem. Phys. Lett. 361 (2002) 152-158.(32) I. Sylvain, R. Zerrouki, R. Granet, Y.M. Huang, J.-F. Lagorce, M. Guilloton, J.-C. Blais, P. Krausz, Synthesis and Biological Evaluation of Thioglycosylated Porphyrins for an Application in Photodynamic Therapy. Bioorg.

Chem. 10 (2002) 57-69.

(33) A.M.G. Silver, A.C. Tomé, M.G.P.M.S. Neves, A.M.S. Silva, J.A.S. Cavaleiro, D. Perrone, Porphyrins in 1,3-dipolar cycloaddition reactions with sugar nitrones. Synthesis of glycoconjugated isoxazolidine-fused chlorins and bacteriochlorins. Tetrahedron Lett. 43 (2002) 603-605.

(34) S. Tamaru, S. Uchino, M. Takeuchi, M. Ikeda, T. Hatano, S. Shinkai, A porphyrin-based gelator assembly which is reinforced by periphyral urea groups and chirally twisted by chiral urea additives. Tetrahedron Lett. 43 (2002) 3751-3755.

(35) M.-H. Teiten, P. Even, P. Burgos, C. Frochot, S. Aubert, M.-C. Carre, L. Bolotine, J.-L. Merlin, F. Guillemin, M.-I. Viriot, Specific fluorescent tracers. Imaging and applications for photpdynamic therapy. C. R. Biologies. 325 (2002) 487-493.

(36) M. Egyeki, G. Turóczy, Zs. Majer, K. Tóth, A. Fekete, Ph. Maillard, Photosnesitized inactivation of T7 phage as surrogate of non-enveloped DNA viruse: efficiency and mechanism of action. Biochem. Biophys. Acta. 1624 (2003) 115-124.

(37) I. Laville, T. Figueiredo, B. Loock, S. Pigaglio, Ph. Maillard, D.S. Grierson, D. Carrez, A. Croisy, J. Blais, Synthesis, Cellular Internalization and Photodynamic Activity of Glycoconjugated Derivatives of tri and Tetra(*meta*-hydroxyphenyl)chlorins. Bioorg. Med. Chem. 11 (2003) 1643-1652.

(38) I. Laville, S. Pigaglio, J.-C. Blais, B. Loock, Ph. Maillard, D.S. Grierson, J. Blais, A study of the stability of tri(glucosyloxyphenyl)chlorin, a sensitizer for photodynamic therapy, in human colon tumoural cells: a liquid chromatography and MALDI-TOF mass spectrometry analysis. Bioorg. Med. Chem. 12 (2004) 3673-3682.

Chapter 2

Synthesis of Glycoconjugated Porphyrins

2-1. Introduction

meso-tetraphenylporphyrin (TPP) is synthesized by condensation between pyrrole and benzaldehyde using Rothemund-Adler method [1-3] or Lindsey method [1-3]. The Rothemund-Adler method uses a relatively small volume of solvents (propionic acid) and short reaction time. However this method requires harsh condition (high temperature over 150 °C) and affords quite low yield (less than 20 %). In the Lindsey method, on the other hand, the reaction condition is quite mild and yield is relatively high (over 45 %). Glycoconjugated porphyrins have been synthesized generally from glycosylated benzaldehyde with pyrrole by means of the Lindsey method [4-9]. The Lindsey method affords relatively low yield in the condensation of *m*-substituted glucosylated benzaldehyde and pyrrole [4,6], presumably because of steric hindrance of the sugar moiety. Metal ions are frequently used as a "template" for hardly constructed molecules such as phthalocyanine [10]. This chapter describes a Zn^{2+} ion-templated condensation to the synthesis of glycoconjugated porphyrins. The resulting zinc porphyrins readily afford the corresponding free-base porphyrins in moderate yield upon treatment with HCl, even in the case of 5,10,15,20-tetrakis[3-(2,3,4,6-tetra-*O*-acetyl-β-D-glucopyranosyloxy)phenyl]porphyrin. The versatility of this method for the synthesis of *para*- and *meta*-substituted glycoconjugated porphyrins was examined with D-glucose, D-galactose, D-xylose and D-arabinose. All of photosensitizers have been characterized by ^1H and ^{13}C NMR, electronic absorption, IR, ESI-TOF and FAB mass spectra.

2-2. Results and Discussions

2-2-1. Synthesis of glycoconjugated porphyrins

The glycoconjugated benzaldehydes **4** were prepared according to the literature (Scheme 2-1) [7,11]. The peracetylated 1-bromoglycopyranosides **3a** and **3d** were prepared from sugar **1a** and **1d**, respectively, and acetyl bromide with 56 % and 82 % yields. On the other hand, the peracetylated 1-bromoglycopyranosides **3b** and **3c** were prepared from peracetylated sugar **2b** and **2c**, respectively, and HBr with 83 % and 87 % yields. The glycoconjugated benzaldehydes **4** were prepared from *p*- or *m*-hydroxybenzaldehyde and peracetylated 1-bromoglycopyranosides **3** according to the Halazys or Knorrs methods in ca. 50 % yield. Glycoconjugated porphyrins **5** were synthesized as shown in Scheme 2-2. The condensations of **4** with pyrrole were conducted using $BF_3{\cdot}OEt_2$ in the presence of $Zn(OAc)_2{\cdot}2H_2O$. After addition of $BF_3{\cdot}OEt_2$ to initiate the condensation, the reaction mixture slowly became pale red, indicating chelation with Zn^{2+} ion. This suppressed the formation of polymeric by-products (e.g.,

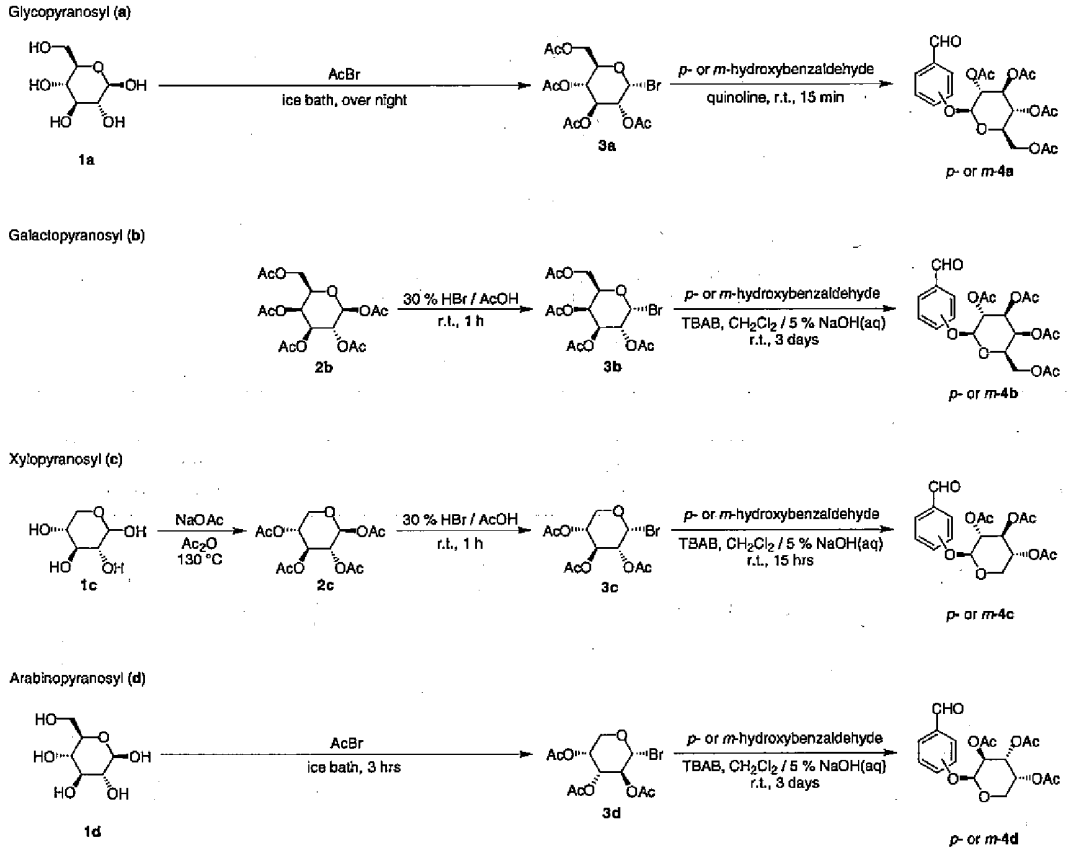
Glycopyranosyl (a)
AcBr
ice bath, over night
p- or m-hydroxybenzaldehyde
quinoline, r.t., 15 min
1a
3a
p- or m-4a
Galactopyranosyl (b)
30 % HBr / AcOH
r.t., 1 h
p- or m-hydroxybenzaldehyde
TBAB, CH2Cl2 / 5 % NaOH(aq)
r.t., 3 days
2b
3b
p- or m-4b
Xylopyranosyl (c)
NaOAc
Ac2O
130 °C
30 % HBr / AcOH
r.t., 1 h
p- or m-hydroxybenzaldehyde
TBAB, CH2Cl2 / 5 % NaOH(aq)
r.t., 15 hrs
1c
2c
3c
p- or m-4c
Arabinopyranosyl (d)
AcBr
ice bath, 3 hrs
p- or m-hydroxybenzaldehyde
TBAB, CH2Cl2 / 5 % NaOH(aq)
r.t., 3 days
1d
3d
p- or m-4d

Scheme 2-1

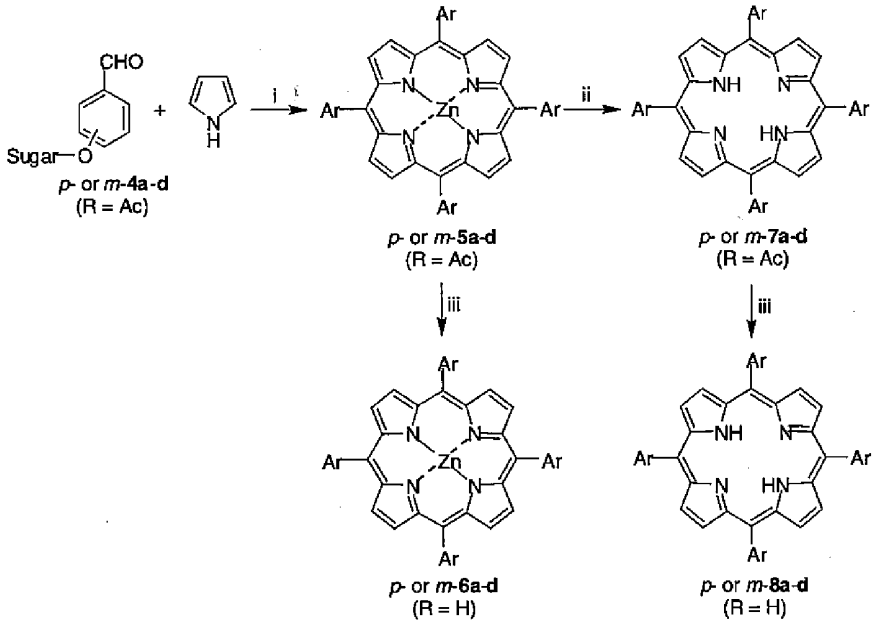

Reagents and Conditions: i) $BF_3{\cdot}OEt_2$, $Zn(OAc)_2{\cdot}H_2O$,$CHCl_3$, r.t., 24 h; then chloranil, reflux, 1 h. ii) 4 M HCl, $CHCl_3$. iii) NaOMe, THF (or $CHCl_3$ - MeOH)

(Ar)$_4$—porphyrin

Types of Glycopyranosyl Groups	Substitution Position: *para*-Substituted (denoted as *p*-)	Substitution Position: *meta*-Substituted (denoted as *m*-)
a: D-glucose R = Ac for **4**, **5** and **7** R = H for **6** and **8**	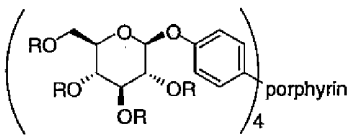	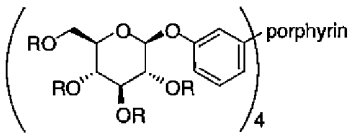
b: D-galactose R = Ac for **4**, **5** and **7** R = H for **6** and **8**	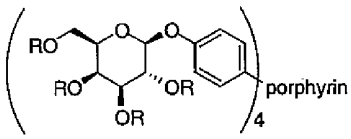	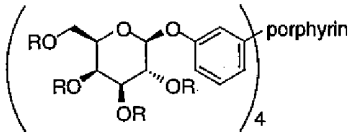
c: D-xylose R = Ac for **4**, **5** and **7** R = H for **6** and **8**	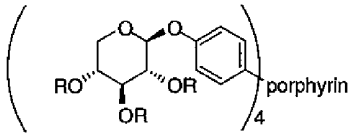	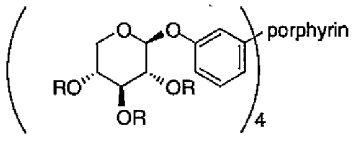
d: D-arabinose R = Ac for **4**, **5** and **7** R = H for **6** and **8**	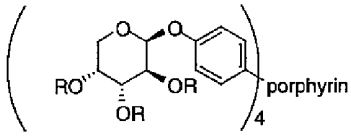	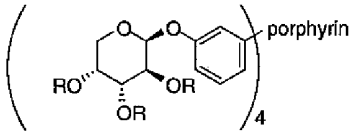

Scheme 2-2

oligopyrroles) at the porphyrinogen formation stage. The oxidation of the porphyrinogen with *p*-chloranil gave zinc porphyrins **5** in 53 ~ 93 % yield. The yield of zinc porphyrin **5** depends on the amount of zinc acetate used. In order to synthesize the zinc porphyrin **5**, hence, the large excess amount of zinc acetate was used to suppress the formation of free-base porphyrin. The detailed condition on the synthesis of the glycoconjugated porphyrin **5** was slightly depends on the glycoconjugated benzaldehyde used. The amount of BF_3·OEt_2 and *p*-chloranil was determined by repeating trial. The Zn^{2+} ion in **5** was easily removed by washing with 4 M HCl to give the free-base porphyrins **7** in 36 ~ 86 % yield (Table 2-1). For the synthesis of porphyrins **7**, however, the excess amount of zinc acetate reduced the overall yield, probably due to the careful purification. Porphyrins **7** were easily obtained by demetalation with 4 M HCl. The Zn^{2+} ion template strategy improved the yield about 3-fold in the case of 5,10,15,20-tetrakis[3-(2,3,4,6-tetra-*O*-acetyl-β-D-glucopyranosyloxy)phenyl]porphyrin [4,6] using modified Lindsey method in spite of the additional step. Deprotection of **5** and **7** was carried out using NaOMe in THF or in a mixture of MeOH and CH_2Cl_2 [4-9]. Eventually, 16 deacetylated glycoconjugated porphyrins **6** and **8** were obtained in moderate yield. All glycoconjugated porphyrins were confirmed by ^1H and ^{13}C NMR, ESI-TOF and FAB mass, IR, and electronic absorption spectroscopy. The purity of all photosensitizers was >95 % as evaluated by HPLC using an octadecylsilyl-supported silica gel column.

Table 2-1 Synthesis of glycoconjugated tetraphenylporphyrins **7**

	yield / %			yield / %	
	BF_3·OEt_2	BF_3·OEt_2 / Zn^{2+}		BF_3·OEt_2	BF_3·OEt_2 / Zn^{2+}
p-**7a**	53.2[a]	64	*p*-**7c**	-	64
m-**7a**	26.0[a]	68	*m*-**7c**	-	86
p-**7b**	20[b]	62	*p*-**7d**	-	36
m-**7b**	-	57	*m*-**7d**	-	37

[a] Kobata et. al. *Bull. Chem. Soc. Jpn.* **1994**, *67*, 668-679. [b] Oulmi et. al. *J. Org. Chem.* **1995**, *60*, 1554-1564.

2-2-2. Electronic absorption spectra of glycoconjugated porphyrins

The absorption of longer wavelength light is one of the important performances for PDT drugs. The electronic absorption spectra of glycoconjugated porphyrins were recorded in DMSO (Figure 2-1). The maximum absorption wavelength (λ_{max}) and molar extinction coefficient (ε) are listed in Table 2-2 and 2-3. The free-base porphyrins **7** and **8** have a strong Soret band (sometimes called as a B band) at ca. 420 nm and four weak Q bands at ca. 520 nm (Q_{IV}), 550 (Q_{III}), 600 (Q_{II}), and 650 nm (Q_I) with etioporphyrin-like shape [1,4,6,8,12-14] owing to the D_{2h} symmetry. The zinc porphyrins **5** and **6** show the electronic absorption spectra of typical metalloporphyrins, i.e., a strong Soret band at ca. 430 nm and two weak Q bands at ca. 560 nm (Q_{II}) and 600 nm (Q_I) owing to the D_{4h} symmetry [12-14]. Both Soret and Q bands of *meta*-substituted porphyrins shifted toward shorter wavelength (i.e., blue shift) than those of *para*-substituted porphyrins. And, both Soret bands of zinc porphyrins shifted longer wavelength (i.e., red shift) than one of free-base porphyrins. Electronic absorption spectra measured in DMSO did not depend on the sugar unit attached. The Q_I band (630 nm) of porphyrin derivatives is known to be useful for the PDT treatment because of its skin cell permeability [1,4,14].

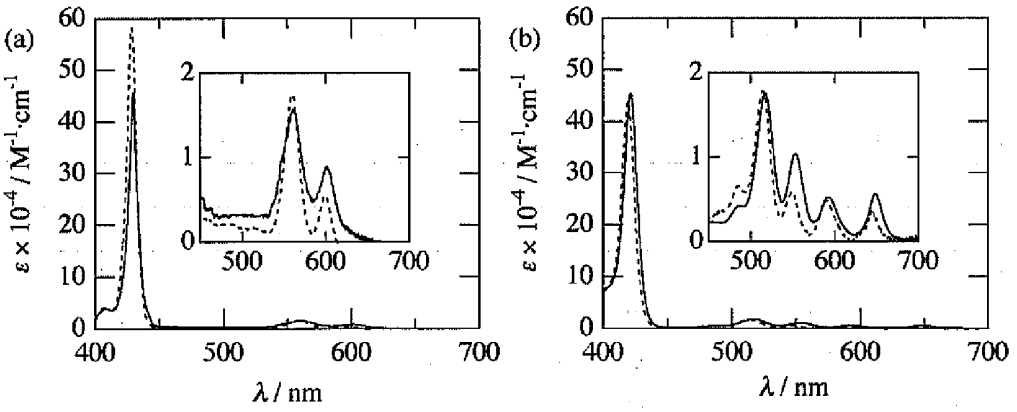

Figure 2-1 Electronic absorption spectra of *p*-**5a** (solid line) and *m*-**5a** (broken line) (a), *p*-**7a** (solid line) and *m*-**7a** (broken line) (b) in $CDCl_3$.

Table 2-2 Electronic absorption spectral data of **7** and **8**

	λ_{max} / nm ($\varepsilon \times 10^{-4}$ / $M^{-1} \cdot cm^{-1}$)				
	Soret Band	Q Bands			
		IV	III	II	I
p-**7a**	421 (45.4)	517 (1.75)	552 (1.03)	591 (0.53)	648 (0.56)
p-**8a**	423 (46.2)	518 (1.74)	555 (1.17)	594 (0.54)	647 (0.67)
m-**7a**	419 (44.0)	513 (1.79)	547 (0.59)	587 (0.49)	643 (0.37)
m-**8a**	420 (40.0)	514 (2.05)	548 (0.96)	589 (0.76)	644 (0.54)
p-**7b**	421 (40.8)	517 (1.59)	553 (0.97)	593 (0.49)	648 (0.52)
p-**8b**	421 (45.2)	517 (1.75)	553 (1.18)	593 (0.56)	649 (0.65)
m-**7b**	419 (38.0)	513 (1.67)	548 (0.68)	589 (0.54)	646 (0.39)
m-**8b**	420 (44.1)	515 (1.81)	548 (0.68)	589 (0.55)	645 (0.43)
p-**7c**	422 (47.0)	517 (1.61)	555 (0.87)	593 (0.36)	648 (0.43)
p-**8c**	422 (46.1)	517 (1.61)	555 (0.88)	593 (0.87)	648 (0.44)
m-**7c**	419 (41.1)	513 (1.61)	553 (0.39)	589 (0.40)	643 (0.29)
m-**8c**	419 (37.9)	513 (1.51)	553 (0.38)	589 (0.41)	643 (0.30)
p-**7d**	422 (47.0)	517 (1.67)	555 (0.93)	594 (0.43)	648 (0.50)
p-**8d**	421 (46.2)	517 (1.58)	555 (0.85)	594 (0.34)	648 (0.41)
m-**7d**	419 (37.9)	514 (1.55)	550 (0.57)	589 (0.42)	646 (0.27)
m-**8d**	419 (44.1)	515 (1.80)	550 (0.71)	589 (0.55)	645 (0.41)

Table 2-3 Electronic absorption spectral data of **5** and **6**

	λ_{max} / nm ($\varepsilon \times 10^{-4}$ / $M^{-1} \cdot cm^{-1}$)		
	Soret Bands	Q Bands	
		II	I
p-**5a**	430 (45.6)	561 (1.56)	602 (0.90)
p-**6a**	430 (52.1)	562 (1.54)	603 (1.04)
m-**5a**	428 (58.4)	560 (1.76)	599 (0.57)
m-**6a**	429 (50.3)	560 (1.46)	600 (0.53)
p-**5b**	430 (58.7)	563 (1.87)	602 (1.14)
p-**6b**	431 (54.1)	559 (1.73)	602 (1.17)
m-**5b**	428 (36.3)	559 (1.43)	598 (0.59)
m-**6b**	428 (40.1)	561 (1.49)	599 (0.59)
p-**5c**	430 (45.5)	561 (1.41)	601 (0.75)
p-**6c**	431 (42.9)	562 (1.18)	601 (0.76)
m-**5c**	428 (40.9)	560 (1.30)	600 (0.45)
m-**6c**	429 (42.5)	560 (1.19)	600 (0.39)
p-**5d**	430 (58.7)	560 (1.80)	604 (1.02)
p-**6d**	431 (54.0)	561 (1.57)	604 (1.07)
m-**5d**	428 (40.8)	559 (1.42)	598 (0.50)
m-**6d**	429 (40.7)	559 (1.26)	598 (0.34)

2-2-3. NMR spectra of glycoconjugated porphyrins

Figure 2-2 shows the representative ^{1}H NMR spectra of zinc(II) 5,10,15,20-tetrakis[4-(2,3,4,6-tetra-*O*-acetyl-β-D-arabinopyranosyloxy)phenyl]porphyrin (*p*-**5d**), zinc(II) 5,10,15,20-tetrakis[4-(β-D-arabinopyranosyloxy)phenyl]porphyrin (*p*-**6d**), 5,10,15,20-tetrakis[4-(2,3,4,6-tetra-*O*-acetyl-β-D-arabinopyranosyloxy)phenyl]porphyrin (*p*-**7d**) and 5,10,15,20-tetrakis[4-(β-D-arabinopyranosyloxy)-phenyl]porphyrin (*p*-**8d**). All photosensitizers were fully assigned using 2D NMR technique (COSY and HMQC). The peak due to β-pyrrole proton are found around 8.9 ppm for all glycoconjugated porphyrins. The peaks attributable to the phenyl protons are ranged from 8.1 to 7.0 ppm. After demetalation, the characteristic peak attributable to the inner proton appears at ca. -2.9 ppm for free-base compound *p*-**7d** and *p*-**8d**. Figure 2-3 shows the ^{13}C NMR spectra of *p*-**5d**, *p*-**6d**, *p*-**7d** and *p*-**8d**. In the ^{13}C NMR spectra of all porphyrins, the characteristic peaks for porphyrin ring were found at 150.47, 132.06 and 120.46 ppm which can be assigned to α position, β-pyrrole and *meso* positions, respectively. In the case of *m*-**5** and *m*-**7**, HMQC spectra indicated that the peaks owing to acetyl groups were divided into two regions, i.e., 2.1 ~ 2.0 ppm and 1.5 ~ 1.3 ppm (Figure 2-4) [6]. This is plausibly caused by atropisomeric forms of *meta*-substituted porphyrins. All glycoconjugated porphyrins were fairly caracterized by ^{1}H and ^{13}C NMR spectroscopy.

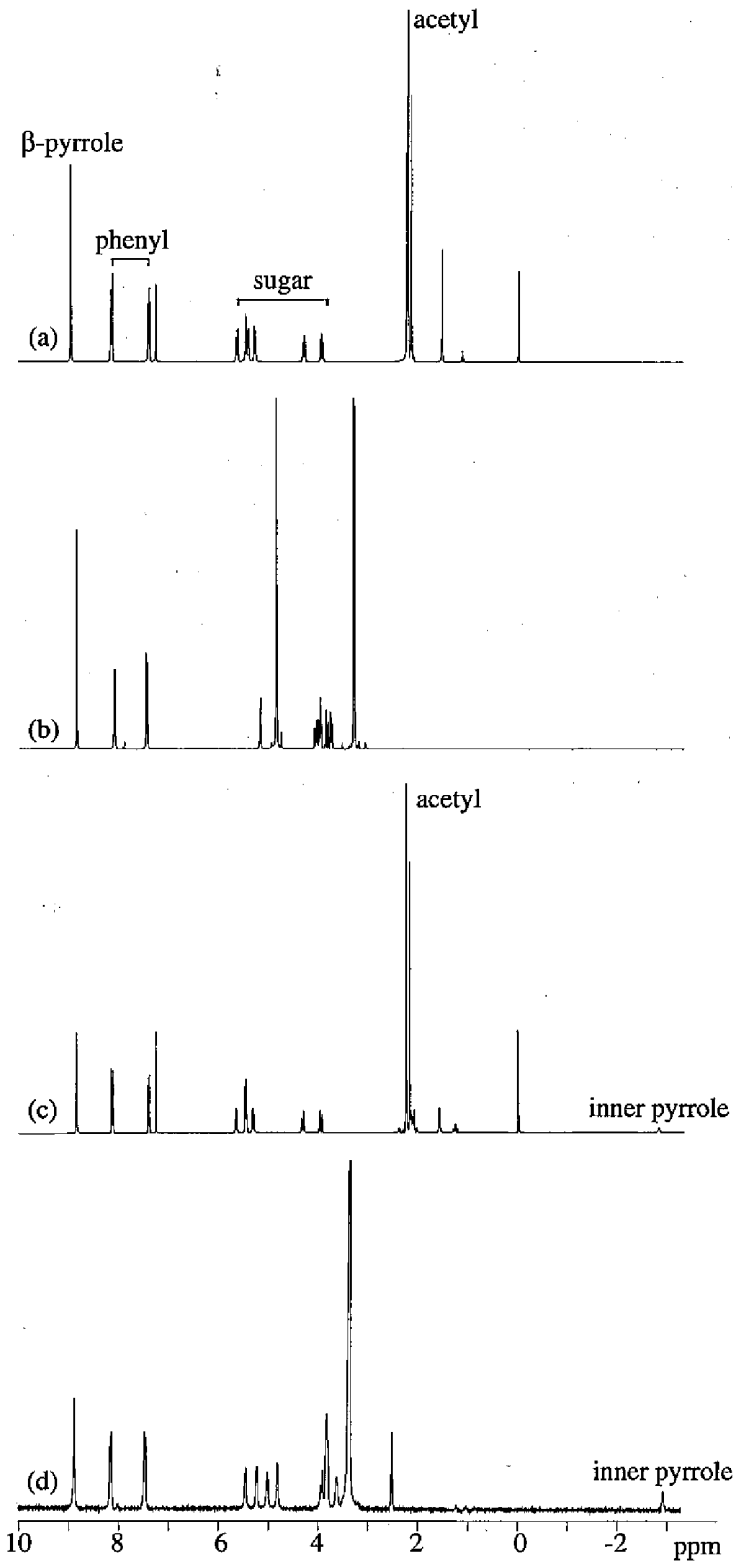

Figure 2-2 ^{1}H NMR spectra of *p*-**5d** (a) and *p*-**7d** (c) in $CDCl_3$ and *p*-**6d** (b) and *p*-**8d** (d) in DMSO-d_6.

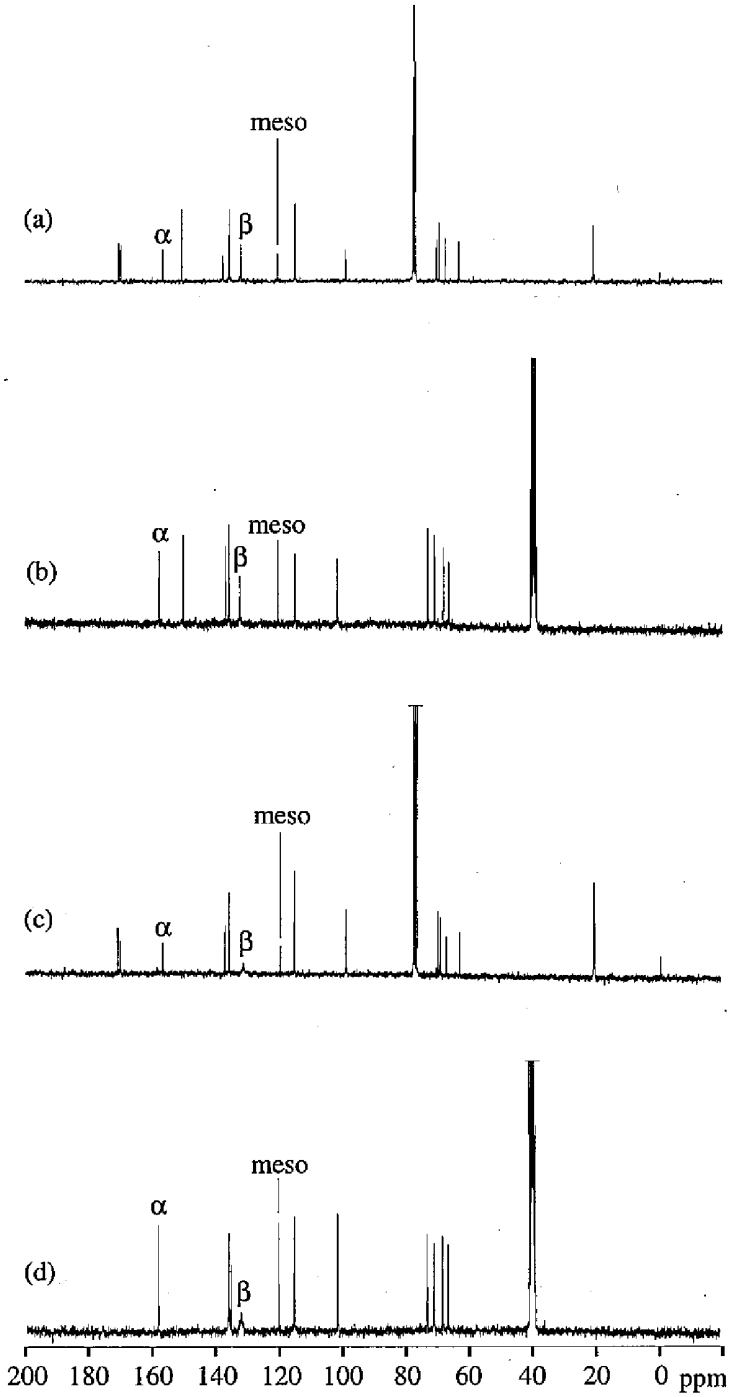

Figure 2-3 ^{13}C NMR spectra of *p*-**5d** (a) and *p*-**7d** (c) in $CDCl_3$ and *p*-**6d** (b) and *p*-**8d** (d) in DMSO-d_6.

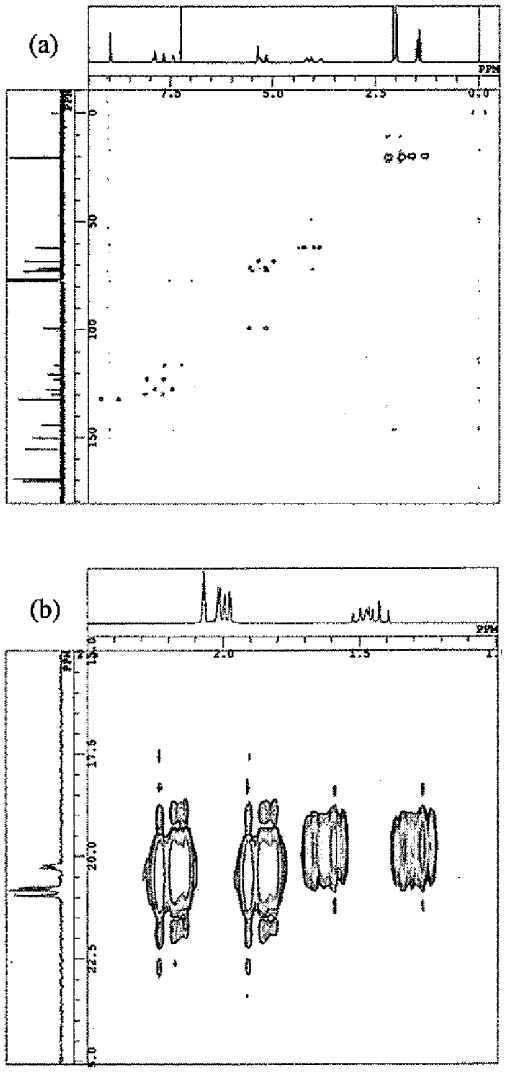

Figure 2-4 HMQC spectrum of *m*-**5a** in $CDCl_3$ (a) and its expanded spectrum (b)

2-2-4. ESI-TOF mass spectra of glycoconjugated porphyrins (p-8a and p-8c)

Figure 2-5 shows the electron-spray ionization time-of-flight (ESI-TOF) mass spectroscopy of *p*-**8a** and *p*-**8c** in MeOH. In ESI-TOF mass, porphyrins **8** were detected as $[M+Na]^+$ species in the positive mode. The results obtained by this measurement agree closely with calculated isotope pattern.

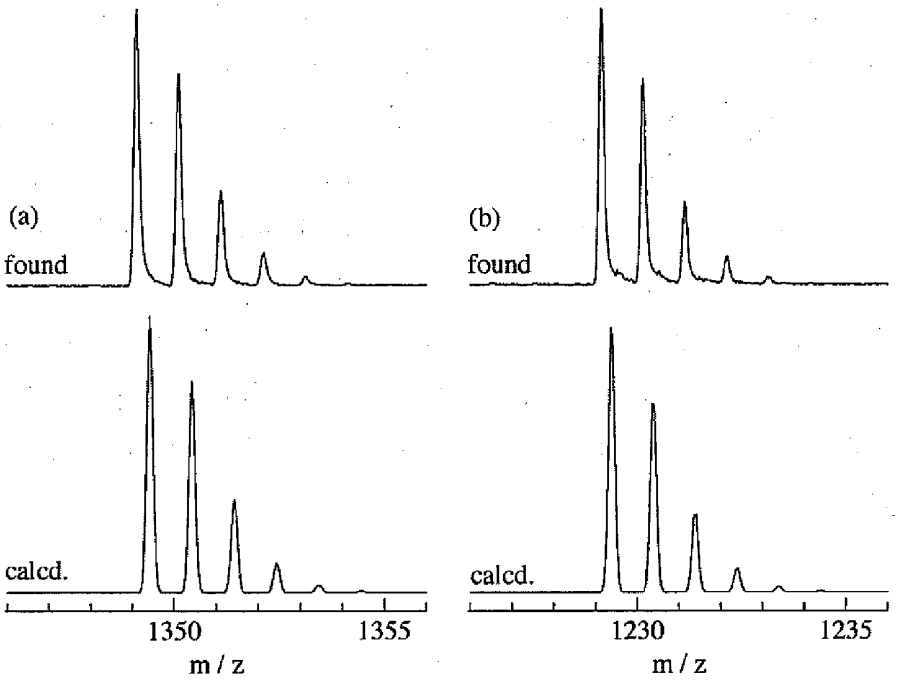

Figure 2-5 ESI-TOF mass spectra of *p*-**8a** (a) and *p*-**8c**. $[M+Na]^+$ species were found.

2-2-5. IR spectra of glycoconjugated porphyrins

The infra-red absorption spectra of glycoconjugated porphyrins were recorded using ATR instrument (Figure 2-6). The band assignments and wavenumbers (cm^{-1}) are listed in Table 2-4, 2-5, 2-6, 2-7, 2-8, 2-9, 2-10 and 2-11. All porphyrins show absorption in the regions from 3000 to 2900 cm^{-1} due to C-H stretch in the phenyl ring ($\nu_{C\text{-}H}$) and the pyrrole ring β-carbon ($\nu_{Cp\text{-}H}$) (Figure 2-6) [14-16]. In addition, the characteristic absorption for tetraphenylporphyrin was found at 666.5 cm^{-1} due to out-of-plane C-H bending in the phenyl ring ($op\delta_{C\text{-}H}$) for all glycoconjugated porphyrins [14-16]. All *para*-substituted porphyrins show one peak around 1600 cm^{-1} due to C=C stretch ($\nu_{C=C}$) and C=N stretch ($\nu_{C=N}$) in the porphyrin ring (Figure 2-6a, b and d) [14-16]. On the other hand, the top of this peak was splitted in all *meta*-substituted porphyrins. (Figure 2-6c). This may reflect that the porphyrin ring is distorted in the *meta*-substituted porphyrins. In the case of acetylated photosensitizers, all zinc porphyrins **5** and all free-base porphyrins **7** show absorption around 1490 cm^{-1} and 1470 cm^{-1}, respectively, due to asymmetric CH_3 bending (δ_{as},CH_3) in the acetyl groups (Figure 2-6a and b) [14-16]. In addition, all zinc porphyrins **5** and free-base porphyrins **7** show absorption around 1750 cm^{-1} and 1370 cm^{-1} due to symmetric CH_3 scissoring ($\nu_{C=O}$) and C-O-CH_3 stretching ($\nu_{C\text{-}O\text{-}CH3}$), respectively (Figure 2-6a-c) [14-16]. After deprotection, the absorption band attributable to the acetyl group disappeared completely, and then huge absorption due to O-H stretch (ν_{OH}) of alcohol groups emerges around 3380 cm^{-1} for all deacetylated porphyrins **6** and **8** (Figure 2-6d) [14-16].

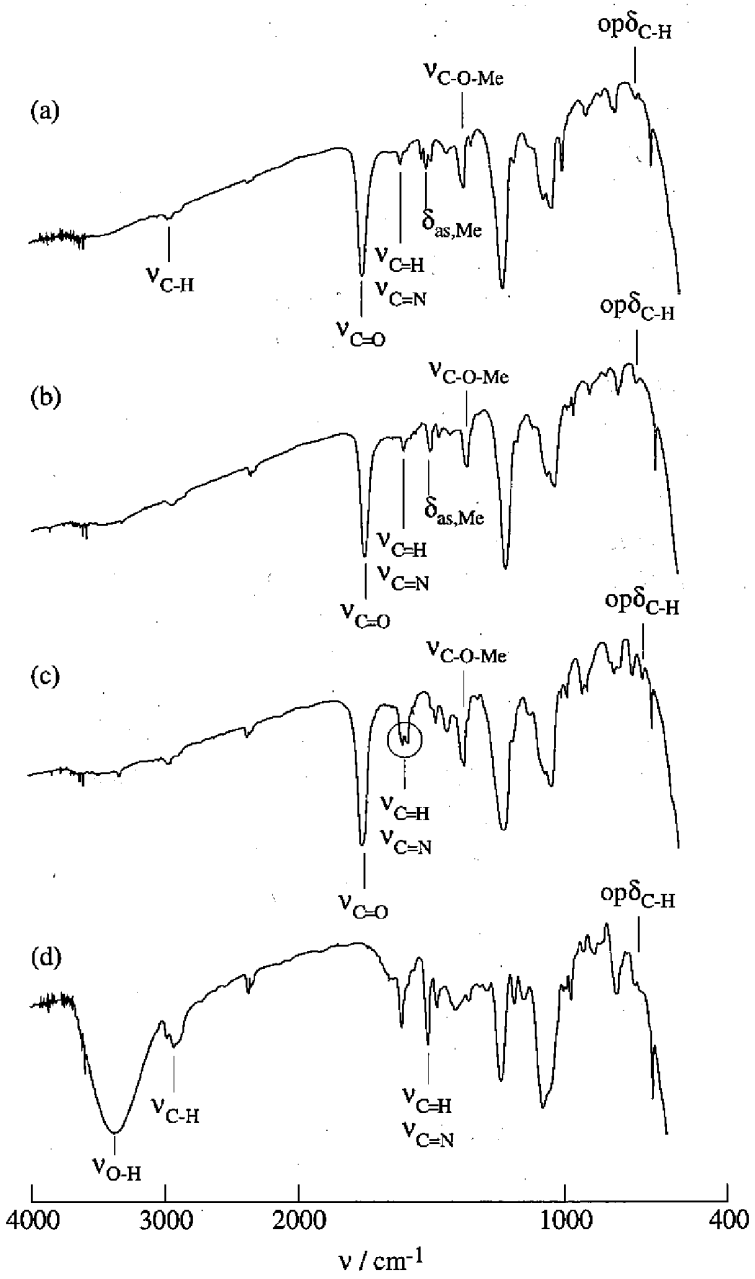

Figure 2-6 IR spectra of *p*-**5a** (a), *p*-**7a** (b), *m*-**7a** (c) and *p*-**8a** (d).

Table 2-4 IR spectral data of *p*-**5**[a]

assignment[b]	*p*-5a	*p*-5b	*p*-5c	*p*-5d	assignment[c]
ν_{NH}	3800 ~ 3300	3800 ~ 3300	3800 ~ 3300	3800 ~ 3300	ν_{NH}
$\nu_{a,C-H}$			3036.33		ν_{C-H}
	2959.16	2982.32	2939.87	2923.48	
	2934.09	2932.16			
$\nu_{s,C-H}$	2844.38	2864.64	2862.71	2850.17	
	2279.17		2338.97		
$\nu_{C=O}$	1755.44	1751.58	1755.44	1747.72	
$\nu_{C=C}$	1604.97	1605.93	1605.93	1605.93	$\nu_{C=C},\nu_{C=N}$
$\nu_{C=N}$	1523.95	1523.95	1524.91	1524.91	
	1508.52	1507.55	1507.55	1506.59	
$\delta_{as,CH3}$	1491.16	1491.16	1491.16	1493.09	
$\nu_{C=C},\nu_{C=N}$		1429.43	1430.39	1429.43	$\nu_{C=N},\delta_{CCN}$
$\delta_{s,CH3}$	1368.66	1369.63	1370.59	1371.55	$\nu_{C=C},\delta_{Cp-H}$
	1339.73	1339.73	1339.73	1339.73	δ_{Cp-H}
$\nu_{C-O-CH3}$	1224.95	1224.95	1224.95	1223.98	
$\nu_{C-O-CH3}$		1179.61	1178.65	1169.00	
		1125.60	1121.74		
$ip\delta_{CH}$	1068.69	1077.37	1071.59	1087.98	
	1038.79		1039.76	1047.47	$\delta_{Cp-H},\nu_{C=C}$
Ring deform.	997.32	997.32	996.35	996.35	ν_{C-C},ν_{C-C}
		954.88			
	907.62	916.30	905.69		
$op\delta_{CH(Au)}$			876.75		πCH
		853.60	853.60		πCH
		810.20	810.20		
	798.63	799.59	798.63	798.63	
$\pi_{(ring)}$		734.97	734.97	735.93	
			700.25		
	666.49	666.49	666.49	666.49	
			598.97		
	425.36	425.36		425.36	
			413.78		
	406.07				

[a] ATR method. [b] Empirical assignment from Caughey et al [16]. The abbreviations are as follows: ip, in plane; op, out of plane; a, asymmetric; s, symmetric; p, pyrrole β-carbon (Cp). [c] Assignments are made from normal coordinate analysis of 18 E_u bands [16].

Table 2-5 IR spectral data of *m*-5[a]

assignment[b]	*m*-5a	*m*-5b	*m*-5c	*m*-5d	assignment[c]
ν_{NH}	3800 ~ 3300	3800 ~ 3300	3800 ~ 3300	3800 ~ 3300	ν_{NH}
$\nu_{a,C-H}$	2927.33	2926.37	2923.48	2922.51	ν_{C-H}
	2848.24	2848.24	2850.17	2848.24	
$\nu_{s,C-H}$	2364.05				
$\nu_{C=O}$	1756.40	1751.58	1752.54	1747.72	
$\nu_{C=C}$	1600.15	1600.15	1605.93	1600.15	$\nu_{C=C}$,$\nu_{C=N}$
		1583.75			
			1502.73		
$\delta_{as,CH3}$	1479.58	1480.55	1473.80	1479.58	
$\nu_{C=C}$,$\nu_{C=N}$	1431.36	1432.32		1432.32	$\nu_{C=N}$,δ_{CCN}
$\delta_{s,CH3}$	1368.66	1370.59	1370.59	1371.55	$\nu_{C=C}$,δ_{Cp-H}
	1338.76	1337.80			δ_{Cp-H}
$\nu_{C-O-CH3}$	1223.98	1221.09	1223.98	1221.09	
$\nu_{C-O-CH3}$		1160.32			
		1124.64			
ipδ_{CH}	1041.69	1077.37	1071.59	1087.98	
			1041.69	1048.44	δ_{Cp-H},$\nu_{C=C}$
Ring deform.	1001.18	1001.18			ν_{C-C},ν_{C-C}
		954.88			
	935.59	935.59	967.42	937.52	
op$\delta_{CH(Au)}$			877.72		πCH
	820.81	819.85		819.85	πCH
	796.70	795.73	802.49	795.73	
$\pi_{(ring)}$		735.93	734.97		
		721.46		721.46	
		702.17	666.49	666.49	
	666.49	666.49			
		417.97	413.78		

[a] ATR method. [b] Empirical assignment from Caughey et al [16]. The abbreviations are as follows: ip, in plane; op, out of plane; a, asymmetric; s, symmetric; p, pyrrole β-carbon (Cp). [c] Assignments are made from normal coordinate analysis of 18 E_u bands [16].

Table 2-6 IR spectral data of *p*-**6**[a]

assignment[b]	*p*-**6a**	*p*-**6b**	*p*-**6c**	*p*-**6d**	assignment[c]
ν_{OH}	3363.30	3383.21	3387.41	3382.59	ν_{OH}
$\nu_{a,C-H}$				2965.92	ν_{C-H}
	2924.44	2923.48	2924.07	2916.72	
$\nu_{s,C-H}$	2847.28				
	2363.09		2359.23	2364.05	
			2341.87		
$\nu_{C=C}$	1604.97	1604.01	1604.97	1604.97	$\nu_{C=C}$,$\nu_{C=N}$
$\nu_{C=N}$			1522.99	1522.99	
	1507.55	1505.62	1504.66	1505.62	
$\nu_{C=C}$,$\nu_{C=N}$	1406.28	1401.46	1400.49	1400.49	$\nu_{C=N}$,δ_{CCN}
		1338.76	1339.73	1338.76	δ_{Cp-H}
	1227.84	1227.84	1226.88	1226.88	
		1178.65	1177.69	1177.69	
ν_{C-O}		1142.00			
ipδ_{CH}	1072.55	1074.48		1071.59	
			1039.76	1047.47	δ_{Cp-H},$\nu_{C=C}$
Ring deform.	997.32	996.35	998.28	998.28	ν_{C-C},ν_{C-C}
				949.09	
				913.41	
op$\delta_{CH(Au)}$		889.29	895.08		πCH
				870.97	πCH
	796.70	797.66	796.70	795.73	
$\pi_{(ring)}$				772.58	
				718.57	
	666.49	666.49	666.49	666.49	
	425.36	429.21	425.36	421.50	
	413.78		413.78	413.78	
		409.92			

[a] ATR method. [b] Empirical assignment from Caughey et al [16]. The abbreviations are as follows: ip, in plane; op, out of plane; a, asymmetric; s, symmetric; p, pyrrole β-carbon (Cp). [c] Assignments are made from normal coordinate analysis of 18 E_u bands [16].

Table 2-7 IR spectral data of *m*-**6**[a]

assignment[b]	*m*-**6a**	*m*-**6b**	*m*-**6c**	*m*-**6d**	assignment[c]
ν_{OH}	3380.66	3398.02	3365.23	3320.86	ν_{OH}
$\nu_{a,C-H}$	2924.80	2923.48	2917.69	2912.87	ν_{C-H}
$\nu_{s,C-H}$	2846.31	2846.31	2844.38		
		2370.80	2362.12	2364.05	
				2340.90	
$\nu_{C=C}$	1599.18	1602.08	1600.15	1598.22	$\nu_{C=C}$,$\nu_{C=N}$
$\nu_{C=N}$			1580.86		
δ_{N-H}	1468.97		1477.65	1469.94	
$\nu_{C=C}$,$\nu_{C=N}$	1425.57	1439.07	1422.67	1425.57	$\nu_{C=N}$,δ_{CCN}
	1353.23	1339.73	1336.83	1349.37	δ_{Cp-H}
			1251.95		
			1181.54	1165.15	
				1425.57	
				1349.37	
ν_{C-O}				1165.15	
ipδ_{CH}	1071.59	1073.52		1073.52	
			1039.76	1044.58	δ_{Cp-H},$\nu_{C=C}$
Ring deform.	919.19		999.25		ν_{C-C},ν_{C-C}
			931.73	922.09	
op$\delta_{CH(Au)}$			892.19		πCH
			820.81	877.72	πCH
	795.73	794.77	795.73	797.66	
$\pi_{(ring)}$			720.50		
	666.49	666.49	666.49	666.49	
	421.50	425.36	425.36	428.25	
	413.78			409.92	
		406.07	406.07		

[a] ATR method. [b] Empirical assignment from Caughey et al [16]. The abbreviations are as follows: ip, in plane; op, out of plane; a, asymmetric; s, symmetric; p, pyrrole β-carbon (Cp). [c] Assignments are made from normal coordinate analysis of 18 E_u bands [16].

Table 2-8 IR spectral data of *p*-7[a]

assignment[b]	*p*-7a	*p*-7b	*p*-7c	*p*-7d	assignment[c]
ν_{NH}	3800 ~ 3300	3800 ~ 3300	3800 ~ 3300	3800 ~ 3300	ν_{NH}
$\nu_{a,C-H}$		3037.29			ν_{C-H}
	2959.16	2982.31	2925.41	2923.48	
	2866.57	2868.50	2850.17	2847.28	
$\nu_{s,C-H}$		2706.46			
		2535.74			
		2522.23			
	2347.65	2350.55	2363.09	2351.51	
		2119.06			
$\nu_{C=O}$	1755.44	1755.44	1755.44	1748.68	
$\nu_{C=C}$	1605.93	1606.90	1605.93	1605.93	$\nu_{C=C}$,$\nu_{C=N}$
		1580.60			
		1558.67			
δ_{N-H}	1507.55	1506.59	1503.70	1505.62	
$\delta_{as,CH3}$	1473.80	1472.83	1473.80	1473.80	
$\nu_{C=C}$,$\nu_{C=N}$		1429.43			$\nu_{C=N}$,δ_{CCN}
$\delta_{s,CH3}$	1368.66	1370.59	1370.59	1371.55	$\nu_{C=C}$,δ_{Cp-H}
	1226.88	1225.91	1223.98	1225.91	δ_{Cp-H}
$\nu_{C-O-CH3}$	1180.58	1179.61		1169.00	
$\nu_{C-O-CH3}$		1165.15			
		1125.69			
ipδ_{CH}	1068.69	1078.34	1071.59	1088.95	
	1039.76		1041.69	1048.44	δ_{Cp-H},$\nu_{C=C}$
				1025.29	
Ring deform.	982.85	993.46	992.50	993.46	ν_{C-C},ν_{C-C}
		982.85			
	967.42	967.42	967.42	966.45	
	907.62	916.30			
op$\delta_{CH(Au)}$		899.90	877.72	873.86	πCH
	847.82	847.82			πCH
	803.45	804.41	801.52	803.45	
$\pi_{(ring)}$	735.93	735.93	734.97	736.90	
	666.49	666.49	666.49	666.49	
	425.36	621.15	421.50		
	409.92		413.78		

[a] ATR method. [b] Empirical assignment from Caughey et al [16]. The abbreviations are as follows: ip, in plane; op, out of plane; a, asymmetric; s, symmetric; p, pyrrole β-carbon (Cp). [c] Assignments are made from normal coordinate analysis of 18 E_u bands [16].

Table 2-9 IR spectral data of *m*-7[a]

assignment[b]	*m*-7a	*m*-7b	*m*-7c	*m*-7d	assignment[c]
ν_{NH}	3800 ~ 300	3800 ~ 3300	3800 ~ 3300	3800 ~ 3300	ν_{NH}
$\nu_{a,C-H}$	2947.59	2937.94	2924.44	2921.55	ν_{C-H}
	2852.10	2860.78	2850.17	2852.10	
$\nu_{s,C-H}$	2360.19	2360.19	2346.69	2359.23	
		2339.94			
$\nu_{C=O}$	1758.33	1751.58	1756.40	1748.68	
$\nu_{C=C}$	1599.18	1599.18	1601.11	1600.15	$\nu_{C=C}$,$\nu_{C=N}$
			1577.96		
δ_{N-H}			1523.95		
			1479.58		
$\delta_{as,CH3}$	1473.80	1472.83		1468.01	
$\nu_{C=C}$,$\nu_{C=N}$	1431.36	1431.36	1432.32	1432.32	$\nu_{C=N}$,δ_{CCN}
$\delta_{s,CH3}$	1368.66	1369.63	1371.55	1371.55	$\nu_{C=C}$,δ_{Cp-H}
			1338.76		δ_{Cp-H}
$\nu_{C-O-CH3}$	1227.84	1220.12	1224.24	1220.12	
$\nu_{C-O-CH3}$		1160.32	1221.09		
		1125.60	1185.40		
ipδ_{CH}		1076.41	1071.59	1088.95	
	1041.69		1042.65	1049.40	δ_{Cp-H},$\nu_{C=C}$
Ring deform.		978.03	1002.14		ν_{C-C},ν_{C-C}
		954.84			
	920.16	923.05	935.59		
op$\delta_{CH(Au)}$			877.72		πCH
	802.49	815.99	821.78	801.51	πCH
			796.70		
$\pi_{(ring)}$	734.97	735.93	734.97		
			721.46	734.97	
		701.21	700.25	666.49	
	666.49	666.49	666.49		
		445.61			
		411.85	413.78		

[a] ATR method. [b] Empirical assignment from Caughey et al [16]. The abbreviations are as follows: ip, in plane; op, out of plane; a, asymmetric; s, symmetric; p, pyrrole β-carbon (Cp). [c] Assignments are made from normal coordinate analysis of 18 E_u bands [16].

Table 2-10 IR spectral data of *p*-**8**[a]

assignment[b]	*p*-**8a**	*p*-**8b**	*p*-**8c**	*p*-**8d**	assignment[c]
ν_{OH}	3379.70	3378.73	3382.59	3382.59	ν_{OH}
$\nu_{a,C-H}$				2968.81	ν_{C-H}
			2896.47	2915.76	
$\nu_{s,C-H}$	2889.72	2882.00			
	2360.19	2363.09	2360.19	2351.51	
$\nu_{C=C}$	1604.97	1604.01	1604.97	1604.97	$\nu_{C=C}$,$\nu_{C=N}$
δ_{N-H}	1502.73	1502.73	1503.70	1505.62	
δ_{N-H}	1473.80		1472.83	1471.87	
$\nu_{C=C}$,$\nu_{C=N}$	1400.49	1401.46	1407.24	1400.49	$\nu_{C=N}$,δ_{CCN}
				1398.56	
			1350.34	1348.41	δ_{Cp-H}
	1230.73	1229.77	1227.84	1226.88	
	1178.65		1177.69	1177.69	
ipδ_{CH}	1073.52	1073.52	1101.49	1070.62	
			1037.83		δ_{Cp-H},$\nu_{C=C}$
Ring deform.			992.50	1011.79	ν_{C-C},ν_{C-C}
	967.42	967.42	966.45	966.45	
				949.09	
op$\delta_{CH(Au)}$			896.04		πCH
			846.85	870.00	πCH
	796.70	795.73	796.70	795.73	
$\pi_{(ring)}$			730.15	771.62	
				729.18	
	666.49	666.49	666.49	666.49	
	429.21	429.21	425.36	425.36	
		413.78	413.78		
				409.92	
	403.17				

[a] ATR method. [b] Empirical assignment from Caughey et al [16]. The abbreviations are as follows: ip, in plane; op, out of plane; a, asymmetric; s, symmetric; p, pyrrole β-carbon (Cp). [c] Assignments are made from normal coordinate analysis of 18 E_u bands [16].

Table 2-11 IR spectral data of *m*-**8**[a]

assignment[b]	*m*-**8a**	*m*-**8b**	*m*-**8c**	*m*-**8d**	assignment[c]
ν_{OH}	3374.87	3382.59	3377.77	3383.55	ν_{OH}
$\nu_{a,C-H}$	2975.56			2914.80	ν_{C-H}
	2923.48		2915.76		
$\nu_{s,C-H}$		2878.14	2846.31		
			2359.23	2361.16	
$\nu_{C=C}$	1599.18	1601.11	1587.61	1597.25	$\nu_{C=C}$,$\nu_{C=N}$
$\nu_{C=N}$	1577.96				
δ_{N-H}	1478.62	1468.01	1473.80		
$\nu_{C=C}$,$\nu_{C=N}$	1425.57	1430.39	1427.50	1438.11	$\nu_{C=N}$,δ_{CCN}
	1336.83	1349.37	1349.37		δ_{Cp-H}
	1253.88	1242.31	1260.63		
			1235.56		
	1206.62		1205.66		
	1183.47	1178.65	1178.65		
ν_{C-O}	1155.50	1136.21	1100.52		
ipδ_{CH}	1070.62	1081.23	1038.79	1070.62	
			1039.76		δ_{Cp-H},$\nu_{C=C}$
Ring deform.	1001.18				ν_{C-C},ν_{C-C}
	951.02		919.19		
	932.70	917.26			
op$\delta_{CH(Au)}$	874.82				πCH
	819.85				πCH
	794.77	798.63			
	776.44		777.41		
$\pi_{(ring)}$	719.54		721.46		
	666.49	666.49	666.49	666.49	
	425.36	425.36	429.21	421.50	
			413.78	406.07	
	406.07	406.07			

[a] ATR method. [b] Empirical assignment from Caughey et al [16]. The abbreviations are as follows: ip, in plane; op, out of plane; a, asymmetric; s, symmetric; p, pyrrole β-carbon (Cp). [c] Assignments are made from normal coordinate analysis of 18 E_u bands [16].

2-3. Summary

Thirty-two glycoconjugated porphyrins were synthesized by a modification of Lindsey method in the presence of $Zn(OAc)_2 \cdot 2H_2O$ as a template, and fully characterized by ^1H and ^{13}C NMR, ESI-TOF and FAB mass, IR and electronic absorption spectroscopy. The Zn^{2+} ion temperate strategy improved the yield about 3-fold in the case of 5,10,15,20-tetrakis[3-(2,3,4,6-tetra-*O*-acetyl-β-D-glucopyranosyloxy)phenyl]porphyrin (*m*-**7a**). In addition, free-base porphyrins **7** were obtained almost quantitatively by demetaration of corresponding zinc porphyrin **5** precursor with 4 M HCl. This provides an efficient means to prepare wide variety of glycoconjugated porphyrins, which can be used as a precursor for glycoconjugated chlorins having similar structures to tetrakis(3-hydroxyphenyl)chlorin, i.e., Foscan®. In electronic absorption spectroscopy, the free-base porphyrins **7** and **8** have a strong Soret band at ca. 420 nm and four weak Q bands at ca. 520, 550, 600 and 650 nm with etioporphyrin-like shape. The zinc porphyrins **5** and **6** show the electronic absorption spectra of typical metalloporphyrins, i.e., a strong Soret band at ca. 430 nm and two weak Q bands at ca. 560 and 600 nm. The Q_1 band (about 630 nm) of porphyrin derivatives is known to be useful for the PDT treatment because of its skin cell permeability. All porphyrins **7** and **8** have a Q_1 band at ca. 650 nm which is almost same as that of Foscan® and is longer than that of Photofrin®. Hence the porphyrins **7** and **8** are potential PDT drugs in terms of the availability of the long wavelength region for excitation.

2-4. Experimentals

Materials and Measurements

^1H NMR spectra were recorded on Bruker AVANCE 800 (800 MHz) (National Food Research Institute), Bruker DRX600 (600 MHz) (National Food Research Institute), JEOL JNM-AL400 (400 MHz) (Nara Women's University) and VARIAN GEMINI 2000 (300 MHz) (Nara Women's University) instruments. NMR assignment appears with following abbreviations; "P" is porphyrin ring, "R" is saccharide residue, and "Ar" is aromatic group or bridging phenylene group between P and R. Electronic absorption spectra in dimethyl sulfoxide (DMSO) were recorded on a JASCO V-570 spectrophotometer (Nara Women's University). IR spectra were recorded on FT/IR-8900 JASCO (Osaka Prefectural College of Technology) using an ATR-500/M instrument. Mass spectra in methanol were recorded on JMS T100LC JEOL (Nara Women's University), JEOL JMS-700 (Nara Institute of Science and Technology) and JMS-100LC JEOL (National Food Research Institute) instruments. The purity of the acetylated

compounds **5** and **7** was estimated by liquid chromatography (SHIMADZU, CLASS-VP ver 5.02 system) (Nara Women's University) equipped with a silica gel-ODS (Kanto, Mightysil RP-18 4.6 mmϕ × 200 mm) column and a UV-vis detector (SPD-M10A VP) using MeOH / H_2O = 8 / 2 as an eluent. The purity of the deacetylated compounds **3** was determined by high performance liquid chromatography (HPLC, HITACHI, L-6000) (Osaka Prefectural College of Technology) equipped with an octadecylsilyl-bounded silica gel (HITACHI, HITACHI GEL 4 mmϕ × 150 mm) column and a diode array detector (HITACHI L-4000) using acetonitrile / water = 1 / 1 as an eluent.

*2-4-1. Glucopyranosylated Compounds (**a**)*

*2,3,4,6-Tetra-O-acetyl-α-D-glucopyronosyl Bromide (**3a**)*

Procedure A: 1,2,3,4,6-penta-*O*-acetyl-α-D-glucose (25.8 g, 66.1 mmol) and 30 % HBr/AcOH (300 mL) were stirred for 1 h in room temperature. After 1 h, the solution was added to $CHCl_3$ (600 mL). The solution was washed with ice water (600 mL × 2), saturated cold $NaHCO_3$(aq) (600 mL × 2) and dried over Na_2SO_4. The filtered solution was evaporated to dryness and pure product was crystallized from CH_2Cl_2/Et_2O to give a white solid (17.7 g, 64.9 %).

Procedure B: Anhydrous D-glucose (39 g, 236 mmol) and acetyl bromide (98 mL, 577 mmol) were stirred. This mixture was stirred for 12 h in ice water bath. After 12 h, the solution was added Et_2O (390 mL). The solution was washed with ice water (400 mL × 2), saturated cold $NaHCO_3$(aq) (400 mL × 2), and dried over Na_2SO_4. The filtered solution was evaporated to dryness and pure product was crystallized from CH_2Cl_2/Et_2O to give a white solid (53 g, 56 %). ^{1}H NMR ($CDCl_3$, 300.07 MHz): δ (ppm) = 6.62 (1H, d, ^3J = 3.9 Hz, 1-R), 5.57 (1H, t, ^3J= 9.3 MHz, 3-R), 5.17 (1H, t, ^3J= 10.05 MHz, 4-R), 4.85 (1H, dd, ^3J= 10.2 Hz, ^2J = 3.9 Hz, 2-R), 4.32 (2 H, m, 6-R), 4.13 (1H, dd, ^3J= 12.6 Hz, ^2J= 2.1 Hz, 5-R), 2.10, 2.08, 2.07, 2.05 ((3H, s, Me) × 4).

*4-(2,3,4,6-Tetra-O-actyl-β-D-glucopyranosiloxy)benzaldehyde (**p-4a**)*

p-Hydroxyenzaldehyde (1.5 g, 12 mmol), quinoline (15 mL) and **3a** (10.1 g, 25 mmol) were stirred. Silver oxide(I) (5.8 g, 25 mmol) was added to the stirred solution. This mixture was stirred for 15 min at room temperature. To the solution was added 25 % acetic acid (aq) (100 mL), and then was stirred for 1 h in ice water bath. The reaction mixture was filtered, and resulting solid was poured in hot MeOH (150 mL). The insoluble silver oxide was removed by celite filtration. The filtrate was evaporated to dryness

and crude product was crystallized from hot MeOH to give a white solid (2.7 g, 50 %). ^{1}H NMR ($CDCl_3$, 300.07 MHz): δ (ppm) = 9.94 (1H, s, aldehyde), 7.86 (2H, d, ^3J = 6.6 Hz, 2,6-Ar*H*), 7.01 (2H, d, ^3J = 6.9 Hz, 3,5-Ar*H*), 5.33 (2H, m, 1,2-R), 5.16 ~ 5.24 (2H, m, 3,4-R), 4.30 (1H, dd, ^3J= 12.6 Hz, ^2J = 5.1 Hz, 6-R), 4.18 (1H, dd, ^3J= 12.3 Hz, ^2J = 2.4 Hz, 6-R), 3.94 (1H, m, 5-R), 2.10, 2.08, 2.07, 2.05 ((3H, s, Me)×4).

3-(2,3,4,6-Tetra-O-actyl-β-D-glucopyranosiloxy)benzaldehyde (m-4a)

The similar procedure for *p*-**4a** was applied to *m*-hydroxyenzaldehyde (1.5 g, 12 mmol) and **3a** (10.1 g, 25 mmol) to give *m*-**4a** as a light yellow solid (3.4 g, 63 %). ^{1}H NMR ($CDCl_3$, 300.07 MHz): δ (ppm) = 9.99 (1H, s, aldehyde), 7.61 ~ 7.58 (1H, m, 2-Ar*H*), 7.52 ~ 7.47 (2H, m, 5,6-Ar*H*), 7.29 ~ 7.25 (1H, m, 4-Ar*H*), 5.30 (2H, m, 1,2-R), 5.20 ~ 5.12 (2H, m, 3,4-R), 4.24 (2H, m, 6-R), 3.94 (1 H, m, 5-R), 2.11, 2.10, 2.07, 2.05 ((3H, s, Me) × 4).

Zinc(II) 5,10,15,20-tetrakis[4-(2,3,4,6-tetra-O-acetyl-β-D-glucopyranosyloxy)phenyl]porphyrin (p-5a)

p-**4a** (1.9 g, 3.9 mmol), pyrrole (0.27 mL, 3.9 mmol) and dry $CHCl_3$ (430 mL) were stirred with Ar flushing for 30 min. BF_3·OEt_2 (0.2 mL, 0.10 mmol) and $Zn(OAc)_2$·$2H_2O$ (3.8 g, 17 mmol) were added, and the mixture was stirred for 24 h at room temperature. To the solution was added chloranil (0.73 g, 2.9 mmol), and the whole was refluxed for 1 h. The solution was evaporated under reduced pressure. The crude product was purified by column chromatography (silica gel, $CHCl_3$/acetone (15/1 ~ 8/1)), followed by recrystallization from $CHCl_3$/EtOH to give *p*-**5a** (1.1 g, yield 87 %) as a red solid. Purity (HPLC): >99 %. ^{1}H NMR ($CDCl_3$, 600.13 MHz): δ (ppm) = 8.89 (8H, s, β-P), 8.12 (8H, d, ^3J = 8.7 Hz, 2,6-Ar), 7.38 (8H, d, ^3J = 8.4 Hz, 3,5-Ar), 5.48 ~ 5.42 (12H, m, 1,2,3-R), 5.30 (4H, t, ^3J = 9.6 Hz, 4-R), 4.40 (4H, dd, ^3J = 12.3 Hz, ^2J = 5.4 Hz, 6-R), 4.31 (4H, dd, ^3J = 12.3 Hz, ^2J = 2.4 Hz, 6-R), 4.06 (4H, m, 5-R), 2.21, 2.11, 2.10, 2.09 ((12H, s, Me) × 4). ^{13}C NMR ($CDCl_3$, 75.46 MHz): δ (ppm) = 170.80, 170.49, 169.65 (CO × 3), 156.63 (4-Ar), 150.45 (α-P), 137.88 (1-Ar), 135.47 (2,6-Ar), 132.09 (β-P), 120.39 (meso-P), 114.99 (3,5-Ar), 99.18 (1-R), 72.81 (3-R), 72.23 (5-R), 71.29 (2-R), 68.35 (4-R), 62.04 (6-R), 20.70, 20.65, 20.55, 20.52 (Me × 4). ESI-HRMS (m/z) = $[M+Na]^+$ calcd for $C_{100}H_{100}N_4O_{40}ZnNa$, 2083.5103; found, 2083.5117.

Zinc(II) 5,10,15,20-tetrakis[3-(2,3,4,6-tetra-O-acetyl-β-D-glucopyranosyloxy)phenyl]porphyrin (m-5a)

The similar procedure for *p*-**5a** was applied to *m*-**4a** (1.2 g, 2.4 mmol) to give *m*-**5a** as a red solid (0.89 g, 93 %). Purity (HPLC): 96.1 %. ^{1}H NMR ($CDCl_3$, 300.07 MHz): δ (ppm) = 8.97 (8H, br, β-P), 7.97 ~ 7.85 (8H, m, 2,6-Ar), 7.72 ~ 7.62 (4H, m, 5-Ar), 7.47 ~ 7.21 (4H, m, 4-Ar), 5.40 ~ 5.25 (12H, m, 1,2,3-R), 5.20 ~ 5.25 (4H, m, 4-R), 4.25 ~ 4.12 (4H, m, 6-R), 4.12 ~ 4.00 (4H, m, 6-R), 3.89 ~ 3.77 (4H, m, 5-R), 2.16 ~ 1.99 + 1.53 ~ 1.34 (48H, m, Me). ^{13}C NMR ($CDCl_3$, 75.46 MHz): δ (ppm) = 170.56, 170.37, 169.52 (CO × 3), 155.32 (3-Ar), 150.11 (α-P), 144.37 (1-Ar), 132.17 (β-P), 129.90 (5-Ar), 127.67 (6-Ar), 122.93 (4-Ar), 120.39 (meso-P), 116.31 (2-Ar), 99.20 (1-R), 72.65 (3-R), 72.00 (5-R), 71.21 (2-R), 68.20 (4-R), 61.87 (6-R), 20.57, 20.44, 20.38, 19.83 (Me× 4). ESI-HRMS (m/z) = $[M+Na]^+$ calcd for $C_{100}H_{100}N_4O_{40}ZnNa$, 2083.5103; found, 2083.5090.

5,10,15,20-Tetrakis[4-(2,3,4,6-tetra-O-acetyl-β-D-glucopyranosyloxy)phenyl]porphyrin (p-7a)

p-**4a** (1.9 g, 3.8 mmol), pyrrole (0.27 mL, 3.8 mmol) and dry $CHCl_3$ (430 mL) were stirred with Ar flushing for 30 min. $BF_3{\cdot}OEt_2$ (0.06 mL, 0.48 mmol) and $Zn(OAc)_2{\cdot}2H_2O$ (2.5 g, 11 mmol) were added, and the mixture was stirred for 24 h at room temperature. To the solution was added chloranil (0.44 g, 1.7 mmol), and the whole was refluxed for 1 h. The solution was washed with 4 M HCl (100 mL × 3), distilled water (100 mL × 2) and saturated $NaHCO_3$ (aq) (100 mL × 2). The solution was dried over Na_2SO_4, and the solvent was taken off under reduced pressure. The crude product was purified by column chromatography (silica gel, $CHCl_3$/acetone (15/1 ~ 8/1)), followed by recrystallization from $CHCl_3$/EtOH to give *p*-**7a** (1.2 g, 64 %) as a red solid. Purity (HPLC): 99.7 %. ^{1}H and ^{13}C NMR spectrum of *p*-**7a** was agreed with the literature [4,6,8].

5,10,15,20-Tetrakis[3-(2,3,4,6-tetra-O-acetyl-β-D-glucopyranosyloxy)phenyl]porphyrin (m-7a)

The similar procedure for *p*-**7a** was applied to *m*-**4a** (1.2 g, 2.4 mmol) to give *m*-**7a** as a red solid (1.3 g, 68 %). Purity (HPLC): >99 %. ^{1}H and ^{13}C NMR spectrum of *m*-**7a** was agreed with the literature [4,6,8].

Zinc(II) 5,10,15,20-tetrakis[4-(β-D-glucopyranosyloxy)phenyl]porphyrin (p-6a)

p-**5a** (0.25 g, 0.12 mmol) was dissolved in THF (30 mL). To the solution, sodium methoxide was added until pH 9. This mixture was stirred for 24 h at room temperature, then 25 % acetic acid (aq) was

added to neutralize it. The solvent was evaporated, and the crude product was purified by gel filtration on a Sephadex LH-20® column eluted with methanol. The solvent was evaporated. The precipitate was washed with water and lyophilized to give *p*-**6a** as a purple red powder (0.15 g, 94 %). Purity (HPLC): >99 %. ^{1}H NMR (CD_3OD, 300.07 MHz): δ (ppm) = 8.83 (8H, s, β-P), 8.10 (8H, d, ^3J = 8.4 Hz, 2,6-Ar), 7.49 (8H, d, ^3J = 8.4 Hz, 3,5-Ar), 5.26 (4H, d, ^3J = 4.5 Hz, 1-R), 4.01 (4H, dd, ^3J = 1.8 Hz, ^2J = 12.0 Hz, 6-R), 3.80 (4H, dd, ^3J = 5.1 Hz, ^2J = 11.7 Hz, 6-R), 3.69 ~ 3.48 (16H, m, 2,3,4,5-R). ^{1}H NMR (DMSO-d_6, 300.07 MHz): δ (ppm) = 8.81 (8H, s, β-P), 8.08 (8H, d, ^3J = 8.1 Hz, 2,6-Ar), 7.44 (8H, d, ^3J = 7.8 Hz, 3,5-Ar), 5.51 (4H, d, ^3J = 5.1 Hz, 2-RO*H*), 5.21 (4H, m, 2-R), 5.21 (4H, br, 1-R), 5.11 (8H, br, 3,4-RO*H*), 4.88 ~ 4.64 (4H, m, 6-RO*H*), 3.80 (4H, m, 6-R), 3.62 ~ 3.42 (20H, m, 2,3,4,5,6-R). ^{13}C NMR (DMSO-d_6, 75.46 MHz): δ (ppm) = 157.54 (4-Ar), 149.95 (α-P), 136.62 (1-Ar), 135.43 (2,6-Ar), 131.95 (β-P), 120.24 (meso-P), 114.52 (3,5-Ar), 100.97 (1-R), 77.54 (3-R), 77.02 (5-R), 73.77 (2-R), 70.10 (4-R), 61.09 (6-R). ESI-HRMS (m/z) = $[M-H]^-$ calcd for $C_{68}H_{67}N_4O_{24}Zn$, 1387.3437; found, 1387.3391.

Zinc(II) 5,10,15,20-tetrakis[3-(β-D-glucopyranosyloxy)phenyl]porphyrin (m-6a)

The similar procedure for *p*-**6a** was applied to *m*-**5a** (91 mg, 43.7 μmol) to give *m*-**6a** as a red solid (54.0 mg, 89 %). Purity (HPLC): >99 %. 1H NMR (CD_3OD, 600.13 MHz): δ (ppm) = 8.90 ~ 8.84 (8H, m, β-P), 7.95 ~ 7.85 (8H, m, 2,6-Ar), 7.68 ~ 7.64 (4H, m, 5-Ar), 7.53 ~ 7.49 (4H, m, 4-Ar), 5.22 ~ 5.20 (4H, m, 1-R), 3.82 ~ 3.81 (4H, m, 6-R), 3.68 ~ 3.66 (4H, m, 6-R), 3.56 ~ 3.43 (12H, m, 2,3,5-R), 3.39 (4H, m, 4-R). 1H NMR (DMSO-d6, 300.07 MHz): δ (ppm) = 8.84 (8H, m, β-P), 7.81 ~ 7.79 (8H, m, 2,6-Ar), 7.73 ~ 7.70 (4H, m, 5-Ar), 7.51 ~ 7.48 (4H, m, 4-Ar), 5.42 (4H, d, ^3J = 4.2 Hz, 2-RO*H*), 5.19 (4H, m, 3 or 4-RO*H*), 5.11 (4H, m, 1-R), 5.01 (4H, br, 3 or 4-RO*H*), 4.60 (4H, m, 6-RO*H*), 3.82 (4H, d, ^2J = 12.0 Hz, 6-R), 3.67 (4H, dd, ^3J = 5.4 Hz, ^2J = 13.2 Hz, 6-R), 3.62 ~ 3.31 (16H, m, 2,3,4,5-R). ^{13}C NMR (DMSO-d_6, 75.46 MHz): δ (ppm) =155.12 (3-Ar), 149.60 (α-P), 144.41 (1-Ar), 132.06 (β-P), 128.87 (5-Ar), 127.84 (6-Ar), 122.79 (4-Ar), 120.22 (meso-P), 115.48 (2-Ar), 100.85 (1-R), 77.31 (3-R), 76.85 (5-R), 73.72 (2-R), 69.95 (4-R), 60.91 (6-R). ESI-HRMS (m/z) = $[M+H]^+$ calcd for $C_{68}H_{68}N_4O_{24}Zn$, 1389.2845; found, 1389.2853.

5,10,15,20-Tetrakis[4-(β-D-glucopyranosyloxy)phenyl]porphyrin (p-8a)

The similar procedure for *p*-**6a** was applied to *p*-**7a** (203 mg, 102 μmol) to give *p*-**8a** as a red solid (123 mg, 91 %). Purity (HPLC): 96 %. 1H and 13C NMR spectrum of *p*-**8a** was agreed with the

literature [4,6,8].

5,10,15,20-Tetrakis[3-(β-D-glucopyranosyloxy)phenyl]porphyrin (m-8a)

The similar procedure for *p*-**6a** was applied to *m*-**7a** (510 mg, 255 μmol) to give *m*-**8a** as a red solid (325 mg, 96 %). Purity (HPLC): 98 %. ^{1}H and ^{13}C NMR spectrum of *m*-**8a** was agreed with the literature [4,6,8].

*2-4-2. Galactopyranosylated Compounds (**b**)*

*2,3,4,6-Tetra-O-acetyl-α-D-galactopyronosyl bromide (**3b**)*

1,2,3,4,6-penta-*O*-acetyl-α-D-galactose (10.3 g, 26.4 mmol) and 25 % HBr/AcOH (50 mL) were stirred for 1 h in room temperature. After 1 h, the solution was added $CHCl_3$ (600 mL). The solution was washed with ice water (200 mL x 2), saturated cold $NaHCO_3$ (aq) (200 mL x 2), and dried over Na_2SO_4. The filtered solution was evaporated to dryness and pure product was crystallized from CH_2Cl_2/Et_2O to give white solid (9.0 g, 83.3 %). ^{1}H NMR ($CDCl_3$, 300.07 MHz): δ (ppm) = 6.70 (1H, d, ^{3}J = 3.9 Hz, 1-R), 5.52 (1H, d, ^{3}J= 3.3 MHz, 4-R), 5.41 (1H, dd, ^{3}J= 10.5 MHz, ^{2}J = 3.00 Hz, 3-R), 5.06 (1H, dd, ^{3}J= 10.5 Hz, ^{2}J = 3.9 Hz, 2-R), 4.49 (1H, t, ^{3}J= 5.4 Hz, 5-R), 4.15 (2H, m, 6-R), 2.16, 2.12, 2.07, 2.02 ((3H, s, Me) × 4).

*4-(2,3,4,6-Tetra-O-actyl-β-D-galactopyranosiloxy)benzaldehyde (p-**4b**)*

p-Hydroxybenzaldehyde (1.5 g, 12 mmol) was dissolved into the mixture of CH_2Cl_2 (14 mL) and 5 % NaOH (aq) (20 mL). Tetrabutylammonium bromide (0.66 g, 2.0 mmol) was added to the solution with stirring. To the solution was added CH_2Cl_2 solution (8 mL) of **3b** (3.5 g, 8.4 mmol). The mixture was stirred for 2 days at room temperature. The solution was washed with NaOH (aq) (5 %, 20 mL× 3), saturated $NaHCO_3$ (aq) (20 mL × 1), water (20 mL × 1). After drying over Na_2SO_4, the filtrate was evaporated to dryness and give colorless oil (2.3 g, 41 %). ^{1}H NMR ($CDCl_3$, 300.07 MHz): δ (ppm) = 9.94 (1H, s, aldehyde), 7.86 (2H, d, ^{3}J = 6.9 Hz, 2,6-Ar*H*), 7.14 (2H, d, ^{3}J = 6.9 Hz, 3,5-Ar*H*), 5.56 ~ 5.48 (2H, m, 4,3-R), 5.21 ~ 5.13 (2H, m, 1,2-R), 4.24 ~ 4.15 (3H, m, 5,6-R), 2.19, 2.09, 2.08, 2.03 ((3H, s, Me) × 4).

3-(2,3,4,6-Tetra-O-actyl-β-D-galactopyranosiloxy)benzaldehyde (m-4b)

The similar procedure for *p*-**4b** was applied to *m*-hydroxyenzaldehyde (1.5 g, 12 mmol) and **3b** (3.6 g, 8.6 mmol) to give *m*-**4b** as colorless oil (2.2 g, 39 %). ^{1}H NMR ($CDCl_3$, 300.07 MHz): δ (ppm) = 9.93 (1H, s, aldehyde), 7.62 ~ 7.57 (1H, m, 2-Ar*H*), 7.57 ~ 7.51 (2H, m, 6,5-Ar*H*), 7.32 ~ 7.25 (1H, m, 4-Ar*H*), 5.57 ~ 5.41 (2H, m, 4,3-R), 5.18 ~ 5.12 (2H, m, 1,2-R), 4.27 ~ 4.04 (3H, m, 5,6-R), 2.20, 2.08, 2.06, 2.03 ((3H, s, Me) × 4).

Zinc(II) 5,10,15,20-tetrakis[4-(2,3,4,6-tetra-O-acetyl-β-D-galactopyranosyloxy)phenyl]porphyrin (p-5b)

The similar procedure for *p*-**5a** was applied to *p*-**4b** (3.3 g, 6.9 mmol) to give *p*-**5b** as a red solid (1.4 g, 53 %). Purity (HPLC): >99 %. ^{1}H NMR ($CDCl_3$, 300.07 MHz): δ (ppm) = 8.81 (8H, s, β-P), 8.13 (8H, d, ^3J = 8.6 Hz, 2,6-Ar), 8.74 (8H, d, ^3J = 8.1 Hz, 3,5-Ar), 5.86 (4H, m, 4-R), 5.33 (8H, m, 1,3-R), 4.62 ~ 4.56 (4H, m, 2-R), 4.28 ~ 4.08 (12H, m, 5,6-R), 2.27, 2.23, 2.20, 2.04 ((12H, s, Me) × 4). ^{13}C NMR ($CDCl_3$, 75.46 MHz): δ (ppm) = 170.51, 170.32, 169.69 (CO × 3), 156.57 (4-Ar), 150.39 (α-P), 137.81 (1-Ar), 135.44 (2,6-Ar), 132.02 (β-P), 120.31 (meso-P), 114.92 (3,5-Ar), 99.57 (1-R), 71.10 (5-R), 70.87 (2-R), 68.72 (3-R), 66.86 (4-R), 61.34 (6-R), 20.70, 20.65, 20.55, 20.52 (Me × 4). ESI-HRMS (m/z) = $[M+Na]^+$ calcd for $C_{100}H_{100}N_4O_{40}ZnNa$, 2083.5103; found, 2083.5083.

Zinc(II) 5,10,15,20-tetrakis[3-(2,3,4,6-tetra-O-acetyl-β-D-galactopyranosyloxy)phenyl]porphyrin (m-5b)

The similar procedure for *p*-**5a** was applied to *m*-**4b** (2.1 g, 4.4 mmol) to give *m*-**5b** as a red solid (1.6 g, 72 %). Purity (HPLC): 96.9 %. ^{1}H NMR ($CDCl_3$, 600.13 MHz): δ (ppm) = 8.95 (8H, br, β-P), 7.91 ~ 7.88 (8H, m, 2,6-Ar), 7.68 ~ 7.64 (4H, m, 5-Ar), 7.44 (4H, m, 4-Ar), 5.59 ~ 5.57 (4H, m, 4-R), 5.42 ~ 5.40 (4H, m, 1-R), 5.34 ~ 5.32 (4H, m, 3-R), 5.14 ~ 5.12 (4H, m, 2-R), 4.14 ~ 4.01 (12H, m, 5,6-R), 2.15 ~ 2.00 + 1.37 ~ 1.28 (48H, m, Me). ^{13}C NMR (DMSO-d_6, 75.46 MHz): δ (ppm) = 170.38, 170.28, 169.62 (CO × 3), 155.40 (3-Ar), 150.17 (α-P), 144.25 (1-Ar), 132.25 (β-P), 129.81 (5-Ar), 127.72 (6-Ar), 122.70 (4-Ar), 120.55 (meso-P), 116.33 (2-Ar), 99.80 (1-R), 71.10 (5-R), 70.79 (3-R), 68.68 (2-R), 66.89 (4-R), 61.40 (6-R), 20.72, 20.50, 19.71 (Me × 3). ESI-HRMS (m/z) = $[M+Na]^+$ calcd for $C_{100}H_{100}N_4O_{40}ZnNa$, 2083.5103; found, 2083.5110.

5,10,15,20-Tetrakis[4-(2,3,4,6-tetra-O-acetyl-β-D-galactopyranosyloxy)phenyl]porphyrin (p-7b)

The similar procedure for *p*-**7a** was applied to *p*-**4b** (1.5 g, 3.12 mmol) to give *p*-**7b** as a red solid

(0.98 g, 62 %). Purity (HPLC): >99 %. ^{1}H and ^{13}C NMR spectrum of *p*-**7b** was agreed with the literature [4,6,8].

5,10,15,20-Tetrakis[3-(2,3,4,6-tetra-O-acetyl-β-D-galactopyranosyloxy)phenyl]porphyrin (m-7b)

The similar procedure for *p*-**7a** was applied to *m*-**4b** (0.6 g, 1.6 mmol) to give *m*-**7b** as a red solid (0.69 g, 57 %). Purity (HPLC): 98 %. ^{1}H NMR ($CDCl_3$, 300.07 MHz): δ (ppm) = 8.89 (8H, br, β-P), 7.95 ~ 7.84 (8H, m, 2,6-Ar), 7.73 ~ 7.62 (4H, m, 5-Ar), 7.50 ~ 7.42 (4H, m, 4-Ar), 5.68 ~ 5.54 (4H, m, 4-R), 5.54 ~ 5.38 (4H, m, 3-R), 5.38 ~ 5.20 (4H, m, 1-R), 5.20 ~ 4.93 (4H, m, 2-R), 4.16 ~ 4.04 (12H, m, 5,6-R), 2.17 ~ 2.01 + 1.29 ~ 1.22 (48H, m, Me), -2.88 (2H, br, NH). ^{13}C NMR ($CDCl_3$, 75.46 MHz): δ (ppm) = 170.37, 170.27, 169.60 (CO × 3), 155.45 (3-Ar), 150.13 (α-P), 143.54 (1-Ar), 131.42 (β-P), 129.84 (5-Ar), 127.85 (6-Ar), 122.59 (4-Ar), 119.52 (meso-P), 116.59 (2-Ar), 99.76 (1-R), 71.11 (5-R), 70.76 (3-R), 66.64 (2-R), 66.87 (4-R), 61.40 (6-R), 20.68, 20.49, 20.43, 19.62 (Me × 4). ESI-HRMS (m/z) = [M-H]$^-$ calcd for $C_{100}H_{101}N_4O_{40}$, 1997.5992; found, 1997.5996.

Zinc(II) 5,10,15,20-tetrakis[4-(β-D-galactopyranosyloxy)phenyl]porphyrin (p-6b)

The similar procedure for *p*-**6a** was applied to *p*-**5b** (510 mg, 245 μmol) to give *p*-**6b** as a red solid (306 mg, 90 %). Purity (HPLC): >99 %. ^{1}H NMR (CD_3OD, 300.07 MHz): δ (ppm) = 8.84 (8H, s, β-P), 8.10 (8H, d, ^3J = 8.4 Hz, 2,6-Ar), 7.49 (8H, d, ^3J = 8.4 Hz, 3,5-Ar), 5.20 (4H, d, ^3J = 7.8 Hz, 1-R), 4.02 ~ 3.80 (20H, m, 2,4,5,6-R), 3.74 ~ 3.70 (4H, m, 3-R). ^{1}H NMR (DMSO-d_6, 300.07 MHz): δ (ppm) = 8.81 (8H, s, β-P), 8.08 (8H, d, ^3J = 8.4 Hz, 2,6-Ar), 7.45 (8H, d, ^3J = 8.1 Hz, 3,5-Ar), 5.37 (4H, d, ^3J= 5.1 Hz, 2-RO*H*), 5.11 (4H, d, ^3J = 7.5 Hz, 1-R), 4.99 (4H, d, ^3J = 5.4 Hz, 3-RO*H*), 4.77 (4H, m, 6-RO*H*), 4.63 (4H, d, ^3J = 4.5 Hz, 4-RO*H*), 3.83 ~ 3.77 (12H, m, 4,2,6-R), 3.77 ~ 3.63 (8H, m, 6,5-R), 3.63 ~ 3.50 (4H, m, 3-R). ^{13}C NMR (DMSO-d_6, 75.46 MHz): δ (ppm) = 157.64 (4-Ar), 149.95 (α-P), 136.54 (1-Ar), 135.43 (2,6-Ar), 131.93 (β-P), 120.25 (meso-P), 114.57 (3,5-Ar), 101.66 (1-R), 76.00 (5-R), 73.71 (3-R), 70.79 (2-R), 68.56 (4-R), 60.81 (6-R). ESI-HRMS (m/z) = [M-H] calcd for $C_{68}H_{67}N_4O_{24}Zn$, 1387.3437; found, 1387.3418.

Zinc(II) 5,10,15,20-tetrakis[3-(β-D-galactopyranosyloxy)phenyl]porphyrin (m-6b)

The similar procedure for *p*-**6a** was applied to *m*-**5b** (77 mg, 37.0 μmol) to give *m*-**6b** as a red solid (462 mg, 90 %). Purity (HPLC): 98 %. ^{1}H NMR (CD_3OD, 300.07 MHz): δ (ppm) = 8.87 (8H, br, β-P),

7.96 (4H, br, 2-Ar), 7.60 (4H, m, 6-Ar), 7.81 (4H, m, 5-Ar), 7.56 (4H, m, 4-Ar), 5.17 (4H, d, ^3J = 7.5 Hz, 1-R), 3.93 ~ 3.87 (8H, m, 2,4-R), 3.87 ~ 3.71 (8H, m, 6-R), 3.71 ~ 3.59 (8H, m, 3,5-R). ^{1}H NMR (DMSO-d_6, 300.07 MHz): δ (ppm) = 8.84 (8H, br, β-P), 7.83 ~ 7.72 (8H, m, 2,6-Ar), 7.72 ~ 7.61 (4H, m, 5-Ar), 7.49 ~ 7.47 (4H, m, 4-Ar), 5.28 (4H, d, ^3J = 4.8 Hz, 2-RO*H*), 5.13 (4H, d, ^3J = 6.6 Hz, 1-R), 5.01 ~ 4.72 (4H, d, ^3J = 2.7 Hz, 3-RO*H*), 4.58 ~ 4.52 (8H, m, 4,6-RO*H*), 3.73 ~ 3.32 (24H, m, 2,3,4,5,6-R). ^{13}C NMR (DMSO-d_6, 75.46 MHz): δ (ppm) =156.15 (3-Ar), 149.62 (α-P), 144.39 (1-Ar), 131.95 (β-P), 128.79 (5-Ar), 127.81 (6-Ar), 122.68 (4-Ar), 120.27 (meso-P), 115.69 (2-Ar), 101.40 (1-R), 75.70 (5-R), 73.58 (3-R), 70.79 (2-R), 68.27 (4-R), 60.44 (6-R). ESI-HRMS (m/z) = [M-H]$^-$ calcd for $C_{68}H_{67}N_4O_{24}Zn$, 1387.3437; found, 1387.3433.

5,10,15,20-Tetrakis[4-(β-D-galactopyranosyloxy)phenyl]porphyrin (p-8b)

The similar procedure for *p*-**6a** was applied to *p*-**7b** (257 mg, 123 μmol) to give *p*-**8b** as a red solid (142 mg, 87 %). Purity (HPLC): >99 %. ^{1}H and ^{13}C NMR spectrum of *p*-**8b** was agreed with the literature [4,6,8].

5,10,15,20-Tetrakis[3-(β-D-galactopyranosyloxy)phenyl]porphyrin (m-8b)

The similar procedure for *p*-**6a** was applied to *m*-**7b** (172 mg, 86.1 μmol) to give *m*-**8b** as a red solid (86.8 mg, 76 %). Purity (HPLC): >99 %. ^{1}H NMR (CD_3OD, 300.07 MHz): δ (ppm) = 8.92 (8H, br, β-P), 7.97 (4H, br, 2-Ar), 7.85 (4H, m, 6-Ar), 7.67 (4H, m, 5-Ar), 7.57 (4H, m, 4-Ar), 5.17 (4H, d, ^3J = 7.5 Hz, 1-R), 3.93 ~ 3.87 (8H, m, 2,4-R), 3.71 (8H, m, 6-R), 3.65 ~ 3.58 (8H, m, 3,5-R). ^{1}H NMR (DMSO-d_6, 300.07 MHz): δ (ppm) = 8.89 (8H, br, β-P), 7.89 (4H, br, 2-Ar), 7.82 (4H, br, 6-Ar), 7.73 (4H, m, 5-Ar), 7.51 (4H, m, 4-Ar), 5.29 (4H, d, ^3J = 4.8 Hz, 2-RO*H*), 5.14 (4H, d, ^3J = 7.5 Hz, 1-R), 4.88 (4H, d, ^3J = 5.4 Hz, 3-RO*H*), 4.55 ~ 4.53 (8H, m, 4,6-RO*H*), 3.68 (8H, br, 2,4-R), 3.64 ~ 3.44 (16H, m, 3,5,6-R), -2.97 (2H, br, N*H*). ^{13}C NMR (DMSO-d_6, 75.46 MHz): δ (ppm) =156.35 (3-Ar), 142.74 (α-P and 1-Ar), 131.56 (β-P), 128.71 (5-Ar), 128.24 (6-Ar), 122.65 (4-Ar), 119.94 (meso-P), 116.26 (2-Ar), 101.23 (1-R), 75.700 (5-R), 73.53 (3-R), 70.68 (2-R), 68.34 (4-R), 60.51 (6-R). ESI-HRMS (m/z) = [M-H]$^-$ calcd for $C_{68}H_{69}N_4O_{24}$, 1325.43027; found, 1325.4304.

2-4-3. Xylopyranosylated Compounds (c)

2,3,4-Tri-O-acetyl-α-D-xylose (2c)

Sodium acetate (3.0 g, 35.8 mmol) and Ac_2O (36 mL) were stirred in 130 °C. D-Xylose (5.0g, 33.3 mmol) was added carefully to the mixture. After dissolving completely, reaction solution was cooled to room temperature. The solution was poured into ice water (150 g), and then was stirred for overnight. The filtered solid was crystallized from hot MeOH to give a white solid (5.6 g, 53 %). ^{1}H NMR ($CDCl_3$, 300.07 MHz): δ (ppm) = 5.72 (1H, d, ^3J = 6.6 Hz, 1-R), 5.57 (1H, t, ^3J= 8.4 MHz, 3-R), 5.05 (1H, t, ^3J= 6.6 MHz, 2-R), 4.98 (1H, m, 5-R), 4.16 (1H, dd, ^3J= 11.7 Hz, ^2J = 4.8 Hz, 5-R), 3.53 (1H, dd, ^3J= 12.0 Hz, ^2J= 8.4 Hz, 5-R), 2.12, 2.07, 2.06 ((3H, s, Me) × 3).

2,3,4-Tri-O-acetyl-α-D-xylopyronosyl bromide (3c)

The similar procedure for **2b** was applied to **2c** (5.0 g, 15.7 mmol) and 30 % HBr/AcOH (25 mL) to give **3c** as white solid (4.6 g, 87 %). ^{1}H NMR ($CDCl_3$, 300.07 MHz): δ (ppm) = 6.59 (1H, d, ^3J = 3.9 Hz, 1-R), 5.57 (1H, t, ^3J= 9.6 MHz, 3-R), 5.04 (1H, m, 4-R), 4.78 (1H, dd, ^3J= 9.8 Hz, ^2J = 3.9 Hz, 2-R), 4.06 (1H, dd, ^3J= 11.1 Hz, ^2J = 6.3 Hz, 5-R), 3.88 (1H, t, ^3J= 11.1 Hz, 5-R), 2.26, 2.13, 2.09 ((3H, s, Me) × 3).

4-(2,3,4-Tri-O-acetyl-β-D-xylopyranosyloxy)benzaldehyde (p-4c)

p-Hydroxybenzaldehyde (4.7 g, 38 mmol) was dissolved into the mixture of CH_2Cl_2 (70 mL) and 5 % NaOH (aq) (70 mL). Tetrabutylammonium bromide (1.2 g, 3.8 mmol) was added to the solution with stirring. To the solution was added CH_2Cl_2 solution (10 mL) of **3c** (8.5 g, 27 mmol). The mixture was stirred for 15 h at room temperature. The solution was washed with NaOH (aq) (5 %, 70 mL × 3), saturated $NaHCO_3$ (aq) (70 mL × 1) and water (70 mL × 1). After drying over Na_2SO_4, the filterate was evaporated to dryness and the residue was crystallized from CH_2Cl_2/Et_2O to give white solid (2.1 g, 21 %). ^{1}H NMR ($CDCl_3$, 300.07 MHz): δ (ppm) = 9.91 (1H, s, CHO), 7.84 (2H, d, ^3J = 8.4 Hz, 2,6-Ar), 7.11 (2H, d, ^3J = 8.7 Hz, 3,5-Ar), 5.32 (^{1}H, d, ^3J = 4.8 Hz, 1-R), 5.25~5.18 (2H, m, 2,3-R), 5.00~4.99 (1H, m, 4-R), 4.22 (1H, dd, ^3J = 4.2 Hz, ^2J = 12.3 Hz, 5-R), 3.59 (1H, dd, ^3J = 6.6 Hz, ^2J = 11.7 Hz, 5-R), 2.08 (9H, s, Me). ^{13}C NMR ($CDCl_3$, 75.46 MHz): δ (ppm) = 190.94 (CHO), 169.94, 169.48 (CO × 2), 161.18 (4-Ar), 131.68 (1-Ar), 131.67 (2,6-Ar), 116.72 (3,5-Ar), 97.39 (1-R), 69.96 (3-R), 69.48 (2-R), 68.09 (4-R), 61.68 (5-R), 20.55, 20.65 (Me × 2).

3-(2,3,4-Tri-O-acetyl-β-D-xylopyranosyloxy)benzaldehyde (m-4c)

The similar procedure for *p*-**4c** was applied to *m*-hydroxybenzaldehyde (4.3 g, 35 mmol) and **3c** (6.1 g, 19 mmol) to give *m*-**4c** (0.99 g, 14 %). ^{1}H NMR ($CDCl_3$, 300.07 MHz): δ (ppm) = 9.99 (1H, s, CHO), 7.60 (1H, m, 2-Ar), 7.57~7.46 (2H, m, 6,5-Ar), 7.29~7.25 (1H, m, 4-Ar), 5.29~5.17 (3H, m, 1,2,3-R), 5.06~4.99 (1H, m, 4-R), 4.24 (1H, dd, ^3J = 4.8 Hz, ^2J = 12.3 Hz, 5-R), 3.59 (1H, dd, ^3J = 7.8 Hz, ^2J = 12.3 Hz, 5-R), 2.12 (3H, s, Me), 2.10 (6H, s, Me × 2). ^{13}C NMR ($CDCl_3$, 75.46 MHz): δ (ppm) = 191.75 (CHO), 169.98, 169.49 (CO × 2), 157.12 (1-Ar), 130.39 (3,5-Ar), 125.28 (6-Ar), 123.40 (4-Ar), 116.91 (2-Ar), 98.11 (1-R), 70.34 (3-R), 69.83 (2-R), 68.231 (4-R), 61.78 (5-R), 20.62 (Me).

Zinc(II) 5,10,15,20-tetrakis[4-(2,3,4-tri-O-acetyl-β-D-xylopyranosyloxy)phenyl]porphyrin (p-5c)

The similar procedure for *p*-**5a** was applied to *p*-**4c** (1.0 g, 3.1 mmol) to give *p*-**5c** as a red solid (1.3 g, 84 %). Purity (HPLC): >99 %. ^{1}H NMR ($CDCl_3$, 300.07 MHz): δ (ppm) = 8.96 (8H, s, β-P), 8.14 (8H, d, ^3J = 8.7 Hz, 2,6-Ar), 7.39 (8H, d, ^3J = 8.4 Hz, 3,5-Ar), 5.54 (4H, t, ^3J = 6.0 Hz, 2-R), 5.39 ~ 5.37 (8H, m, 1,3-R), 5.15 (4H, m, 4-R), 4.43 (4H, dd, ^3J = 4.8 Hz, ^2J = 12.3 Hz, 5-R), 3.73 (4H, dd, ^3J = 7.8 Hz, ^2J = 12.3 Hz, 5-R), 2.22, 2.17, 2.13 ((9H, s, Me) × 3). ^{13}C NMR ($CDCl_3$, 75.46 MHz): δ (ppm) = 170.22, 170.09, 169.72 (CO × 3), 156.40 (4-Ar), 150.47 (α-P), 137.64 (1-Ar), 135.53 (2,6-Ar), 132.07 (β-P), 120.47 (meso-P), 114.91 (3,5-Ar), 98.63 (1-R), 70.76 (3-R), 70.25 (2-R), 68.54 (4-R), 62.04 (5-R), 20.76, 20.72 (Me × 2). Fast atom bombardment (FAB)-HRMS (m/z) = $[M]^+$ calcd for $C_{88}H_{84}N_4O_{32}Zn$, 1772.436; found, 1772.4304.

Zinc(II) 5,10,15,20-tetrakis[3-(2,3,4-tri-O-acetyl-β-D-xylopyranosyloxy)phenyl]porphyrin (m-5c)

The similar procedure for *p*-**5a** was applied to *m*-**4c** (1.5 g, 3.9 mmol) to give *m*-**5c** as a red solid (1.6 g, 84 %). Purity (HPLC): >99 %. ^{1}H NMR ($CDCl_3$, 300.07 MHz): δ (ppm) = 8.97 (8H, br, β-P), 7.93~7.87 (8H, m, 2,6-Ar), 7.68 (4H, m, 5-Ar), 7.43 (4H, m, 4-Ar), 5.38 (4H, m, 2-R), 5.25 (8H, m, 1,3-R), 5.05 (4H, m, 4-R), 4.26 (4H, m, 5-R), 3.57 (4H, m, 5-R), 2.12, 2.06, 2.04 ((9H, s, Me) × 3). ^{13}C NMR ($CDCl_3$, 75.46 MHz): δ (ppm) = 170.07, 169.96, 169.59 (CO × 3), 155.03 (3-Ar), 150.14 (α-P), 144.37 (1-Ar), 132.14 (β-P), 129.76 (5-Ar), 127.67 (6-Ar), 123.16 (4-Ar), 120.42 (meso-P), 116.09 (2-Ar), 98.63 (1-R), 70.58 (3-R), 70.09 (2-R), 68.36 (4-R), 61.81 (5-R), 20.59 (Me). FAB-HRMS (m/z) = $[M]^+$ calcd for $C_{88}H_{84}N_4O_{32}Zn$, 1772.436; found, 1772.4303.

5,10,15,20-Tetrakis[4-(2,3,4-tri-O-acetyl-β-D-xylopyranosyloxy)phenyl]porphyrin (p-7c)

The similar procedure for *p*-**7a** was applied to *p*-**4c** (284 mg, 738 μmol) to give *p*-**7c** as a red purple solid (202 mg, 64 %). Purity (HPLC): >99 %. ^{1}H NMR ($CDCl_3$, 800.03 MHz): δ (ppm) = 8.85 (8H, br, β-P), 8.13 (8H, d, ^3J = 8.7 Hz, 2,6-Ar), 7.39 (8H, d, ^3J = 8.4 Hz, 3,5-Ar), 5.53 ~ 5.55 (4H, m, 1-R), 5.40 ~ 5.38 (8H, m, 2,3-R), 5.17 ~ 5.15 (4H, m, 4-R), 4.44 (4H, dd, ^3J = 4.5 Hz, ^2J = 11.9 Hz, 5-R), 3.74 (4H, dd, ^3J = 7.6 Hz, ^2J = 11.9 Hz, 5-R), 2.23, 2.18, 2.14 ((9H, s, Me) × 3), -2.815 (2H, br, N*H*). ^{13}C NMR ($CDCl_3$, 75.46 MHz): δ (ppm) = 170.22, 170.11, 169.73 (CO × 3), 156.55 (4-Ar), 136.99 (α-P and 1-Ar), 135.71 (2,6-Ar), 130.10 (β-P), 119.45 (meso-P), 115.02 (3,5-Ar), 98.58 (1-R), 70.752 (3-R), 70.24 (2-R), 68.52 (4-R), 62.04 (5-R), 20.71 (Me). FAB-HRMS (m/z) = $[M+H]^+$ calcd for $C_{88}H_{87}N_4O_{32}$, 1711.52979; found, 1711.53108.

5,10,15,20-Tetrakis[3-(2,3,4-tri-O-acetyl-β-D-xylopyranosyloxy)phenyl]porphyrin (m-7c)

The similar procedure for *p*-**7a** was applied to *m*-**4c** (882 mg, 2.32 mmol) to give *m*-**7c** as a red purple solid (854 mg, 86 %). Purity (HPLC): >99 %. UV-vis (DMSO): λ_{max} (nm) ($\varepsilon \times 10^{-3}$ / $M^{-1}\cdot cm^{-1}$) = 420 (41.2), 514 (2.72), 549 (1.46), 589 (1.28), 644 (1.09). ^{1}H NMR ($CDCl_3$, 300.07 MHz): δ (ppm) = 8.88 (8H, s, β-P), 7.94 (4H, m, 2-Ar), 7.87 (4H, m, 6-Ar), 7.68 ~ 7.43 (8H, m, 4,5-Ar), 5.38 (4H, m, 2-R), 5.25 (8H, m, 1,3-R), 5.05 (4H, m, 4-R), 4.26 (4H, m, 5-R), 3.57 (4H, m, 5-R), 2.10, 2.06, 2.04 ((9H, s, Me) × 3), -2.87 (2H, br, N*H*). ^{13}C NMR ($CDCl_3$, 75.46 MHz): δ (ppm) = 170.10, 169.98, 169.60 (CO × 3), 155.16 (3-Ar), 143.65 (α-P, 1-Ar), 132.20 (β-P), 129.83 (5-Ar), 128.25 (6-Ar), 123.22 (4-Ar), 119.48 (meso-P), 116.28 (2-Ar), 98.66 (1-R), 70.59 (3-R), 70.28 (2-R), 68.38 (4-R), 61.86 (5-R), 20.61 (Me). FAB-HRMS (m/z) = $[M+H]^+$ calcd for $C_{88}H_{87}N_4O_{32}$, 1711.52979; found, 1711.52702.

Zinc(II) 5,10,15,20-tetrakis[4-(β-D-xylotopyranosyloxy)phenyl]porphyrin (p-6c)

The similar procedure for *p*-**6a** was applied to *p*-**5c** (201 mg, 113 μmol) to give *p*-**6c** as a red purple solid (141 mg, 98 %). Purity (HPLC): >99 %. ^{1}H NMR (CD_3OD, 300.07 MHz): δ (ppm) = 8.81 (8H, s, β-P), 8.05 (8H, d, ^3J = 8.4 Hz, 2,6-Ar), 7.37 (8H, d, ^3J = 8.7 Hz, 3,5-Ar), 5.18 (4H, d, ^3J = 7.5 Hz, 1-R), 4.06 ~ 4.00 (8H, m, 5-R), 3.76 ~ 3.43 (12H, m, 2,3,4-R). ^{1}H NMR (DMSO-d_6, 300.07 MHz): δ (ppm) = 8.82 (8H, s, β-P), 8.10 (8H, br, 2,6-Ar), 7.45 (8H, br, 3,5-Ar), 5.54 (4H, br, 2 or 4-RO*H*), 5.23 (8H, br, 1-R, 3-ROH), 5.17 (4H, br, 2 or 4-RO*H*), 3.91 (8H, br, 5-R), 3.91 ~ 3.58 (12H, m, 2,3,4-R). ^{13}C NMR (DMSO-d_6, 75.46 MHz): δ (ppm) =157.20 (4-Ar), 149.94 (α-P), 136.67 (1-Ar), 135.44 (2,6-Ar), 131.90

(β-P), 120.20 (meso-P), 114.56 (3,5-Ar), 101.26 (1-R), 76.88 (3-R), 73.56 (2-R), 69.78 (4-R), 66.12 (5-R). FAB-HRMS (m/z) = $[M]^+$ calcd for $C_{64}H_{60}N_4O_{20}Zn$, 1268.30869; found, 1268.30900.

Zinc(II) 5,10,15,20-tetrakis[3-(β-D-xylotopyranosyloxy)phenyl]porphyrin (m-6c)

The similar procedure for *p*-**6a** was applied to *m*-**5c** (183 mg, 103 μmol) to give *m*-**6c** as a red purple solid (120 mg, 92 %). Purity (HPLC): 95 %. ^{1}H NMR (CD_3OD, 300.07 MHz): δ (ppm) = 8.88 (8H, s, β-P), 7.94 ~ 7.87 (8H, m, 2,6-Ar), 7.70 ~ 7.65 (4H, m, 5-Ar), 7.51 ~ 7.49 (4H, m, 4-Ar), 5.15 (4H, d, ^3J = 7.5 Hz, 1-R), 3.94 ~ 3.89 (4H, m, 5-R), 3.63 ~ 3.36 (16H, m, 2,3,4,5-R). ^{1}H NMR (DMSO-d_6, 300.07 MHz): δ (ppm) = 8.81 (8H, s, β-P), 7.79 (8H, br, 2,6-Ar), 7.70 ~ 7.67 (4H, m, 5-Ar), 7.48 ~ 7.45 (4H, m, 4-Ar), 5.47 (4H, br, 2-RO*H*), 5.14 (8H, br, 1-R, 3-RO*H*), 5.05 (4H, m, 4-RO*H*), 3.82 ~ 3.66 (4H, m, 5-R), 3.51 ~ 3.17 (16H, m, 2,3,4,5-R). ^{13}C NMR (DMSO-d_6, 75.46 MHz): δ (ppm) =155.88 (3-Ar), 149.57 (α-P), 144.36 (1-Ar), 132.01 (β-P), 128.81 (5-Ar), 127.82 (6-Ar), 122.82 (4-Ar), 120.22 (meso-P), 115.79 (2-Ar), 101.42 (1-R), 76.65 (3-R), 73.56 (2-R), 69.65 (4-R), 65.94 (5-R). FAB-HRMS (m/z) = $[M]^+$ calcd for $C_{64}H_{60}N_4O_{20}Zn$, 1268.30869; found, 1268.30957.

5,10,15,20-Tetrakis[4-(β-D-xylotopyranosyloxy)phenyl]porphyrin (p-8c)

The similar procedure for *p*-**6a** was applied to *p*-**7c** (118 mg, 68.9 mmol) to give *p*-**8c** as a red solid (78.1 mg, 94 %). Purity (HPLC): 98 %. ^{1}H NMR (CD_3OD, 300.07 MHz): δ (ppm) = 8.85 (8H, br, β-P), 8.10 (8H, d, ^3J = 8.4 Hz, 2,6-Ar), 7.48 (8H, d, ^3J = 8.4 Hz, 3,5-Ar), 5.24 (4H, d, ^3J = 7.2 Hz, 1-R), 4.11 ~ 4.05 (4H, m, 5-R), 3.81 ~ 3.51 (16H, m, 2,3,4,5-R). ^{1}H NMR (DMSO-d_6, 300.07 MHz): δ (ppm) = 8.86 (8H, s, β-P), 8.14 (8H, m, 2,6-Ar), 7.52 ~ 7.43 (8H, m, 3,5-Ar), 5.24 (4H, d, ^3J = 7.2 Hz, 1-R), 5.77 ~ 4.80 (12H, m, 2,3,4-RO*H*), 3.90 (4H, d, ^3J = 6.3 Hz, 5-R), 3.77 ~ 3.34 (16H, m, 2,3,4,5-R), -2.92 (2H, br, N*H*). ^{13}C NMR (DMSO-d_6, 75.46 MHz): δ (ppm) = 157.61 (4-Ar), 135.64 (α-P and 1-Ar), 135.09 (2,6-Ar), 131.18 (β-P), 119.94 (meso-P), 114.91 (3,5-Ar), 101.24 (1-R), 76.86 (3-R), 73.55 (2-R), 69.74 (4-R), 66.15 (5-R). FAB-HRMS (m/z) = [M+H]+ calcd for $C_{64}H_{63}N_4O_{20}$, 1207.40302; found, 1207.40263.

5,10,15,20-Tetrakis[3-(β-D-xylotopyranosyloxy)phenyl]porphyrin (m-8c)

The similar procedure for *p*-**6a** was applied to *m*-**7c** (105 mg, 61.3 mmol) to give *m*-**8c** as a (67.3 mg, 91 %). Purity (HPLC): 95 %. ^{1}H NMR (DMSO-d_6, 300.07 MHz): δ (ppm) = 8.88 (8H, br, β-P), 7.85 (8H, m, 2,6-Ar), 7.77 ~ 7.71 (4H, m, 5-Ar), 7.56 ~7.46 (4H, m, 4-Ar), 5.17 (4H, d, ^3J = 6.9 Hz, 1-R), 3.75

~ 3.73 (4H, m, 5-R), 3.73 ~ 3.25 (16H, m, 2,3,4,5-R), -2.96 (2H, br, N*H*). ^{13}C NMR (DMSO-d_6, 75.46 MHz): δ (ppm) = 156.12 (3-Ar), 124.80 (α-P, 1-Ar), 131.72 (β-P), 128.76 (5-Ar), 128.27 (6-Ar), 122.82 (4-Ar), 119.91 (meso-P), 116.35 (2-Ar), 101.45 (1-R), 76.64 (3-R), 73.46 (2-R), 69.65 (4-R), 65.99 (5-R). FAB-HRMS (m/z) = $[M+H]^+$ calcd for $C_{64}H_{63}N_4O_{20}$, 1207.40302; found, 1207.40359.

2-4-4. Arabinopyranosylated Compounds (d)

2,3,4-Tri-O-acetyl-α-D-arabinopyronosyl bromide (3d)

Anhydrous D-arabinose (6.5 g, 43 mmol) and acetyl bromide (31 mL, 177 mmol) were stirred. This mixture was stirred for 2 ~ 3 h in ice water bath. After 2 ~ 3 h, the solution was added $CHCl_3$ (100 mL). The solution was washed with ice water (150 mL x 2), saturated cold $NaHCO_3$ (aq) (150 mL x 2), and dried over Na_2SO_4. The filtered solution was evaporated to dryness and pure product was crystallized from CH_2Cl_2/Et_2O to give a white solid (12 g, 82 %). ^{1}H NMR ($CDCl_3$, 300.07 MHz): δ (ppm) = 6.71 (1H, d, ^3J = 3.6 Hz, 1-R), 5.41 (2H, m, 3, 4-R), 5.09 (2H, ddd, ^3J= 13.2 MHz, ^3J= 13.2 MHz, ^3J= 11.4 MHz, ^2J= 3.9 MHz, 2-R), 4.22 (1H, d, ^3J= 13.2 Hz, 5-R), 4.13 (1H, dd, ^3J= 13.5 Hz, ^2J= 1.8 Hz, 5-R), 2.16, 2.13, 2.11, 2.05 ((3H, s, Me) × 4).

4-(2,3,4-Tri-O-actyl-β-D-arabinopyranosiloxy)benzaldehyde (p-4d)

The similar procedure for *p*-**4b** was applied to *p*-hydroxybenzaldehyde (2.2 g, 18 mmol) and **3d** (4.0 g, 12 mmol) to give *p*-**4d** as colorless oil (1.9 g, 43 %). ^{1}H NMR ($CDCl_3$, 300.07 MHz): δ (ppm) = 9.93 (1H, s, CHO), 7.86 (2H, d, ^3J = 8.4 Hz, 2,6-Ar), 7.13 (2H, d, ^3J = 8.4 Hz, 3,5-Ar), 5.45 (1H, dd, ^3J = 6.0 Hz, ^2J = 8.1 Hz, 3-R), 5.43 (1H, br, 4-R), 5.24 (1H, d, ^3J = 6.0 Hz, 1-R), 5.20 (1H, dd, ^3J = 3.6 Hz, ^2J = 8.7 Hz, 2-R), 4.13 (1H, dd, ^3J = 4.5 Hz, ^2J = 12.6 Hz, 5-R), 3.80 (1H, dd, ^3J = 2.4 Hz, ^2J = 12.6 Hz, 5-R), 2.15, 2.12, 2.10 ((3H, s, Me) × 3). ^{13}C NMR ($CDCl_3$, 75.46 MHz): δ (ppm) = 190.70 (CHO), 169.96, 169.83, 169.22 (CO × 3), 161.01 (4-Ar), 131.57 (1-Ar), 131.26 (2,6-Ar), 116.38 (3,5-Ar), 97.34 (1-R), 69.09 (3-R), 68.28 (2-R), 66.47 (4-R), 62.25 (5-R), 20.33, 20.20, 19.13 (Me × 3).

3-(2,3,4-Tri-O-actyl-β-D-arabinopyranosiloxy)benzaldehyde (m-4d)

The similar procedure for *p*-**4b** was applied to *m*-hydroxybenzaldehyde (2.2 g, 18 mmol) and **3d** (4.0 g, 12 mmol) to give *m*-**4d** as colorless oil (1.4 g, 32 %). ^{1}H NMR ($CDCl_3$, 300.07 MHz): δ (ppm) = 9.96 (1H, s, CHO), 7.58~7.44 (3H, m, 2,5,6-Ar), 7.27 (1H, m, 4-Ar), 5.42 (1H, m, 3-R), 5.32 (1H, m, 4-

R), 5.16 (1H, m, 1,2-R), 4.10 (1H, dd, ^3J = 4.2 Hz, ^2J = 12.9 Hz, 5-R), 3.78 (1H, dd, ^3J = 2.1 Hz, ^2J = 12.6 Hz, 5-R), 2.13, 2.09, 2.07 ((3H, s, Me) × 3). ^{13}C NMR ($CDCl_3$, 75.46 MHz): δ (ppm) = 191.67 (CHO), 170.14, 170.01, 169.36 (CO × 3), 157.02 (1-Ar), 130.19 (3,5-Ar), 125.07 (6-Ar), 123.21 (4-Ar), 115.41 (2-Ar), 98.19 (1-R), 69.40 (3-R), 68.52 (2-R), 66.79 (4-R), 62.55 (5-R), 20.47, 20.36 (Me× 3).

*Zinc(II) 5,10,15,20-tetrakis[4-(2,3,4-tri-O-acetyl-β-D-arabinopyranosyloxy)phenyl]porphyrin (p-**5d**)*

The similar procedure for *p*-**5a** was applied to *p*-**4d** (2.9 g, 7.6 mmol) to give *p*-**5d** as a red solid (1.6 g, 63 %). Purity (HPLC): 96 %. ^{1}H NMR ($CDCl_3$, 300.07 MHz): δ (ppm) = 8.85 (8H, s, β-P), 8.14 (8H, d, ^3J = 8.4 Hz, 2,6-Ar), 7.41 (8H, d, ^3J = 8.7 Hz, 3,5-Ar), 5.58 (4H, dd, ^3J = 6.3 Hz, ^3J = 8.7 Hz, 3-R), 5.44 (8H, m, 1,4-R), 5.15 (4H, dd, ^3J = 9.0 Hz, 2-R), 4.32 (4H, dd, ^3J = 3.6 Hz, ^2J = 11.4 Hz, 5-R), 3.96 (4H, d, ^3J = 11.4 Hz, 5-R), 2.28, 2.24, 2.17 ((9H, s, Me) × 3). ^{13}C NMR ($CDCl_3$, 75.46 MHz): δ (ppm) = 170.53, 170.40, 169.77 (CO × 3), 156.47 (4-Ar), 150.47 (α-P), 137.62 (1-Ar), 135.50 (2,6-Ar), 132.06 (β-P), 120.46 (meso-P), 114.89 (3,5-Ar), 98.87 (1-R), 69.88 (3-R), 69.09 (2-R), 67.25 (4-R), 62.96 (5-R), 20.83, 20.65 (CH_3 × 2). FAB-HRMS (m/z) = $[M]^+$ calcd for $C_{88}H_{84}N_4O_{32}Zn$, 1772.436; found, 1772.4337.

*Zinc(II) 5,10,15,20-tetrakis[3-(2,3,4-tri-O-acetyl-β-D-arabinopyranosyloxy)phenyl]porphyrin (m-**5d**)*

The similar procedure for *p*-**5a** was applied to *m*-**4d** (1.7 g, 4.3 mmol) to give *m*-**5d** as a red solid (1.1 g, 60 %). Purity (HPLC): >99 %. ^{1}H NMR ($CDCl_3$, 300.07 MHz): δ (ppm) = 8.97 (8H, br, β-P), 7.90 (8H, m, 2,6-Ar), 7.67 (4H, m, 5-Ar), 7.43 (4H, m, 4-Ar), 5.54 (4H, m, 3-R), 5.34 (8H, m, 1,4-R), 5.16 (4H, m, 2-R), 4.12 (4H, m, 5-R), 3.73 (4H, m, 5-R), 3.44 ~ 3.40 (4H, m, 5-R), 2.11, 2.09, 2.03 ((9H, s, Me) × 3). ^{13}C NMR ($CDCl_3$, 75.46 MHz): δ (ppm) = 170.40, 170.25, 169.60 (CO × 3), 155.19 (3-Ar), 150.17 (α-P), 144.30 (1-Ar), 132.15 (β-P), 129.69 (5-Ar), 127.65 (6-Ar), 123.09 (4-Ar), 120.49 (meso-P), 116.07 (2-Ar), 98.95 (1-R), 69.80 (3-R), 68.98 (2-R), 67.05 (4-R), 62.81 (5-R), 20.72 (Me). FAB-HRMS (m/z) = $[M]^+$ calcd for $C_{88}H_{84}N_4O_{32}Zn$, 1772.436; found, 1772.4303.

*5,10,15,20-Tetrakis[4-(2,3,4-tri-O-acetyl-β-D-arabinopyranosyloxy)phenyl]porphyrin (p-**7d**)*

The similar procedure for *p*-**7a** was applied to *p*-**4d** (2.10 g, 5.52 mmol) to give *p*-**7d** as a red solid (0.63 g, 36 %). Purity (HPLC): >99 %. ^{1}H NMR ($CDCl_3$, 300.07 MHz): δ (ppm) = 8.85 (8H, s, β-P), 8.14 (8H, d, ^3J = 8.4 Hz, 2,6-Ar), 7.41 (8H, d, ^3J = 8.7 Hz, 3,5-Ar), 5.58 (4H, dd, ^3J = 6.3 Hz, ^3J = 8.7 Hz,

3-R), 5.44 (8H, m, 1,4-R), 5.15 (4H, d, ^3J = 9.0 Hz, 2-R), 4.32 (4H, dd, ^3J = 3.6 Hz, ^2J = 11.4 Hz, 5-R), 3.96 (4H, dd, ^2J = 11.4 Hz, 5-R), 2.28, 2.24, 2.17 ((9H, s, Me) × 3), -2.82 (2H, br, N*H*). ^{13}C NMR ($CDCl_3$, 75.46 MHz): δ (ppm) = 170.53, 170.41, 169.77 (CO × 3), 156.61 (α-P and 1-Ar), 136.96 (4-Ar), 135.68 (2,6-Ar), 131.12 (β-P), 119.47 (meso-P), 115.02 (3,5-Ar), 98.84 (1-R), 69.88 (3-R), 69.09 (2-R), 67.23 (4-R), 62.96 (5-R), 20.88, 20.85, 20.68 (Me × 3). FAB-HRMS (m/z) = $[M+H]^+$ calcd for $C_{88}H_{87}N_4O_{32}$, 1711.52979; found, 1711.53042.

*5,10,15,20-Tetrakis[3-(2,3,4-tri-O-acetyl-β-D-arabinopyranosyloxy)phenyl]porphyrin (m-**7d**)*

The similar procedure for *p*-**7a** was applied to *m*-**4d** (1.62 g, 4.2 mmol) to give *m*-**7d** as a reddish purple solid (493 mg, 37 %). Purity (HPLC): >99 %. ^{1}H NMR ($CDCl_3$, 300.07 MHz): δ (ppm) = 8.88 (8H, s, β-P), 7.95 (8H, m, 2,6-Ar), 7.68 (4H, m, 5-Ar), 7.48 (4H, m, 4-Ar), 5.70 (4H, t, ^3J = 8.7 Hz, 3-R), 5.37 (8H, m, 1,4-R), 5.16 (4H, m, 2-R), 4.16 (4H, m, 5-R), 3.79 (4H, m, 5-R), 2.14, 2.09, 2.06 ((9H, s, Me) × 3), -2.78 (2H, br, N*H*). ^{13}C NMR ($CDCl_3$, 75.46 MHz): δ (ppm) = 170.27, 170.12, 169.52 (CO × 3), 155.16 (3-Ar), 143.51 (α-P and 1-Ar), 131.21 (β-P), 129.63 (5-Ar), 127.75 (6-Ar), 123.11 (4-Ar), 119.42 (meso-P), 116.27 (2-Ar), 98.86 (1-R), 69.69 (3-R), 68.85 (2-R), 67.05 (4-R), 62.81 (5-R), 20.62, 20.44, 20.30 (Me × 3). FAB-HRMS (m/z) = $[M+H]^+$ calcd for $C_{88}H_{87}N_4O_{32}$, 1711.52979; found, 1711.52918.

*Zinc(II) 5,10,15,20-tetrakis[4-(β-D-arabinopyranosyloxy)phenyl]porphyrin (p-**6d**)*

The similar procedure for *p*-**6a** was applied to *p*-**5d** (106 mg, 59.8 μmol) to give *p*-**6d** as a red solid (74.3 mg, 98 %). Purity (HPLC): 99 %. ^{1}H NMR (DMSO-d_6, 300.07 MHz): δ (ppm) = 8.81 (8H, s, β-P), 8.09 (8H, d, ^3J = 8.4 Hz, 2,6-Ar), 7.42 (8H, d, ^3J = 8.4 Hz, 3,5-Ar), 5.39 (4H, d, ^3J = 4.8 Hz, 2-RO*H*), 5.19 (4H, d, ^3J = 6.9 Hz, 1-R), 4.95 (4H, d, ^3J = 5.4 Hz, 3-RO*H*), 4.76 (4H, d, ^3J = 3.9 Hz, 4-RO*H*), 3.92~3.89 (4H, m, 5-R), 3.81 (12H, br, 2,4,3-R), 3.60 (4H, br, 5-R). ^{13}C NMR (DMSO-d_6, 75.46 MHz): δ (ppm) = 157.28 (4-Ar), 149.94 (α-P), 136.56 (1-Ar), 135.48 (2,6-Ar), 131.88 (β-P), 120.20 (meso-P), 114.61 (3,5-Ar), 101.32 (1-R), 73.01 (3-R), 70.83 (2-R), 68.06 (4-R), 66.27 (5-R). FAB-HRMS (m/z) = $[M+Na]^+$ calcd for $C_{64}H_{60}N_4O_{20}ZnNa$, 1291.29846; found, 1291.29604.

*Zinc(II) 5,10,15,20-tetrakis[3-(β-D-arabinopyranosyloxy)phenyl]porphyrin (m-**6d**)*

The similar procedure for *p*-**6a** was applied to *m*-**5d** (100 mg, 56.4 μmol) to give *m*-**6d** as a red solid

(67.3 mg, 96 %). Purity (HPLC): 99 %. ^{1}H NMR (CD_3OD, 300.07 MHz): δ (ppm) = 8.86 (8H, s, β-P), 7.92 (4H, br, 2-Ar), 7.87 ~ 7.84 (4H, m, 6-Ar), 7.69 ~ 7.64 (4H, m, 5-Ar), 7.52 ~ 7.49 (4H, m, 4-Ar), 5.13 (4H, d, ^3J = 7.2 Hz, 1-R), 3.96 ~ 3.34 (20H, m, 2,3,4,5-R). ^{1}H NMR (DMSO-d_6, 300.07 MHz): δ (ppm) = 8.83 (8H, s, β-P), 7.81 (8H, br, 2,6-Ar), 7.73 ~ 7.68 (4H, m, 5-Ar), 7.49 ~ 7.46 (4H, m, 4-Ar), 5.53 ~ 4.54 (12H, br, 2,3,4-RO*H*), 5.13 (4H, d, ^3J = 6.6 Hz, 1-R), 3.76 ~ 3.17 (20H, m, 2,3,4,5-R). ^{13}C NMR (DMSO-d_6, 75.46 MHz): δ (ppm) = 155.96 (3-Ar), 149.63 (α-P), 144.39 (1-Ar), 132.05 (β-P), 128.70 (5-Ar), 127.84 (6-Ar), 122.84 (4-Ar), 120.30 (meso-P), 115.88 (2-Ar), 101.39 (1-R), 72.78 (3-R), 70.78 (2-R), 67.93 (4-R), 66.07 (5-R). FAB-HRMS (m/z) = $[M+Na]^+$ calcd for $C_{64}H_{60}N_4O_{20}ZnNa$, 1291.29846; found, 1291.29759.

5,10,15,20-Tetrakis[4-(β-D-arabinopyranosyloxy)phenyl]porphyrin (p-8d)

The similar procedure for *p*-**6a** was applied to *p*-**7d** (86 mg, 50.2 mmol) to give *p*-**8d** as a red solid (58.1 mg, 96 %). Purity (HPLC): 99 %. ^{1}H NMR (CD_3OD, 300.07 MHz): δ (ppm) = 8.89 (8H, s, β-P), 8.11 (8H, d, ^3J = 8.7 Hz, 2,6-Ar*H*), 7.51 (8H, d, ^3J = 8.1 Hz, 3,5-Ar), 5.21 (4H, d, ^3J = 6.0 Hz, 1-R), 4.11 ~ 3.77 (20H, m, 2,4,3,5-R). ^{1}H NMR (DMSO-d_6, 300.07 MHz): δ (ppm) = 8.87 (8H, s, β-P), 8.14 (8H, d, ^3J = 8.1 Hz, 2,6-Ar), 7.45 (8H, d, ^3J = 8.4 Hz, 3,5-Ar), 5.41 (4H, br, 2-RO*H*), 5.21 (4H, d, ^3J = 7.2 Hz, 1-R), 4.98 (4H, m, 3-RO*H*), 4.77 (4H, m, 4-RO*H*), 3.92 ~ 3.50 (20H, m, 2,3,4,5-R), -2.92 (2H, br, NH). ^{13}C NMR (DMSO-d_6, 75.46 MHz): δ (ppm) =157.72 (4-Ar), 135.67 (α-P and 1-Ar), 134.96 (2,6-Ar), 131.80 (β-P), 119.99 (meso-P), 114.98 (3,5-Ar), 101.26 (1-R), 72.93 (3-R), 70.75 (2-R), 68.08 (4-R), 66.33 (5-R). FAB-HRMS (m/z) = $[M+H]^+$ calcd for $C_{64}H_{63}N_4O_{20}$, 1207.40302; found, 1207.40339.

5,10,15,20-Tetrakis[3-(β-D-arabinopyranosyloxy)phenyl]porphyrin (m-8d)

The similar procedure for *p*-**6a** was applied to *m*-**7d** (72 mg, 42.0 mmol) to give *m*-**8d** as a red solid (49.7 mg, 98 %). Purity (HPLC): >99 %. ^{1}H NMR (CD_3OD, 300.07 MHz): δ (ppm) = 8.91 (8H, br, β-P), 7.94 (4H, br, 2-Ar), 7.85 (4H, m, 6-Ar), 7.70 (4H, m, 5-Ar), 7.56 (4H, m, 4-Ar), 5.13 (4H, d, ^3J = 7.2 Hz, 1-R), 3.94 ~ 3.84 (12H, m, 2,4,5-R), 3.69 ~ 3.63 (8H, m, 3,5-R). ^{1}H NMR (DMSO-d_6, 300.07 MHz): δ (ppm) = 8.89 (8H, s, β-P), 7.84 (4H, br, 2-Ar), 7.74 (4H, br, 6-Ar), 7.60 (4H, m, 5-Ar), 7.49 (4H, m, 4-Ar), 5.30 (4H, d, ^3J = 4.5 Hz, 2-RO*H*), 5.14 (4H, d, ^3J = 7.2 Hz, 1-R), 4.87 (4H, d, ^3J = 5.4 Hz, 3-RO*H*), 4.67 (4H, d, ^3J = 4.2 Hz, 4-RO*H*), 3.71 (8H, m, 2,5-R), 3.66 ~ 3.50 (12H, m, 3,4,5-R), -2.98 (2H, br, N*H*). ^{13}C NMR (DMSO-d_6, 75.46 MHz): δ (ppm) = 156.17 (3-Ar), 142.77 (α-P and 1-Ar), 131.46 (β-P),

128.65 (5-Ar), 128.21 (6-Ar), 122.81 (4-Ar), 119.98 (meso-P), 116.39 (2-Ar), 101.26 (1-R), 72.75 (3-R), 70.73 (2-R), 67.87 (4-R), 66.04 (5-R). FAB-HRMS (m/z) = $[M+H]^+$ calcd for $C_{64}H_{63}N_4O_{20}$, 1207.40302; found, 1207.40118.

2-5. References

1. R. Bonnett, Photosensitizers of the Porphyrin and Phthalocyanine Series for Photodynamic Therapy. Chem. Soc. Rev. 24 (1995) 19-33.
2. I. Okura, Photosensitization of Porphyrins and Phthalocyanines. Kodansha. Tokyo. (2000) 6-7.
3. R. Bonnett, Chemical Aspects of Photodynamic Therapy. Taylor & Francis, London. (2000) 164-165.
4. M. Momenteau, D. Oulmi, Ph. Maillard, A. Croisy, Photodynamic Therapy of cancer II. SPIE. 2325 (1994) 13-23.
5. Ph. Maillard, JL. Guerquin-Kern, M. Momenteau, Catalytic properties of iron and manganese glycoconjugated porphyrins. Tetrahedron Lett. 32 (1991) 4901-4904.
6. K. Kohara, H. Higashio, Y. Yamaguchi, M. Koketsu, T. Odashima, Synthesis and Characterization of New Style of Water-Soluble Glycoconjgated Porphyrins as a Spectrophotometric Reagent for Metal Ions. Bull. Chem. Soc. Jpn. 67 (1994) 668-679.
7. D. Oulmi, P. Maillard, J-L. Guerquin-Kern, C. Huel, M. Momenteau, Glycoconjugated Porphyrins. 3. Synthesis of Flat Amphiphilic Mixed *meso*-(Glycoconjugated aryl)arylporphyrins and Mixed *meso*-(Glycosylated aryl)alkylporphyrins Bearing Some Mono- and Disaccharide Groups. J. Org. Chem. 60 (1995) 1554-1564.
8. Y. Mikata, Y. Onchi, K. Tabata, S. Ogura, I. Okura, H. Ono, S. Yano, Sugar-dependent photocytotoxic property of tetra- and octa- glycoconjugated tetraphenylporphyrins. Tetrahedron Lett. 39 (1998) 4505-4508.
9. A. Hamazawa, I. Kinoshita, B. Breedlove, K. Isobe, M. Shibata, T. Kakuchi, S. Hirohara, M. Obata, Y. Mikata, S. Yano, meso-Tetraphenylporphyrin Having Hexa-maltosyl and Decyl Chain as an Amphiphilic Photosensitizer toward Photodynamic Therapy. Chem. Lett. 3 (2002) 388-389.
10. I. Okura, Photosensitization of Porphyrins and Phthalocyanines. Kodansha. Tokyo. (2000) 9-12.
11. S. Halazy, V. Berges, A. Ehrhard, C. Danzin, *Ortho*- and *para*-(difuluoromethyl)aryl-β-D-glucose: a new class of enzymeactivated irrevesible inhibitors of β-glucosidases. Bioorg. Chem. 18 (1990)

330-344.

12. K. M. Smith, PORPHYRINS AND METALOPORPHYRINS. ELSEVIER SCIENTIFIC PUBLISHING COMPANY. New York. (1975) 19-27.
13. M. Gouterman, A. Absorption Spectra. *The Porphyrins*, 3; D. Dolphine., Academic Press. New York. 3 (1978) 12-24.
14. R. Bonnett, Chemical Aspects of Photodynamic Therapy. Taylor & Francis, London. (2000) 149-156.
15. K. M. Smith, PORPHYRINS AND METALOPORPHYRINS. ELSEVIER SCIENTIFIC PUBLISHING COMPANY. New York. (1975) 526-535.
16. J.O. Alben, Infrared Spectroscopy of Porphyrins. *The Porphyrins*, 3; D. Dolphine., Academic Press. New York. 3 (1978) 323-332.

Chapter 3

In Vitro Study of Glycocojugated Porphyrins

3-1. Introduction

In photodynamic therapy (PDT), photosensitizers generate reactive singlet oxygen ($^1O_2$) which are able to damage tumor cells [1-6]. Hence the quantum yield of $^1O_2$ generation is fundamental performance for photosensitizers. However the photodynamic effect depends on not only $^1O_2$ generation ability but also (1) cellular uptake, (2) subcellular localization and (3) aggregation properties in cytoplasm. Cellular uptake generally depends on hydrophobicity to pass through a hydrophobic cell membrane [7,8]. Hydrophobicity of pharmaceuticals is usually characterized by a partition coefficient (Log *P*) between water and *n*-octanol [9]. Zheng et al. investigated the importance of lipophilicity to the photodynamic effect for purpurin derivatives [10]. On the other hand, the water soluble porphyrin derivative complex with serum albumin, which are most abundant proteins of blood plasma, to penetrate in the cell membranes [7,8,11]. It was reported that (bovine or human) serum albumin has two distinctive binding sites, usually called as site I and site II [11]. Fluorescence energy transfer experiment indicates Hematin and other porphyrin derivatives binds in the vicinity of Trp-214 in human serum albumin. Rosenberger and Margalit reported that the binding constants of hematoporphyrin derivatives whose photocytotoxicity was discovered by Lipson and Schwartz in 1960s [1,12,13]. The binding to serum albumin should play an important role to cellular uptake especially for less hydrophobic porphyrins, while hydrophobic porphyrins strongly interacts with cell membrane [13]. The photodynamic effect is also highly dependent on the localization in cytoplasm [14-20]. Photosensitizers usually distributes in plasma membrane, mitochondria and in some cases lysosomes [14-20]. In addition, photosensitizer such as porphyrin derivatives tends to make an aggregation form in cytoplasm [21-23]. These aggregation forms reduces the fluorescence life time and $^1O_2$ quantum yields [21] to diminish the photocytotoxicity.

In chapter 2, the author designed and synthesized glycoconjugated porphyrins (Chart 3-1). In this chapter, the hydrophobicity parameters of glycoconjugated porphyrins were estimated by Shake-Flask method and reversed phase high performance liquid chromatography (RP-HPLC). In addition, binding equilibrium of some photosensitizers to bovine serum albumin (BSA) were also studied by fluorometric titration. These glycoconjugated porphyrins were subjected to test the cellular uptake by HeLa cells and the photocytotoxicity *in vitro*. These cellular uptake behavior and photocytotoxicity were discussed on the basis of hydrophobicity, binding properties to BSA and photochemical study in aqueous media such as cytoplasm for these photosensitizers.

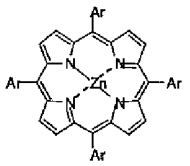

p- or *m*-**5a-d**
(R = Ac)

p- or *m*-**6a-d**
(R = H)

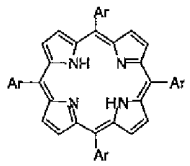

p- or *m*-**7a-d**
(R = Ac)

p- or *m*-**8a-d**
(R = H)

(Ar)$_4$ porphyrin

Types of Glycopyranosyl Groups	Substitution Position: *para*-Substituted (denoted as *p*-)	Substitution Position: *meta*-Substituted (denoted as *m*-)
a: D-glucose R = Ac for **5, 7** R = H for **6, 8**	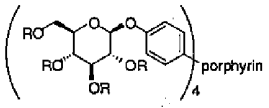	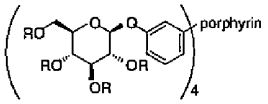
b: D-galactose R = Ac for **5, 7** R = H for **6, 8**	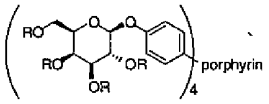	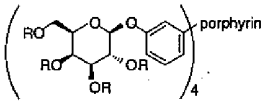
c: D-xylose R = Ac for **5, 7** R = H for **6, 8**	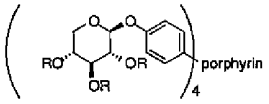	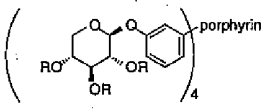
d: D-arabinose R = Ac for **5, 7** R = H for **6, 8**	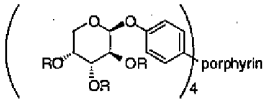	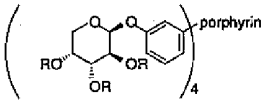

Chart 3-1

3-2. Results and discussion

3-2-1. Hydrophobicity parameters of acetylated glycoconjugated porphyrins 5 and 7

Log *P* values have been usually determined by the conventional Shake-Flask method. However, this method requires trace quantitative analysis, which is difficult for hydrophobic or hydrophilic species and/or strongly aggregating species. An alternative method is reversed phase high performance liquid chromatography (RP-HPLC) [24-26]. The partition ratio can be correlated with the capacity factor *k'*. Figure 3-1 shows typical chromatograms obtained by RP-HPLC. Under the experimental conditions used, the chromatograms and retention times (t_R) of the acetylated glycoconjugated porphyrins **5** and **7** were independent of sample concentration in the range from 1 to 0.01 μM. Hence, value obtained should

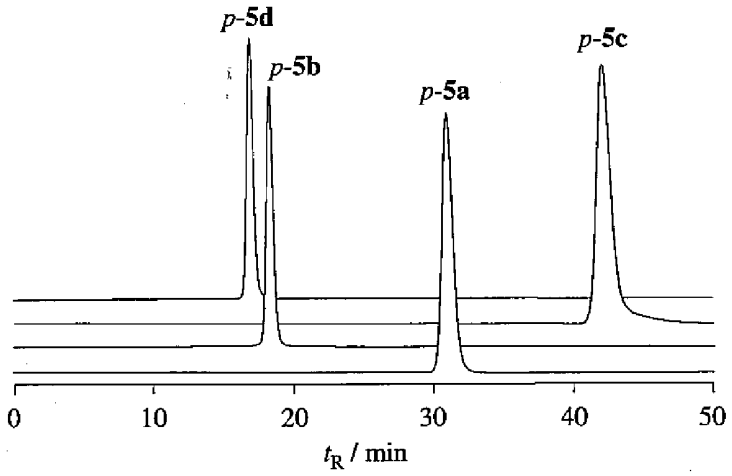

Figure 3-1 Chromatograms of *p*-5 on RP-HPLC.

be those of the monomeric form of the glycoconjugated porphyrins. This represents an advantage of the RP-HPLC method over the Shake-Flask method. The capacity factor *k'* can be calculated by means of the following equation, in which t_R and t_0 are the retention time of the photosensitizers and the dead time, respectively. A good linear relationship between Log *k'* and Log *P* was found as follows, where *a* and *b* are constants for a given HPLC system. Pyridine [9], benzaldehyde [25], quinoline [25], chlorobenzene

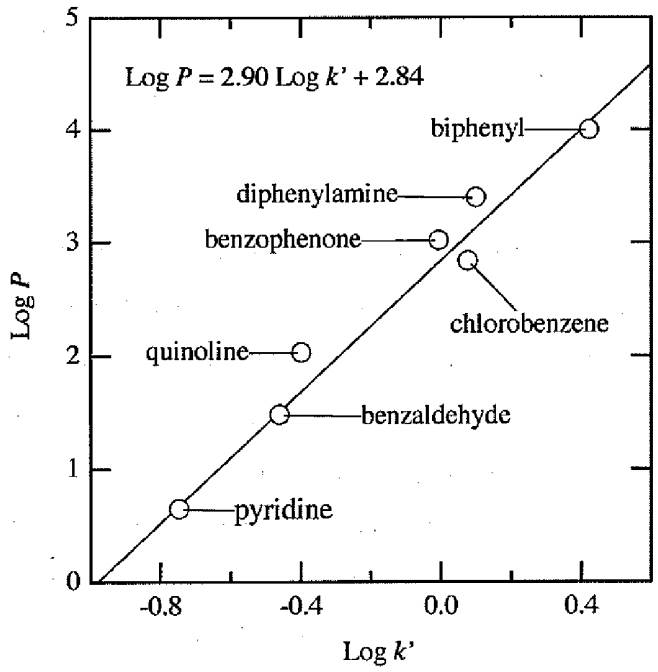

Figure 3-2 Calibration curve of Log *P* versus Log *k'*.

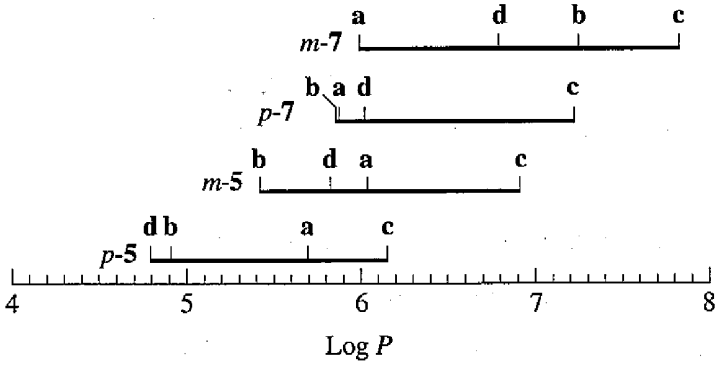

Figure 3-3 Summary of Log *P* values of **5** and **7**.

[9], benzophenone [25], diphenylamine [25] and biphenyl [25] were used as standards to calibrate our HPLC system. Figure 3-2 illustrates the calibration curve, which shows good linearity of Log*P* values against Log *k'* values. The Log *P* values of the porphyrins **5** and **7** were determined on the basis of the calibration. Figure 3-3 summarizes the results. The Log *P* values ranged from +4.8 to +7.8, so that most of the photosensitizers are less hydrophobic (Table 3-1). The hydrophobicity increases in the order of *p*-**5** < *m*-**5** < *p*-**7** < *m*-**7** for every sugar unit attached. The Zn^{2+} ion clearly reduces the hydrophobicity (**5** <

Table 3-1 Retention times (t_R) and Log *P* values of **5** and **7**

compounds	t_R / min	k'^a	Log *P*
p-**5a**	30.86	8.82	5.69
p-**5b**	18.23	4.80	4.91
p-**5c**	42.20	12.67	6.15
p-**5d**	16.84	4.36	4.79
m-**5a**	39.32	11.51	6.03
m-**5b**	25.46	7.10	5.41
m-**5c**	75.72	23.09	6.91
m-**5d**	34.17	9.87	5.83
p-**7a**	34.85	10.09	5.86
p-**7b**	34.50	9.97	5.85
p-**7c**	95.66	29.43	7.22
p-**7d**	39.23	11.48	6.02
m-**7a**	38.35	11.20	5.99
m-**7b**	97.15	29.90	7.24
m-**7c**	15.11	47.05	7.82
m-**7d**	68.81	20.89	6.79

[a] $k' = (t_R - t_0) / t_0$. The t_0 value was determined as 3.14 min using urasil. [b] Log *P* = 2.90 Log *k'* + 2.84, calibration curve is shown in Fig. 3-2.

7). In addition, the sugar units at *meta* position are less effective to gain hydrophilicity, probably due to the intramolecular interaction between vicinal sugar units. Interestingly, glucopyranosyl groups (**a**) seem to negate the chracteristics of the porphyrin ring to keep the Log *P* values constant.

3-2-2. Hydrophobicity parameters of deacetylated glycoconjugated porphyrins p-6 and p-8

The partition coefficients (Log *P* value) of monomeric form of deacetylated glycoconjugated porphyrins *p*-**6** and *p*-**8** ($c = 0.00695$ μM) between phosphate buffered saline (PBS) and *n*-octanol were determined by the conventional Shake-Flask method [9,27-29]. After equilibrating between PBS with *n*-octanol for 18 h, the concentration of photosensitizers in each phase was determined by the HPLC system equipped with UV-vis detector at 420 nm. The average Log *P* values of six replicate experiments ranged from -0.66 to -0.74, hence all photosensitizers are hydrophilic (Table 3-2). Because of the large standard deviation, however, the Shake-Flask method is not suitable to clarify the differences in Log *P* values between glycoconjugated porphyrins. The extremely low concentration condition ($c = 0.00695$ μM) was required to measure the concentration because of strongly aggregating tendency of glycoconjugated porphyrins. This may cause the low signal-to-noise ratio and the large standard deviation. The hydorophobicity of porphyrins *p*-**6** and *p*-**8** was also determined by the RP-HPLC method. Chromatogram of porphyrins *p*-**6** and *p*-**8** were independent of sample concentration in the range from 0.1 to 0.01 μM under the RP-HPLC condition used. The retention time t_R reflects the nature of the monomeric form of these photosensitizers. The t_R value varies ranged from 5.84 to 6.50 min and reflects the hydrophobicity (lipophilicity) of porphyrins *p*-**6** and *p*-**8**. The order of t_R value indicates the hydrophobicity increases in

Table 3-2 Log *P* values and RP-HPLC retaintion time (t_R) of **6** and **8**

	Shake Flask method	RP-HPLC
compounds	Log *P* [a]	t_R / min
p-**6a**	-0.74 ± 0.05	5.88
p-**6b**	-0.71 ± 0.03	5.84
p-**6c**	-0.70 ± 0.03	6.19
p-**6d**	-0.70 ± 0.03	6.10
p-**8a**	-0.71 ± 0.03	6.18
p-**8b**	-0.71 ± 0.02	6.16
p-**8c**	-0.69 ± 0.06	6.50
p-**8d**	-0.70 ± 0.02	6.42

[a] The Log *P* value of deacetylated glycoconjugated porphyrins was determined after incubation for 18 h. The values represent the means ± s.d. of six replicate experiments.

the order of *p*-**6** < *p*-**8** regardless of the sugar unit attached. In addition, the porphyrins having xylopyranosyl (**c**) and arabinopyranosyl (**d**) groups (i.e., pentose groups) showed higher hydrophobicities than those of glucopyranosyl (**a**) and galactopyranosyl (**b**) groups (i.e., hexose groups). The orders of hydrophobicity of glycoconjugated photosensitizers can be determined easily by RP-HPLC method, even though the Shake-Flask method is hardly performed.

3-2-3. Binding properties of deacetylated glycoconjugated porphyrins p-8 to BSA

Most of the deacetylated glycoconjugated porphyrins *p*-**8** might bounds abundant proteins such as serum albumin in *in vitro* experiments. Some water-soluble porphyrins complex with serum albumin to penetrate in cellular membranes [30-33]. Hence binding properties to albumin may affect the interaction with cells. The binding behavior of porphyrins *p*-**8** to BSA was studied by electronic absorption and fluorescence spectrometry. Each photosensitizers ($c = 5$ μM) was stirred gently with various concentration of BSA ($c = 0 \sim 35$ μM) in PBS for 24 h at 37 °C. Figure 3-4 and 3-5 shows the electronic absorption and fluorescence spectra of porphyrins *p*-**8a** after equilibration with various concentration of BSA. The peak area of Soret band of *p*-**8a** increased with an increase of the concentration of BSA, and this peak shows

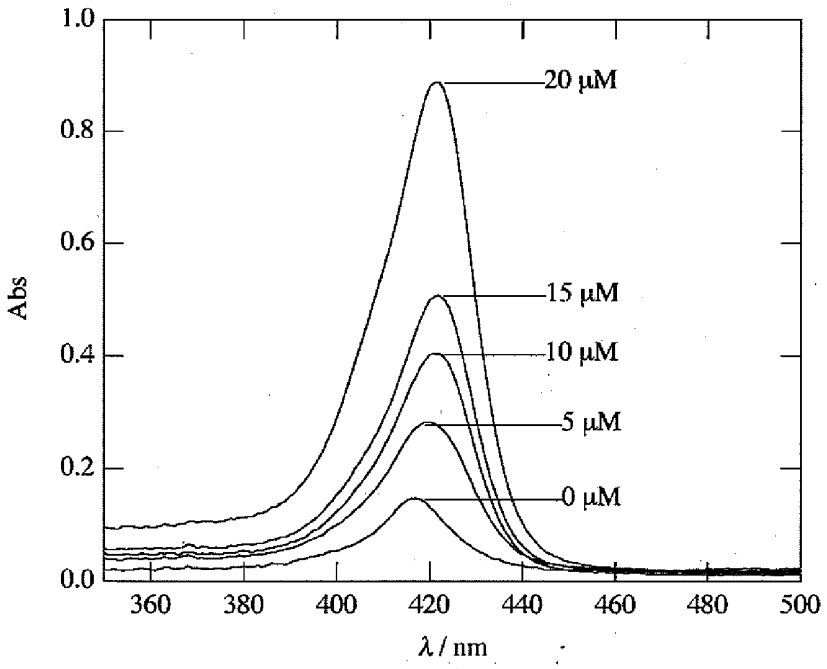

Figure 3-4 Electronic absorption spectra of *p*-**8a** (c = 5 μM) in PBS containing 1 % DMSO, in the presence of BSA at 37 °C. The BSA concentration ranged from 0 to 20 μM.

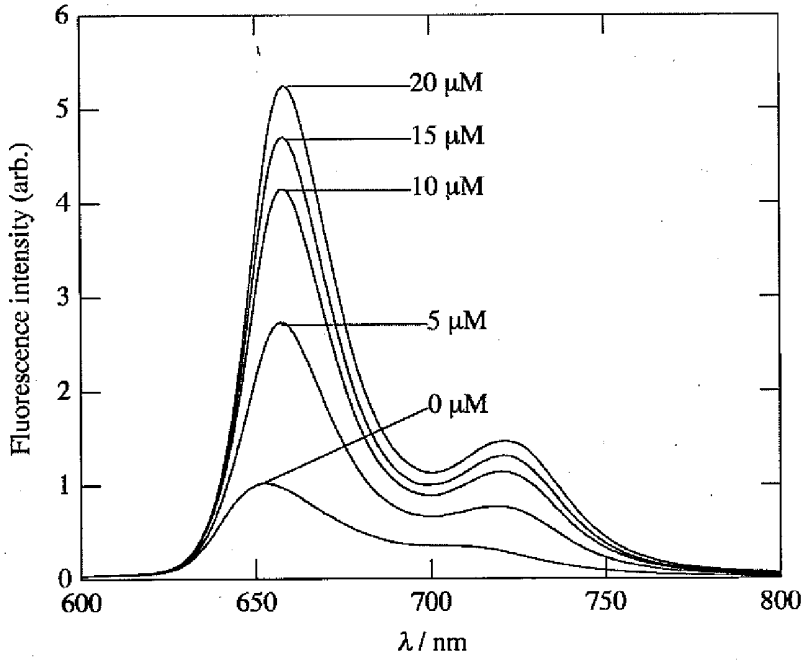

Figure 3-5 Luminescence spectra of *p*-**8a** (c = 5 μM) in PBS containing 1 % DMSO, in the presence of BSA at 37 °C. The BSA concentration ranged from 0 to 20 μM. λ_{ex} = 420 nm.

a bathochromic shift from 417 to 422 nm (Figure 3-4). The porphyrins *p*-**8b-d** showed the similar photochemical behavior of *p*-**8a**. The maximum absorption wavelength (λ_{max}) of Soret band of BSA-free porphyrins are 417 nm (*p*-**8a**), 416.5 nm (*p*-**8b**), 416 nm (*p*-**8c**) and 416.5 nm (*p*-**8d**), while the λ_{max} of Soret band of BSA-porphyrin complexes are 422 nm (*p*-**8a**), 422.5 nm (*p*-**8b**), 423 nm (*p*-**8c**) and 423.5 nm (*p*-**8d**). The fluorescence spectra for each reaction mixture were recorded from 500 to 800 nm using excitation wavelength of λ_{max} in corresponding BSA-porphyrin complex. Figure 3-5 shows that the fluorescence intensity of *p*-**8a** increased with an increase of the concentration of BSA, and the maximum emission wavelength shows a bathochromic shift from 653 to 658 nm. The porphyrins *p*-**8b-d** showed the similar luminescence behavior of *p*-**8a**. The maximum emission wavelength of BSA-free porphyrins are 653 nm (*p*-**8a**), 652.5 nm (*p*-**8b**), 654 nm (*p*-**8c**) and 653.5 nm (*p*-**8d**), while those of BSA-porphyrin complexes are 658 nm (*p*-**8a**), 658 nm (*p*-**8b**), 658.5 nm (*p*-**8c**) and 659.5 nm (*p*-**8d**). Figure 3-6 shows the fluorescence intensity as a function of BSA concentration. The plot can be fitted well with Langmuir isotherm for single high-affinity binding site. The number of binding site per protein n and the equilibrium binding constant K are summarized in Table 3-3. The n and K values varied from 0.41 ± 0.04 to 1.57 ± 0.11 and from (0.25 ± 0.02) × 10^6 to (1.57 ± 0.11) × 10^6 M^{-1} owing to sugar unit attached. The number of

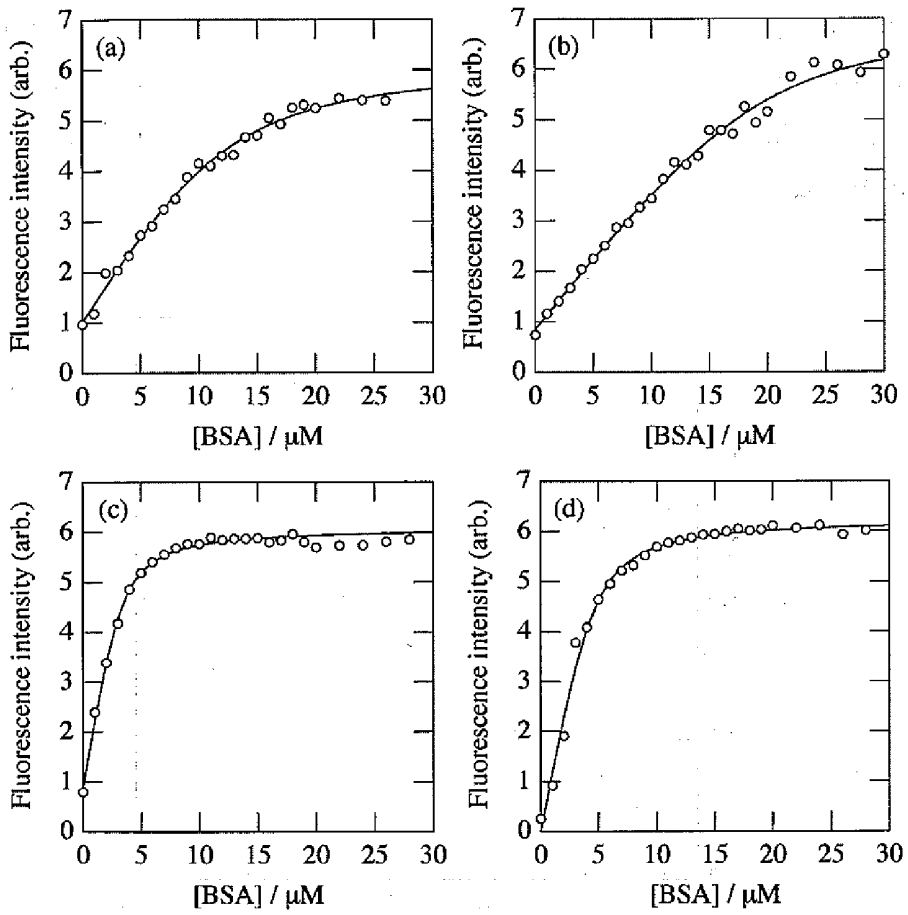

Figure 3-6 Fluorometric titration of *p*-**8** ($c = 5$ μM) in PBS containing 1 % DMSO for *p*-**8a** (a), *p*-**8b** (b), *p*-**8c** (c) and *p*-**8d** (d). The solid curves are best-fit with eq. 7. The fitting parameters are listed in Table 3-3.

Table 3-3 The equilibrium constants of *p*-**8** (5 μM) binding to bovine serum albumin (BSA) at 37 °C in PBS

	n	$K \times 10^{-6}$ / M	$a_f \times 10^{-6}$	$a_b \times 10^{-6}$
p-**8a**	0.41 ± 0.04	1.1 ± 0.5	0.2 ± 0.1	1.23 ± 0.05
p-**8b**	0.25 ± 0.01	2.1 ± 1.3	0.17 ± 0.02	1.39 ± 0.08
p-**8c**	1.10 ± 0.09	1.6 ± 0.5	0	1.25 ± 0.02
p-**8d**	1.57 ± 0.11	1.3 ± 0.3	0.17 ± 0.01	1.22 ± 0.01

binding site (n) of BSA increases in the order of *p*-**8b** < *p*-**8a** < *p*-**8d** < *p*-**8c**. The porphyrins having xylopyranosyl and arabinopyranosyl groups (i.e., pentose groups) showed the greater number of binding sites than those having glucopyranosyl and galactopyranosyl groups (i.e., hexsose groups). Figure 3-7 shows the n value as a function of t_R value. The n value of porphyrins *p*-**8** to BSA increased with an increase of t_R value, i.e., hydrophobicity. While the n value of porphyrins *p*-**8** depends on sugar unit attached, no significant difference was found in binding constant K.

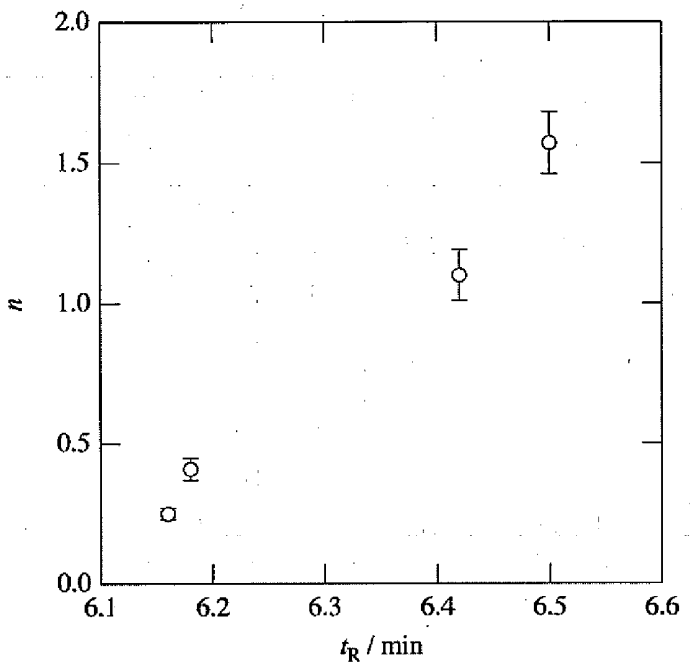

Figure 3-7 The plots of number of bounded porphyrins (n) as a function of retention time t_R on RP-HPLC.

3-2-4. Cellular uptake of glycoconjugated porphyrins

The cellular uptake of all glycoconjugated porphyrins by HeLa cells was examined after incubation with photosensitizers (c = 5 μM) for 24 h. After incubation, however, the precipitates were found by optical microscopy in the case of all acetylated glycoconjugated porphyrins **5** and **7** and the deacetylated glycoconjugated porphyrins *m*-**8c** and *p*-**8b** (Figure 3-8). Since the precipitates were hardly removed from the well, cellular uptake of all porphyrins **5**, **7**, *m*-**8c** and *p*-**8b** could not be determined. The uptake amount of photosensitizer was estimated on the basis of calibration data for each photosensitizer in

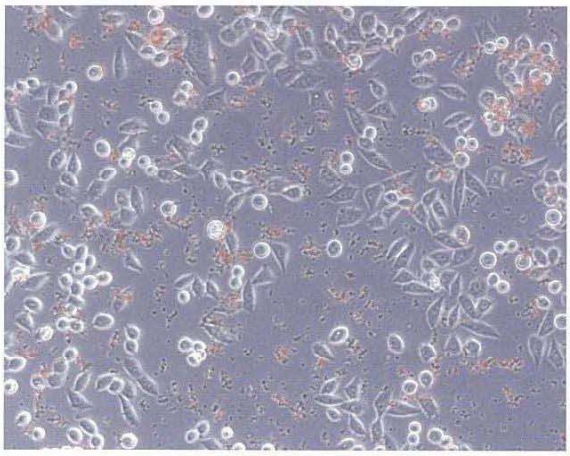

Figure 3-8 The precipitation of *m*-**8c** observed by optical microscopy.

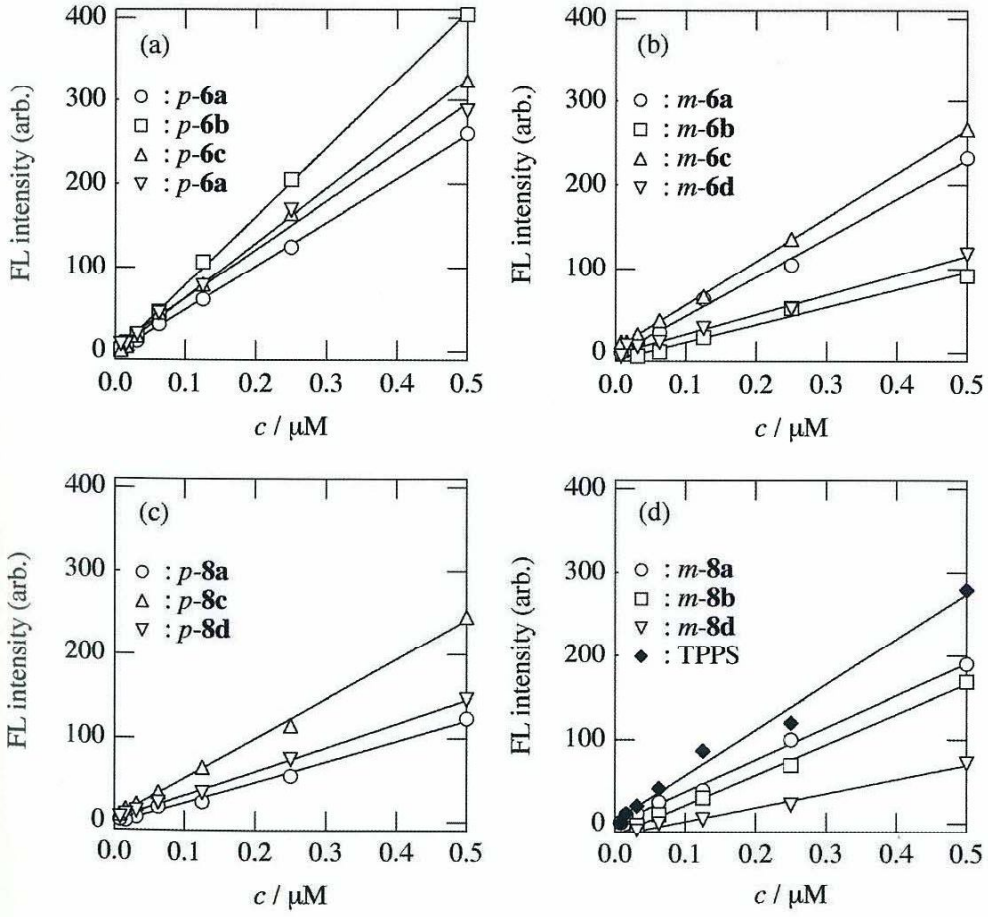

Figure 3-9 Calibration curve of the fluorescence intensity versus the concentration of **6** ((a) and (b)), **8** ((c) and (d)) and TPPS (d).

DMSO. The good linearity was found between the fluorescence intensity and the concentration in each photosensitizer as follows, where a and b are constants for a given plate reader using excitation and emission wavelengths of 430 and 635 nm (Figure 3-9). Figure 3-10 shows the relative value of the cellular uptake against tetraphenylporphyrin tetrasulfonic acid (TPPS) as a standard. All porphyrins **6** and **8** showed higher uptake than TPPS. The order of the cellular uptake amount was determined as *p*-**8d** > *p*-**8a** > *m*-**8a** > *m*-**8d** >*p*-**6d** > *m*-**8b**, *p*-**8c** > *m*-**6d** > *m*-**6c** > *p*-**6c** > *m*-**6a** > *p*-**6b** > *p*-**6a** > *m*-**6b** > *m*-**8b** > TPPS. Interestingly, *p*-**8d** showed an uptake 18-fold greater than that of TPPS. The porphyrins having xylopyranosyl (**c**) and arabinopyranosyl (**d**) groups (i.e., hexose groups) are much more effective to improve cellular uptake than those of glucopyranosyl (**a**) and galactopyranosyl (**b**) groups (i.e., pentose groups). This may reflect the lack of one hydroxymethyl group. In addition, *para*-substituted porphyrins *p*-**8** showed higher uptake than *meta*-substituted ones *m*-**8**, and free-base porphyrins **8** showed higher uptake than corresponding zinc porphyrins **6**. These differences might be related to the shape of the species in water, namely, the globular structure of *meta*-substituted porphyrins and the dimeric form of zinc porphyrins [34]. These findings indicate that glycopyranosyl groups modulate the hydrophobicity parameter (lipophilicity).

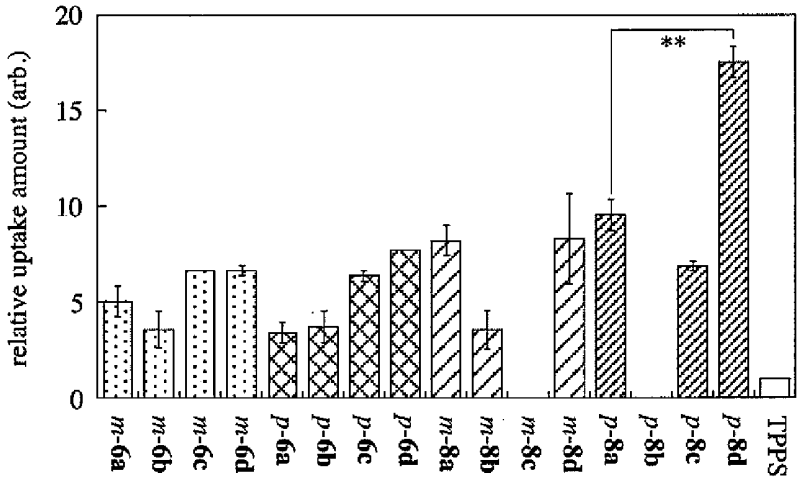

Figure 3-10 The cellular uptake of **6** and **8** by HeLa cells after incubation for 24 h. The values represent the mean ± s.d. of three replicate experiments. The values for *m*-**8c** and *p*-**8b** could not be quantified because of precipitation. **The value of *p*-**8d** was statistically significantly ($p < 0.01$) different from that of *p*-**8a**.

3-2-5. Light dose-dependence of the effect of deacetylated glucosylated porphyrin p-8a

The above results indicate a unique effect of the sugar units on the interaction with HeLa cells. A very interesting question then arises, namely, whether the differences in cellular uptake of photosensitizers affect their photocytotoxicity. In order to examine this issue, the photocytotoxicity of *p*-**8a**, *p*-**8d** and TPPS was assayed *in vitro*. First of all, the photocytotoxicity of *p*-**8a** was examined using a halogen lamp (100 W, $\lambda > 500$ nm) and a thermostated stage in order to find an appropriate light dose. Figure 3-11 shows the light dose dependency of the photocytotoxicity of *p*-**8a**. The cell survival decreased from 110.5 to 17.9 % as the light dose increased, and the lethal dose to 50 % of the population (LD_{50}) was around 16 J/cm^2.

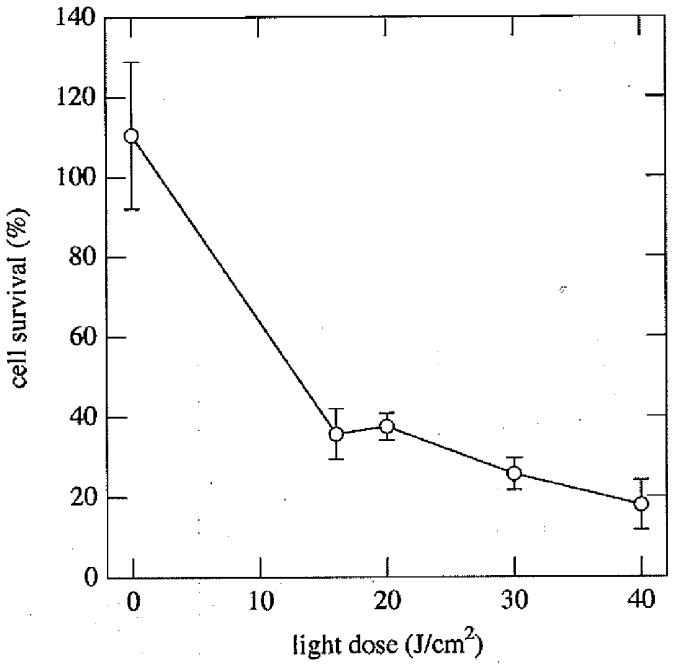

Figure 3-11 Light dose-dependent photocytotoxicity of *p*-**8a** in HeLa cells. [*p*-**8a**] = 5 μM. The light intensity applied was 24 mW/cm^2 using a halogen lamp (100 W, $\lambda > 500$ nm). The percentage cell survival was determined by Cell Titer-Glo™ Luminescent assay after 24 h incubation. The values represent the means ± s.d. of six replicate experiments.

3-2-6. In vitro study of relationship between cellular uptake and photocytotoxicity

The cytotoxicity of deacetylated glycoconjugated porphyrins *p*-**8a**, *p*-**8d** and TPPS to HeLa cells in the dark was examined. Figure 3-12 shows the percentage of cell survival after 48 h incubation without light irradiation. These photosensitizers (*p*-**8a**, *p*-**8d** and TPPS) showed no cytotoxicity in the dark (Figure 3-12a). The photocytotoxicity of *p*-**8a**, *p*-**8d** and TPPS was examined with HeLa cells. The above results show that the light dose of 16 J/cm^2 was appropriate to examine differences of photocytotoxicity between *p*-**8a**, *p*-**8d** and TPPS. Figure 3-12b shows the percentage cell survival after 24 h incubation. Photocytotoxicity of *p*-**8a** (36 %) and *p*-**8d** (28 %) is significantly higher than that of TPPS (70 %). Interestingly, the order of photocytotoxicity (*p*-**8d** > *p*-**8a** > TPPS) seems to be in accord with the order of cellular uptake. The low photocytotoxicity of TPPS could thus be attributable to the lower cellular uptake as compared with *p*-**8a** and *p*-**8d**. The difference in photocytotoxicity between *p*-**8d** and *p*-**8a** was small, even though the cellular uptake of *p*-**8d** was almost twice as that of *p*-**8a**. This may reflects from the differences in aggregation states or in the subcellular localization between *p*-**8a** and *p*-**8d**. This suggests other feature besides cellular uptake plays an important role for photodynamic effect.

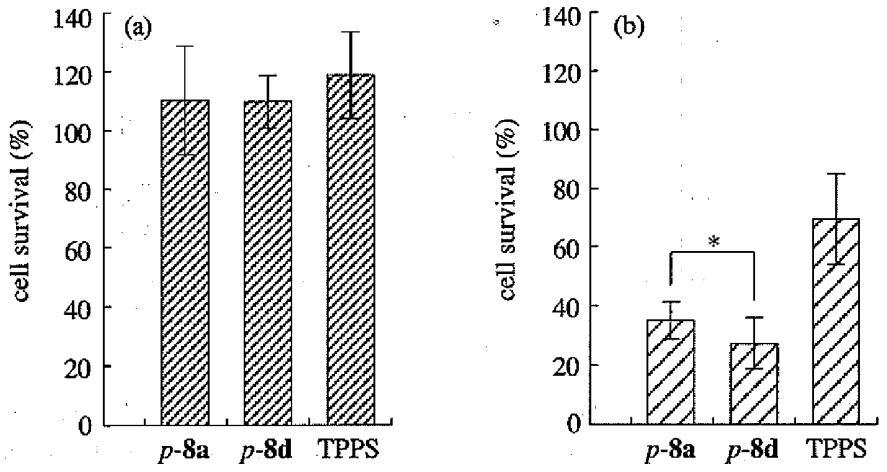

Figure 3-12 Cytotoxicity in the dark (a) and photocytotoxicity (b) of *p*-**8a**, *p*-**8d**, and TPPS in HeLa cells. [Photosensitizer] = 5 μM. The light intensity applied was 24 mW/cm^2 using a 100 W halogen lamp (λ > 500 nm). The percentage cell survival was determined by Cell Titer-Glo™ Luminescent assay after 48 h incubation. The values represent the means ± s.d. of of six replicate experiments. *Significant difference, $p < 0.05$.

3-2-7. Spectroscopic properties of p-8a and p-8d in aqueous media

Porphyrin derivatives are strongly hydrophobic species and it is easy to make an aggregate in aqueous media such as cytoplasm [21-23]. It is well-known that the aggregation states causes the shorter life-time of the excited state [21]. Hence, one of the reasons to make difference in photodynamic effect between *p*-**8a** and *p*-**8d** is a formation of aggregates. The electronic absorption and fluorescence spectra of deacetylated glycoconjugated porphyrins *p*-**8a** and *p*-**8d** (c = 4.97 μM) were measured in various composition of DMSO and PBS to investigate the effect of aggregation state on photochemical properties (Figure 3-13, 3-14 and Table 3-4, 3-5). The porphyrins *p*-**8a** and *p*-**8d** showed strong Soret band, which is typical spectra of monomeric form of porphyrin in DMSO (Figure 3-13) [35]. On the other hand, the Soret band decreased significantly in PBS. The Soret band width of *p*-**8d** is broader than those of *p*-**8a**.

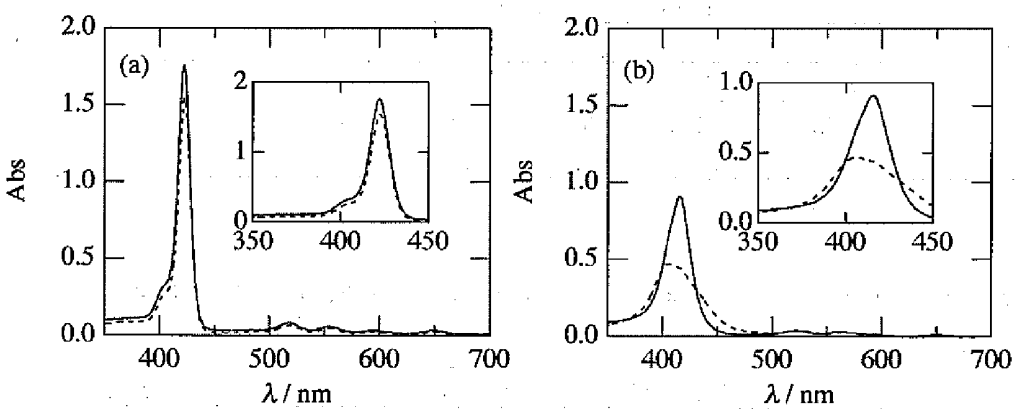

Figure 3-13 Electronic absorption spectra of *p*-**8a** and *p*-**8d** in DMSO (a) and PBS (b) at 37 °C.

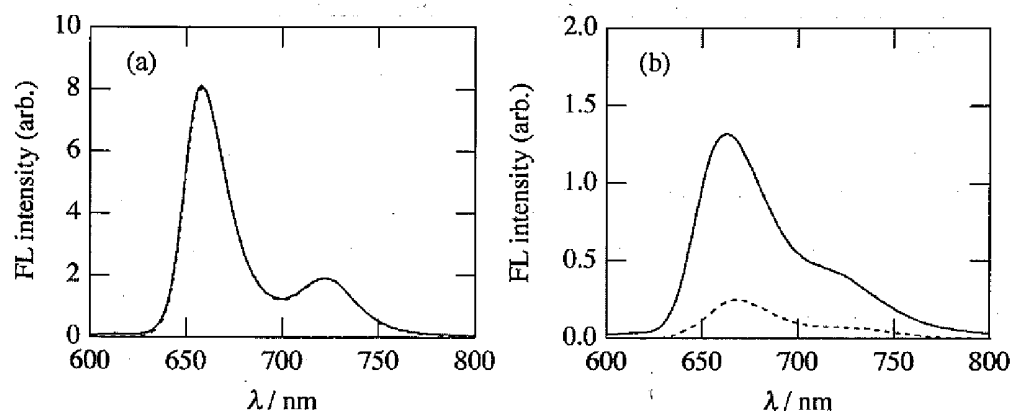

Figure 3-14 Fluorescence spectra of *p*-**8a** and *p*-**8d** in DMSO (a) and in PBS (b) at 37 °C.

The Soret bands of these photosensitizers shifted toward shorter wavelength. This results suggest the aggregation forms of glycocojugated porphyrins depends on sugar unit attached. The aggregation forms of these photosensitizers are H-type structure, i.e. face-to-face π-stacked aggregates [22,36]. Figure 3-14 shows fluorescence spectra of glycoconjugated porphyrins *p*-**8a** and *p*-**8d** in DMSO using a excitation wavelengths of 430 nm at 37 °C. The spectral data are listed in Table 3-4. There are no difference in fluorescence intensities between monomeric forms of porphyrins *p*-**8a** and *p*-**8d**. However the fluorescence intensities of *p*-**8a** were about 5-fold greater than those of *p*-**8d** in PBS (Figure 3-14 and Table 3-5). This suggests that the photochemical properties of aggregates and/or the quantity of remaining monomeric species are different between porphyrins having glucopyranosyl and arabinopyranosyl groups.

Table 3-4 Electronic absorption and fluorescence spectral data of *p*-**8a** and *p*-**8d** in DMSO at 37 °C.[a]

	Electronic absorption spectra					Fluorescence spcetra[b]	
	λ_{max} (nm)					λ_{max} (nm)	
	Soret	IV	III	II	I	(0,0)	(0,1)
p-**8a**	422	518.5	554	593.5	649	658	722
p-**8d**	422	518.5	554	593	651	658	722.5

[a] $c = 4.97$ μM, [b] $\lambda_{ex} = 430$ nm.

Table 3-5 Electronic absorption and fluorescence spectral data of *p*-**8a** and *p*-**8d** in PBS at 37 °C.[a]

	Electronic absorption spectra					Fluorescence spcetra[b]	
	λ_{max} (nm)					λ_{max} (nm)	
	Soret	IV	III	II	I	(0,0)	(0,1)
p-**8a**	416	522	566	592	649.5	663	724.5
p-**8d**	406	525.5	563	594.5	651.5	664	725

[a] $c = 4.97$ μM, [b] $\lambda_{ex} = 430$ nm.

3-3. Summary

The hydrophobicity parameter (Log *P*) of glycoconjugated porphyrins was evaluated by the Shake-Flask and the RP-HPLC methods. RP-HPLC method is very useful to estimate the order of hydrophobicity. The Log *P* values of acetylated glycoconjugated porphyrins **5** and **7** were ranged from +4.8 to +7.8, so that most of the photosensitizers are less hydrophobic. On the other hand, the Log *P* values of deacetylated glycoconjugated porphyrins *p*-**6** and *p*-**8** were ranged from -0.68 to -0.74, hence all photosensitizer are

hydrophilic. Zinc porphyrins **5** and **6** exerted higher hydrophilicity regardless of the sugar unit attached. The porphyrins having hexose groups are more hydrophilic than those having pentose groups. The each sugar unit attached has unique effect on the hydrophobicity. The binding equilibrium of the porphyrins *p*-**8** with BSA were investigated by means of fluorometric titration. The n and K values varied from 0.41 $\pm$ 0.04 to 1.57 $\pm$ 0.11 and from $(0.25 \pm 0.02) \times 10^6$ to $(1.57 \pm 0.11) \times 10^6$ M^{-1} owing to sugar units attached. The number of binding porphyrin to BSA (n) increases monotonically with an increase of retention time t_R on RP-HPLC. Hence the formation of glycoconjugated porphyrins *p*-**8** - BSA complex is simply driven by hydrophobic interaction. Except for *m*-**8c** and *p*-**8b**, the cellular uptake of porphyrins **6** and **8** was evaluated in HeLa cells. All these photosensitizers showed higher cellular uptake than TPPS. The uptake amount of *p*-**8d** showed about 2-fold higher cellular uptake than that of *p*-**8a**. The photocytotoxicity of *p*-**8a**, *p*-**8d**, and TPPS was examined with HeLa cells, using a light dose of 16 J/cm^2. These photosensitizers had no cytotoxicity in the dark, but their photocytotoxicity increased in the order of TPPS < *p*-**8a** < *p*-**8d**. However the difference in photocytotoxicity between *p*-**8d** and *p*-**8a** was small in contrast with the cellular uptake difference. The electronic absorption and fluorescence spectra of the porphyrins *p*-**8a** and *p*-**8d** were measured in DMSO and PBS to explore the photochemical behavior of glycoconjugated porphyrins in aqueous media such as cytoplasm. The fluorescence intensities of *p*-**8a** were about 5-fold greater than those of *p*-**8d** in PBS. This suggests that the photochemical properties of aggregates and/or the quantity of remaining monomeric species are different between porphyrins having glucopyranosyl and arabinopyranosyl groups. It may make difference in photodynamic effect in HeLa cells between *p*-**8a** and *p*-**8d**.

3-4. Experimental

Materials and Measurements

Measurements

Electronic absorption spectra were recorded on a JASCO V-570 spectrophotometer (Nara Women's University). Fluorescence spectra were recorded on a JASCO FP-6300 spectrofluorometer (Nara Women's University). Fluorescence intensity and luminescence intensity were determined by a plate reader (SPECTRA Fluor Plus, TECAN) (Nara Institute of Science and Technology). Image analysis was accomplished with the CLSM (Model LSM 510, Zeiss) (Nara Institute of Science and Technology). The acetylated photosensitizers **5** and **7** was estimated by liquid chromatography (SHIMADZU, CLASS-VP

ver 5.02 system) (Nara Women's University) equipped with silica gel-ODS (Kanto, Mightysil RP-18 4.6 mmϕ × 200 mm) column and a UV-vis detector (SPD-M10A VP) using MeOH / H_2O = 8 / 2 as an eluent. The deacetylated photosensitizers **6** and **8** was estimated by liquid chromatography (HITACHI, L-6000) (Osaka Prefectural College of Technology) equipped with silica gel-ODS (HITACHI, HITACHI GEL 4 mmϕ × 150 mm) column and a diode array detector (HITACHI L-4000) using acetonitrile / water = 1 / 1 as an eluent.

Photosensitizers

Stock solutions of photosensitizers (TPPS, glycoconjugated porphyrins **5**, **6**, **7** and **8**) were prepared by weighing the dried photosensitizers and dissolving them in dimethyl sulfoxide (DMSO, Wako Pure Chemical Industries, Ltd.). Stock solutions of photosensitizers were kept in the freezer (-30 °C).

Materials

Tetraphenylporphyrin tetrasulfonic acid (TPPS) and BSA (fraction V) were purchased from Sigma Aldrich Japan Corporation. All other reagents were of analytical grade.

3-4-1. Hydrophobicity parameters of 5 and 7 determined by RP-HPLC method

RP-HPLC was performed using an octadecylsilyl silica gel ODS column as a stationary phase and MeOH / H_2O = 8 / 2 mixture as the mobile phase (flow rate, 0.85 mL·min^{-1}) on a HPLC system equipped with UV-vis detector. All samples were dissolved in the eluent (1 ~ 0.001 μM), and the solution was filtered just before use. The dead time t_0 was determined using urasil. The capacity factor k' is correlated with Log P values as follows:

$$\mathrm{Log}\,P = a\,\mathrm{Log}\,k' + b \tag{1}$$

where a and b are constants for a given HPLC system. The k' value is calculated as follows:

$$k' = \frac{t_R - t_0}{t_0} \tag{2}$$

where t_R and t_0 are the retention time of sample and uracil (dead time), respectively. Pyridine (Log P = 0.65), benzaldehyde (1.48), quinoline (2.03), chlorobenzene (2.84), benzophenone (3.02), diphenylamine (3.40) and biphenyl (4.00) were used as standards for calibration of Log P and Log k' values.

3-4-2. Partition coefficient of p-8 between PBS and n-octanol

The hydrophobicity was characterized by the Log *P*, the logarithm of partition coefficient, between the two immiscible solvents *n*-octanol (Wako Pure Chemical Industries, Ltd.) and Dulbecco's PBS (13.7 mM NaCl, 2.7 mM KCl, 8.1 mM $Na_2HPO_4 \cdot 12H_2O$, and 1.5 mM KH_2PO_4 pH 7.4) (Nacalai tesque) [9,27-29]. Partition coefficients were determined as follows: DMSO solution (7 μL) of photosensitizer was added to *n*-octanol (0.5 mL) in sampling tube (2 mL). An equal volume of PBS was added to the solution. The sampling tube containing the mixture was vortexed vigorously for 1 min, and was centrifuged for 5 min. The sample tube was kept in standing at room temperature for 18 h. The concentration of each phase was determined by HPLC equipped with an octadecylsilyl silica gel ODS column (acetonitrile / H_2O = 1 / 1; flow rate, 0.25 mL·min^{-1}; UV-vis detector). The concentration of photosensitizers was calculated on the basis of the peak area of the chromatogram recorded at 420 nm. The Log *P* values were calculated as follows:

$$\mathrm{Log}\,P = \mathrm{Log}\frac{C_O}{C_W} \tag{3}$$

where C_O and C_W are the concentrations of *n*-octanol and PBS phases, respectively. The Log *P* value reported was determined by six replicate experiments.

3-4-3. Hydrophobicity parameter of p-8 detremined by RP-HPLC method

RP-HPLC was performed using an octadecylsilyl silica gel ODS column as the stationary phase and acetonitrile / H_2O = 1 / 1 mixture as the mobile phase (flow rate, 0.25 mL·min^{-1}) on a HPLC system equipped with UV-vis detector. All samples were dissolved in the eluent (0.1 ~ 0.01 μM), and the solution was filtered just before use.

3-4-4. Fluorometric titration of p-8 to BSA

Photosensitizers (c = 5 μM (1 % DMSO)) and BSA (c = 0 ~ 35 μM) were dissolved in Dulbecco's PBS (Nacalai tesque). This solution were stirred and shaken in a water bath with slow stirring for 24 h (37 °C, ambient atmosphere). The electronic absorption spectra of these solutions were measured at 37 °C [30-33]. And the fluorescence intensity of these solution were measured using a maximum excitation wavelengths of BSA binding porphyrin at 37 °C. The luminescence intensity was analyzed on the assumption of single high-affinity binding site:

$$M + S \underset{}{\overset{K}{\rightleftharpoons}} M\text{-}S \quad (4)$$

in which M, S and M-S represent the BSA-free porphyrin, free binding site and occupied binding site of BSA, respectively. According to the Langmuir isotherm, the ratio of porphyrin bounded on BSA($[M]_b$) over total BSA concentrations ($[A]_0$) r can be expressed as follows:

$$r = n\theta = \frac{[M]_b}{[A]_0} = \frac{nK[M]_f}{1+K[M]_f} \quad (5)$$

in which θ, n and K means the occupancy of the binding site, the number of binding site per protein and the binding constant, respectively. The luminescence intensity is combination of two contributions, namely BSA-free porphyrin $[M]_f$ and BSA-porphyrin complex $[M]_b$.

$$F = a_f[M]_f + a_b[M]_b = (a_f - a_b)[M]_f + a_b[M]_0 \quad (6)$$

in which a_f and a_b are constants in fluorometric titration. By using eq. 4, the luminescence intensity can be expressed as follows:

$$F = (a_f - a_b)\frac{K([M]_0 - n[A]_0) - 1 + \sqrt{(nK[A]_0 - K[M]_0 + 1)^2 + 4K[M]_0}}{2K} + a_b[M]_0 \quad (7)$$

The plots of luminescence intensity as a function of BSA concentration ($[A]_0$) was fitted with eq. 5 to afford the number of binding site n and binding constant K.

3-4-5. Cellular uptake by HeLa cells

HeLa cells were kindly provided by Professor Jun-ya Kato (Graduate School of Biological Science, Nara Institute of Science and Technology, Japan). They were grown in Dulbecco's modified Eagle's medium (DMEM) with phenol red and 10 % fetal calf serum (FCS) (Hyclone Laboratories, Inc.) [20,23,37-41]. Cellular uptake of glycoconjugated porphyrins **6** and **8** was determined as follows: HeLa cells (5×10^4 cells/well) were plated in a 24-well plate (Nalge Nunc International K.K.) in 500 μL per well of DMEM with phenol red and 10 % FCS, and the plates were incubated for 24 h (37 °C, 5 % CO_2). To each well was added 500 μL of 10 μM (2 % DMSO) photosensitizers in DMEM with phenol red and 10 % FCS (hence the concentration of photosensitzers was 5 μM (1 % DMSO)). In order to estimate the background in fluorometry, in addition, to three wells was added 500 μL of DMEM with phenol red and 10 % FCS (1 % DMSO)) without photosensitizers. The cells were further incubated for 24 h. The medium was removed and the cells were then washed twice with Dulbecco's PBS (Wako Pure Chemical

Industries, Ltd.). The cells were lysed in 100 μL of DMSO to extract the photosensitizers. The fluorescence intensity due to the extracts was measured with a plate reader (TECAN SPECTRA Fluor Plus) using excitation and emission wavelengths of 430 and 635 nm, respectively [23]. The fluorescence intensity of photosensitizers were estimated by removing the averaged background from the averaged fluorescence intensity of extracts. The uptake amount of photosensitizer was calculated on the basis of calibration data for each photosensitizer in DMSO in the range from 500 to 7.81 nM. The fluorescence intensity in each concentration was corrected by removing the scattering contribution from empty wells to give a calibration curve. The fluorescence intensity of each photosensitizer can be correlated with the concentration of each photosensitizer as follows, where a and b are constants for a given plate reader using excitation and emission wavelengths of 430 and 635 nm, respectively. The uptake amount of photosensitizers reported was determined by three replicate experiments.

3-4-6. In vitro photocytotoxicity test against HeLa cells

HeLa cells (5×10^3 cells/well) were plated in 100 μL of DMEM containing 10 % FCS, and incubated overnight (37 °C, 5 % CO_2) in a 96-well plate. To each well was added 100 μL of 10 μM (2 % DMSO) photosensitizers in DMEM with phenol red and 10 % FCS (hence the concentration of photosensitzers was 5 μM (1 % DMSO)). In order to estimate the background in fluorometry, in addition, to three wells was added 100 μL of DMEM with phenol red and 10 % FCS (1 % DMSO)) without photosensitizers. The cells were further incubated for 24 h. The medium was removed and the cells were then washed twice with Dulbecco's PBS , and 100 μL of DMEM containing 10 % FCS was added. The cells were then exposed to light from a 100 W halogen lamp (Ushio, KBEX-102A), equipped with a water jacket and a Y-50 cut-off filter ($\lambda > 500$ nm, Toshiba) for an appropriate time (0 min for evaluation of cytotoxicity in the dark) [39-41]. For all experiments, the light intensity was varied from 0 to 24.5 mW/cm^2 by using an UV-vis power meter (OPHIR, ORION/TH). The light dose was calculated as the product of light intensity (mW/cm^2) and irradiation time. Cell viability was measured after 24 h using a CellTiter-Glo™ Luminescent Assay kit (Promega Corporation) according to the instructions. Then, the 96-well plate was subjected to luminescence measurement using the plate reader. At first, the fluorescence intensity in each wells was estimated by removing the averaged fluorescence intensity from three wells containing Cell Titer-Glo™ only (no cells). The percentage cell survival was calculated by normalization with respect to the value for no drug treatment.

3-4-7 Statistical analysis

All statistical evaluations were performed using Student's *t*-test. All values for cellular uptake and cytotoxicity are expressed as mean ± standard deviation.

3-5. References

1. R. Bonnett, Photosensitizers of the Porphyrin and Phthalocyanine Series for Photodynamic Therapy. Chem. Soc. Rev. 24 (1995) 19-33.
2. Y.N. Konan, R. Gurny, E. Allémann, State of art in the delivery of photosensitizers for photodynamic therapy. J. Photochem. Photobiol. B: Biol. 66 (2002) 89-106.
3. M. Momenteau, D. Oulmi, Ph. Maillard, A. Croisy, Photodynamic Therapy of cancer II. SPIE. 2325 (1994) 13-23.
4. D.M. Tarak, Pharmaceutical development and medical applications of Porphyrin-type macrocycles. J. Porphyrins Phthalocyanines. 4 (2000) 362-367.
5. R. Bonnet, Chemical Aspects of Photodynamic Therapy., Taylor & Francis, UK, 2000.
6. I. Okura, Photosensitization of Porphyrins and Phthalocyanines., Kodansha, Tokyo, 2000.
7. T.T. Tominaga, V.E. Yusbmanov, I.E. Borissevitcb, H. Imasato, Aggregation Phenomena in the Complexes of Iron Tetraphenylporphine Sulfonate with Bovine Serum Albumin. J. Inorg. Chem. 65 (1997) 235-244.
8. P. Kubát, K. Lang, P. Anzenbacher, Jr., Modulation of porphyrin binding to serum albumin by pH. Biochem. Biophys. Acta. 1670 (2004) 40-48.
9. OECD Guidelines for Testing of Chemicals, OECD, Paris 1995; No. 107.
10. G. Zheng, W.R. Potter, A. Sumlin, T.J. Dougherty, R.K. Pandey, Photosensitizers Related to Purpurin-18-*N*-alkylimides: A Comparative in vivo Tumoricidal Ability of Ester versus Amide Functionalities. Bioorg. Med. Chem. Lett. 10 (2000) 123-127.
11. T. Peters, Jr., All about Albumin., ACADEMIC PRESS, California, 1996.
12. I.J. Macdonald, T.J. Dougherty, Basic principles of photodynamic therapy. J. Porphyrins Phthalocyanines. 5 (2001) 105-129.
13. V. Rosenberger, R. Margalit, Thermodynamics of the binding of hematoporphyrin ester, a hematoporphyrin derivative-like photosensitizer, and its components to human serum albumin, human high-density lipoprotein and human low-density lipoprotein. Photochem. Photobiol. 58 (1993) 627-

630.

14. C. Tanielian, C. Schwetzer, R. Mechin, C. Wolff, QUNTUM YIELD OF SINGLRT OXYGEN PRODUCTION BY MONOMERIC AND AGGREGATED FORMS OF HEMATOPORPHYRIN DERIVATIVE. Free Radical Biol. Med. 30 (2001) 208-212.
15. R.D. Almedia, B.J. Manadas, A.P. Carvaiho, C.B. Duarte, Intracellulr signaling mechanisms in photodynamic therapy. Biochem. Biophys. Acta. 1704 (2004) 59-86.
16. S.R. Wood, J.A. Holroyd, S.B. Brow, The Subcellular Localization of Zn(II) Phthalocyanines and Their Redistribution on Exposure to Light. Photochem. Photobiol. 65 (1997) 397-402.
17. M. Mori, T. Kuroda, A. Obana, I. Sakata, T. Hirano, S. Nakajima, M. Hikida, T. Kumagai, *In vitro* Plasma Protein Binding and Cellular Uptake of ATX-S10(Na), a Hydrophilic Chlorin Photosensitizer. Jpn. J. Cancer Res. 91 (2000) 845-852.
18. Y.N. Konan, J. Chevallier, R. Gurny, E. Allémann, Encapulation of p-THPP into Nanoparticles: Cellular Uptake, Subcellular Localization and Effect of Serum on Photodynamic Activity. Photochem. Photobiol. 77 (2003) 638-644.
19. Q. Peng, J. Moan, J.M. Nesland, Correlation of Subcellular and Intratumoral Photosensitizer Localization with Ultrastructural Features After Photodynamic Therapy. Ultrastructural Pathology. 20 (1996) 109-129.
20. C.M.N. Yow, J.Y. Chen, N.K. Mak, N.H. Cheung, A.W.N. Leung, Cellular uptake, subcellular localization and photodamaging effect of Temoporfin (mTHPC) in nasopharygeal carcinoma cells: comparison with hematoporphyrin derivative. Cancer Lett. 157 (2000) 123-131.
21. K. Lang, J. Mosinger, D.M. Wagnerová, Photophysical properties porphyrinoid sensitizers non-covalently bound to host molecules; models for photodynamic therapy. Coord. Chem. Rev. 248 (2004) 321-350.
22. H. García-Ortega, J.L. Bourdelande, J. Crusats, Z. EI-Hachemi, J.M. Ribó, Excitred Triplet States in Aggregates and Monomers of Water Soluble Meso-Aryl Substituted Porphyrins. J. Phys. Chem. B. 108 (2004) 4631-4639.
23. K. Oda, S. Ogura, I. Okura, Preparation of a water-soluble fluorinated zinc phthalocyanine and effect for photodynamic therapy. J. Photochem. Photobiol. B: Biol. 59 (2000) 20-25.
24. A. Rungta, G. Zheng, J.R. Missert, W.R. Potter, T.J. Dougherty, R.K. Pandey, Purpuriimides as Photosensitizers: Effect of the Presence and position of the substituents in the In Vivo Photodynamic

Efficacy. Bioorg. Med. Chem. Lett. 10 (2000) 1463-1466.

25. OECD Guidelines for Testing of Chemicals, OECD, Paris 1989; No. 117.
26. G. Zheng, W.R. Potter, S.H. Camacho, J.R. Missert, G. Wang, D.A. Bellnier, B.W. Henderson, M.A.J. Rodgers, T.J. Dougherty, R.K. Pandey, Synthesis, Photophysical Properties, Tumor Uptake, and Preliminary in Vivo Photosensitizing Efficacy of a Homologous series of 3-(1'-Alkyloxy)ethyl-3-devinyl purpurin-18-*N*-alkylimides with Variable Lipophilicity. J. Med. Chem. 44 (2001) 1540-1559.
27. K.W. Woodburn, N.J. Vardaxis, J.S. Hill, A.H. Kaye, J.A. Reiss, D.R. Phillips, EVALUATION OF PORPHYRIN CHARACTERISTICS REQUIRED FOR PHOTODYNAMIC THERAPY. Photochem. Photobiol. 55 (1992) 697-704.
28. F. Ricchelli, L. Franchi, G. Miotto, L. Borsetto, S. Gobbo, P. Nikolov, J.C. Bommer, E. Reddi, Meso-substituted tetra-cationic porphyrins photosensitize the death of human fibrosarcoma cells via lysosomal targeting. Int. J. Biochem. CellBiol. 37 (2005) 306-319.
29. K.K. Yee, K.C. Soo, B.H. Bay, M. Olivo, A Comparison of Protoporphyrin IX Dimethyl Ester as a Photosensitizer in Poorly Differentiated Human Nasopharyngeal Carcinoma Cells. Photochem. Photbiol. 76 (2002) 678-682.
30. M. Rotenberg, R. Margalit, Deuteroporphyrin-albumin binding equilibrium. Biochem. J. 229 (1985) 197-203.
31. L.I. Grossweiner, G.C. Goyal, BINDING OF HEMATOPORPHYRIN DERIVATIVE TO HUMAN SERUM ALBUMIN. Photochem. Photobiol. 40 (1984) 1-4.
32. A.A. Lamola, I. Asher, U. Muller-Eberhard, M. Poh-Fitzpatrick, Fluorometric study of the binding of protoporphyrin to haemopexin and albumin. Biochem. J. 196 (1981) 693-698.
33. S. Cohen, R. Margalit, Binding of porphyrin to human serum albumin. Biochem. J. 270 (1990) 325-330.
34. B.M. Hoffman, J.A. Ibers, Porphyrinic Molecular Metals. Acc. Chem. Res. 16 (1983) 15-21.
35. F. Ricchelli, S. Gobbo, G. Jori, G. Moreno, F. Vinzens, C. Salet, PHOTOSENSITIZATION OF MITOCHONDRIA BY LIPOSOME-BOUND PORPHYRINS. Photochem. Photobiol. 58 (1993) 53-58.
36. R. Bonnett, B. D. Djelal, A. Nguyen, Physical and chemical studies related to the development of *m*-THPC (FOSCAN®) for the photodynamic therapy (PDT) of tumors. J. Porphyrins Phthalocyanines.

5 (2001) 652-661.

37. F. Lin, C.J. Bertling, P.G. Geiger, A.W. Girtti, Delayed Hyperresistance of Endothelial Cells to Photodynamic Inactivation After Contact with Hemin. Photochem. Photobiol. 68 (1998) 211-217.
38. D.J. Robinson, H.S. de Bruijn, N. van der Veen, M.R. Stringer, S.B. Brown, W.M. Star, Protoporphyrin IX Fluorescence Photobleaching during ALA-mediated Photodynamic Therapy of UVB-Induced Tumors in hairless Mouse Skin. Photochem. Photobiol. 69 (1999) 61-70.
39. I. Laville, T. Figueiredo, B. Loock, S. Pigaglio, Ph. Maillard, D.S. Grierson, D. Carrez, A. Croisy, J. Blais, Synthesis, Cellular Internalization and Photodynamic Activity of Glycoconjugated Derivatives of Tri and Tetra (*meta*-hydroxyphenyl) chlorins. Bioorg. Med. Chem. 11 (2003) 1643-1652.
40. Y. Mikata, Y. Onchi, M. Shibata, T. Kakuchi, H. Ono, S. Ogura, I. Okura, S. Yano, Synthesis and Phototoxic Property of Tetra- and Octa-Glycoconjugated Tetraphenylchlorins. Bioorg. Med. Chem. Lett. 8 (1998) 3543-3548.
41. Y. Mikata, Y. Onchi, K. Tabata, S. Ogura, I. Okura, H. Ono, S. Yano, Sugar-dependent photocytotoxic property of tetra- and octa- glycoconjugated tetraphenylporphyrins. Tetrahedron Lett. 39 (1998) 4505-4508.

Chapter 4

Synthesis of Glycoconjugated Chlorins

4-1. Introduction

5,10,15,20-tetrakis(3-hydroxyphenyl)chlorin (Foscan®, hereinafter referred as *m*-THPC), a second generation photosensitizer, is undergoing clinical trials for use in photodynamic treatment of gynecological, respiratory and head and neck cancers in the USA, Europe and the UK [1-5]. *m*-THPC appears to have many advantages in comparison with Photofrin®. In particular, it is approximately 200 times more effective than Photofrin® at the same photodynamic dose (i.e., drug dose × light dose), allowing the use of lower photosensitiser doses and shorter illumination times to achieve similar results [5]. Several glycoconjugated porphyrins have been synthesized for evaluation of their photocytotoxicity, but there have been few reports on glycoconjugated chlorins, despite their potential utility as photosensitizers. Chlorin derivatives are generally synthesized through reduction of porphyrin derivatives with diimide photosensitizers, i.e., the Whitlock method [6,7]. However, the instability of chlorin macrocycles makes it hard to remove the concomitantly formed porphyrins and bacteriochlorins. This leads to considerable difficulty in the synthesis of glycoconjugated chlorins [8-11]. This chapter, glycoconjugated chlorins were synthesized by means of the Whitlock method with diimide reduction and purified by reversed phase thin layer chromatography (RP-TLC) as shown in scheme 4-1. The versatility of this method for the synthesis of *para*- and *meta*-substituted glycoconjugated chlorins was examined with D-glucose, D-galactose, D-xylose and D-arabinose. All of photosensitizers have been characterized by ^{1}H NMR, electronic absorption, IR and ESI-TOF mass spectra.

4-2. Results and Discussion

4-2-1. Synthesis of deacetylated glycoconjugated chlorins 9

According to chapter 2, the acetylated glycoconjugated porphyrins **7** were prepared by condensation of pyrrole with *p*- or *m*-glycoconjugated benzaldehydes **4** using a modification of the Lindsey method in the presence of $Zn(OAc)_2 \cdot 2H_2O$ as a template, followed by demetalation with 4 M HCl in ca. 36 ~ 86 %. Chlorin derivatives are generally synthesized through reduction of porphyrin derivatives with diimide photosensitizers (i.e., the Whitlock method) [10,11]. The deacetylated glycoconjugated chlorins **9** were synthesized from the corresponding porphyrins **7** as shown in Scheme 4-1. The diimide reduction of porphyrins **7** gave a mixture of dihydro- (i.e., chlorin) and tetrahydro-porphyrin (i.e., bacteriochlorin) [7-11]. After the diimide reduction of porphyrins *p*-**7**, the electronic absorption spectrum of the reaction mixture showed the Q_I band at 650 nm for chlorin and at 740 nm for bacteriochlorin. After the diimide

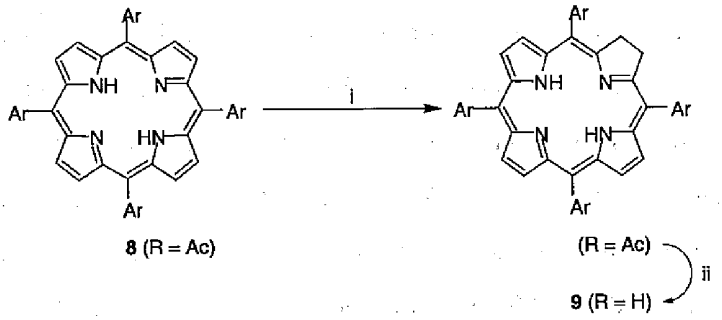

Reagents and Conditions: i) K_2CO_3, *p*-toluenesulfonylhydrazide, pyridine, N_2, 110 °C; then *o*-chloranil, benzene, r.t.. ii) NaOMe, CH_2Cl_2, MeOH.

$(Ar)_4$—chlorin

Types of Glycopyranosyl Groups	Substitution Position: *para*-Substituted (denoted as *p*-)	Substitution Position: *meta*-Substituted (denoted as *m*-)
a: D-glucose R = Ac for **8** R = H for **9**	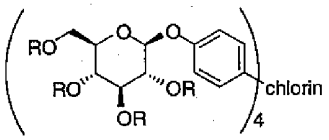	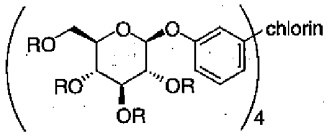
b: D-galactose R = Ac for **8** R = H for **9**	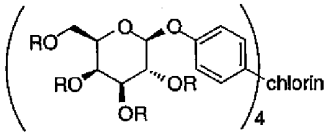	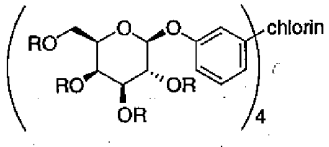
c: D-xylose R = Ac for **8** R = H for **9**	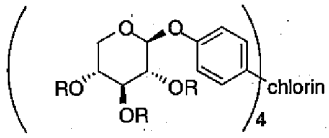	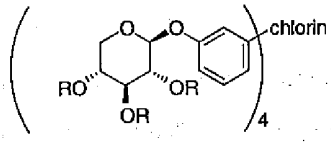
d: D-arabinose R = Ac for **8** R = H for **9**	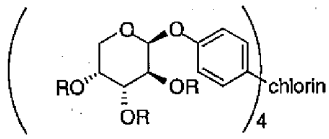	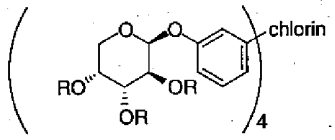

Scheme 4-1

reduction of porphyrins *m*-**7**, on the other hand, the electronic absorption spectrum of the reaction mixture showed only a peak at 740 nm due to bacteriochlorin. These suggest that the macrocycles of porphyrins *m*-**7** are much easier to be reduced than those of porphyrins *p*-**7**. Dehydrogenation with *o*-chloranil cleanly removed the bacteriochlorin (λ_{max}= 740 nm) to afford glycoconjugated chlorins. It was found that some of acetyl groups of sugar unit were cleaved in this diimide reduction. The crude product was used for the synthesis of deacetylated glycoconjugated chlorins **9** without further purification. The saponification of the resulting product was carried out using NaOMe in a mixture of MeOH and CH_2Cl_2 to give chlorins **9**. The crude product was successfully purified by RP-TLC (Table 4-1 and Figure 4-1). The chlorins **9** were obtained in the yields of 14 ~ 49 % with the purities of >95 % evaluated by HPLC using an octadecylsilyl-supported silica gel column. The chlorins **9** were characterized by ^{1}H NMR,

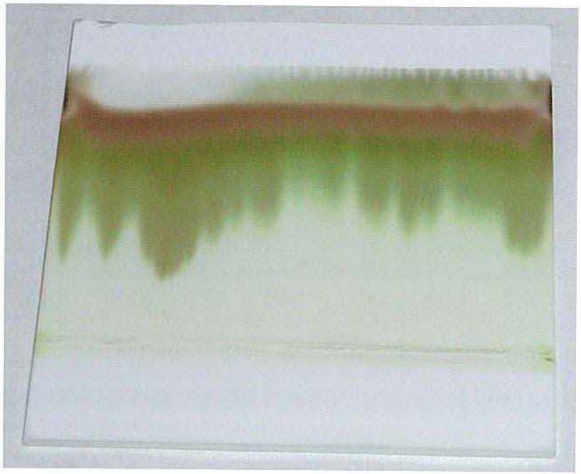

Figure 4-1 The preparative reversed phase thin layer chromatography of *p*-**9a**.

Table 4-1. The relative hydrophobicity of **9** evaluated by reversed phase TLC[a]

Compound	R_f
p-**9a**	0.66
p-**9b**	0.69
p-**9c**	0.14
p-**9d**	0.44
m-**9a**	0.43
m-**9b**	0.49
m-**9c**	0.20
m-**9d**	0.25
TPPS	0.91

[a] stationary phase, octadecylsilyl bounded silica gel, mobile pahse, MeOH / H_2O = 8 / 2.

ESI-TOF mass, IR and electronic absorption spectroscopy.

4-2-2. Electronic absorption spectra of deacetylated glycoconjugated chlorins 9

The absorption of longer wavelength light is one of the important performances for PDTdrugs. The electronic absorption spectra of deacetylated glycoconjugated chlorins **9** were recorded in DMSO (Figure 4-2). The wavelength (λ_{max}) and molar extinction coefficient (ε) of maximum absorption are listed in

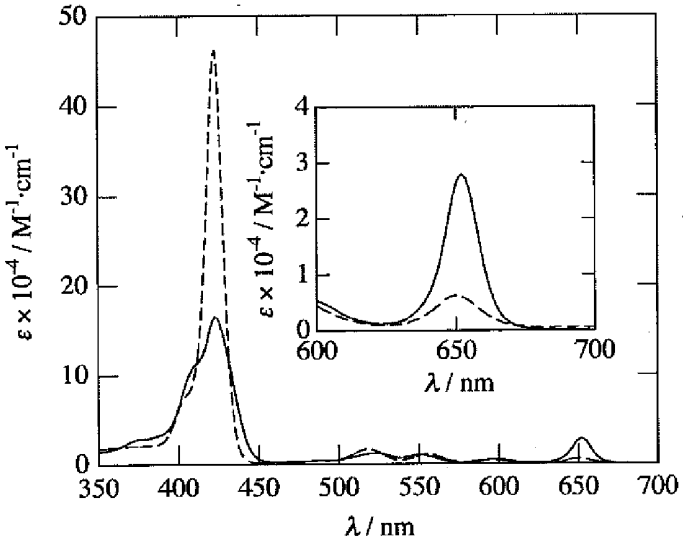

Figure 4-2 Electronic absorption spectra of *p*-**8a** ($c = 4.97$ μM, solid line) and *p***9a** ($c = 4.97$ μM, broken line) in DMSO at 20 °C.

Table 4-2 Electronic absorption spectra data of **9** (4.97 μM) in DMSO at 20 °C.

	λ_{max} / nm (ε x 10^{-4} / cm^2·$mmol^{-1}$)				
	Soret	Q Bands			
		IV	III	II	I
m-**9a**	421 (13.8)	520 (1.40)	546 (0.92)	598 (0.58)	652 (3.22)
m-**9b**	421 (14.4)	517 (1.46)	546 (0.98)	602 (0.62)	651 (2.42)
m-**9c**	421 (14.9)	518 (1.43)	545 (0.94)	597 (0.54)	651 (3.28)
m-**9d**	421 (16.3)	516 (1.62)	547 (0.90)	602 (0.52)	651 (2.22)
p-**9a**	424 (13.1)	522 (1.32)	550 (1.18)	599 (0.66)	652 (2.50)
p-**9b**	421 (15.1)	522 (1.66)	550 (1.54)	598 (0.90)	651 (2.32)
p-**9c**	423 (14.6)	522 (1.34)	550 (1.14)	602 (0.58)	651 (2.56)
p-**9d**	423 (13.6)	521 (1.28)	551 (1.14)	596 (0.60)	650 (2.48)

Table 4-2. All chlorins **9** have a strong Soret band (sometimes called the b band) at ca. 420 nm and four weak Q bands at ca. 520 (Q_{IV}), 550 (Q_{III}), 600 (Q_{II}) and 650 nm (Q_I) [7,8,10]. The Q_I band of all chlorins **9** is greater than that of porphyrins **8**. For example, the Q_I band of chlorin *p*-**9a** (2.79×10^4 $M^{-1} \cdot cm^{-1}$) were about 3-fold greater than that of corresponding porphyrin *p*-**8a** (0.64×10^4 $M^{-1} \cdot cm^{-1}$) (Figure 4-2). Because the Q_I band is usually used for PDT treatment, it is expected that that chlorins have higher photodynamic effect than that of porphyrins.

4-2-3. ^1H NMR spectra of deacetylated glycoconjugated chlorins 9

Figure 4-3 shows the ^1H NMR spectra of 5,10,15,20-tetrakis[3-(β-D-glucopyranosyloxy)phenyl]-porphyrin (*m*-**8a**) and 5,10,15,20-tetrakis[3-(β-D-glucopyranosyloxy)phenyl]chlorin (*m*-**9a**) in CD_3OD. The peak at 8.8 ppm due to the β-pyrrole proton of porphyrins **8** disappeared completely in corresponding chlorins **9** except for *m*-**9b** and *m*-**9d** [8,10,12]. On the other hand, the peaks due to the β-pyrrole protons of chlorins **9** appeared at 8.6, 8.4, 8.2 and 4.2 ppm [8,10,12]. The peaks at 8.6, 8.4, 8.2 and 4.2 ppm are assigned to those of 8,17-β-pyrrole, 12,13-β-pyrrole, 7,18-β-pyrrole and 2,3-β-pyrrole protons, respectively [13-16]. The phenyl protons were found at 8.0-7.4 ppm [13-16]. The anomeric proton of sugar unit was found at 5.2-5.1 ppm. The peaks around 4.1-3.5 ppm are assigned to those of sugar moieties. The

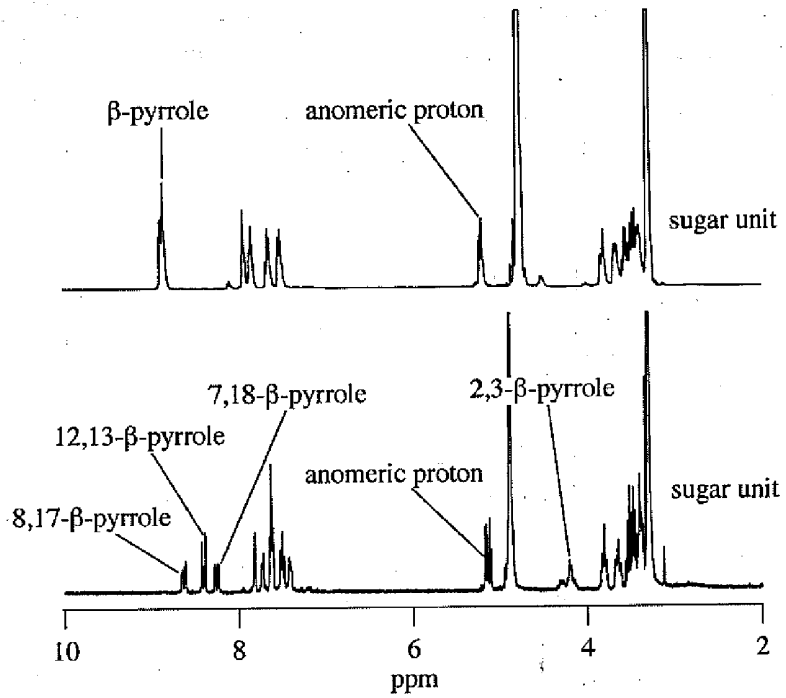

Figure 4-3 ^1H NMR spectra of *m*-**8a** and *m*-**9a** in CD_3OD.

assignment of sugar units was carried out using ^{1}H NMR spectra of the porphyrins and 2D NMR techniques (COSY and HMQC).

4-2-4. ESI-TOF mass spectra of deacetylated glycoconjugated chlorins 9

Mass spectra of deacetylated glycoconjugated chlorins **9** were recorded using the electron-spray ionization time-of-flight (ESI-TOF) mass spectrometry in MeOH. The small difference in the molecular weight between chlorins **9** and corresponding porphyrins **8** was also clearly evidenced by ESI-TOF mass spectrometry as shown in Figure 4-4. All glycoconjugated porphyrins **8** and chlorins **9** were detected as a $[M + Na]^+$ species in the positive mode [10,17]. Figure 4-5a shows the ESI-TOF mass spectrum of crude product of chlorin *p*-**9c**. The spectrum can be divided into two contribution of porphyrin *p*-**8c** and chlorin *p*-**9c** (Figure 4-5b). The peaks due to porphyrin *p*-**8c** dramatically decreased after RP-TLC purification (Figure 4-5c). The mass spectra of all chlorins **9** fairy agreed with the calculated spectra.

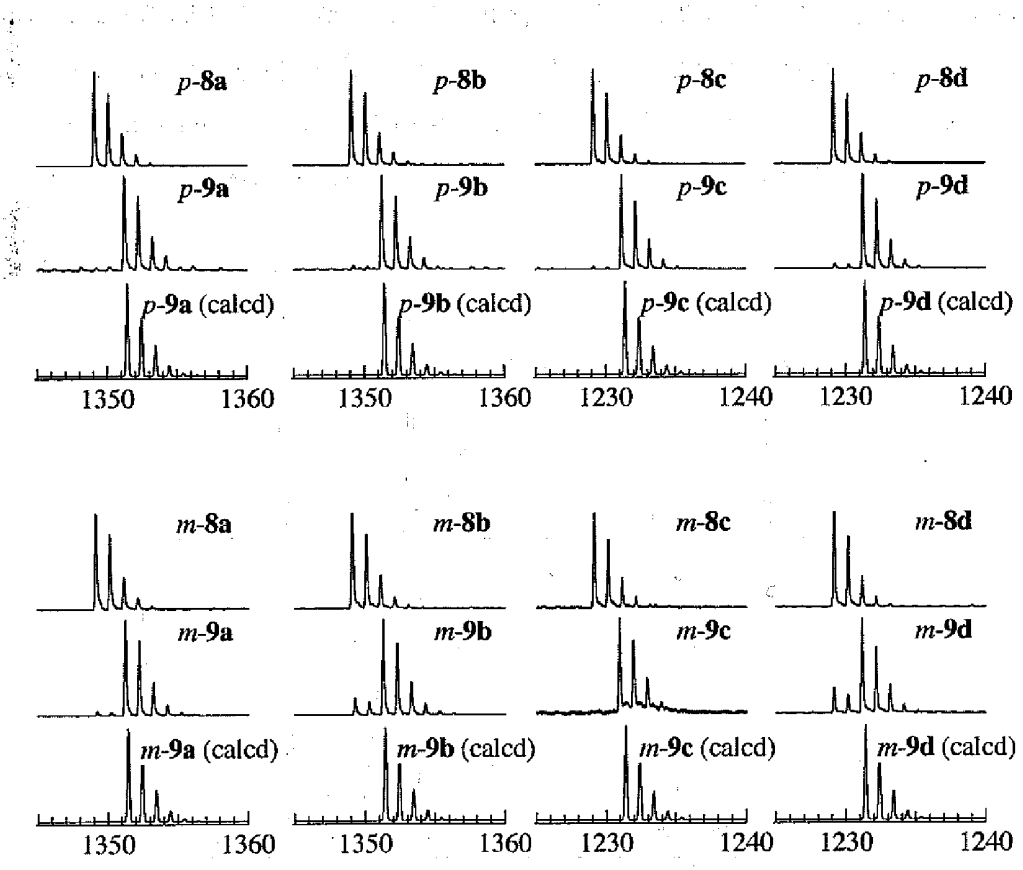

Figure 4-4 ESI-TOF mass spectra of **8** and **9**, calculation spectrum of **9**. $[M+Na]^+$ species were observed on positive mode

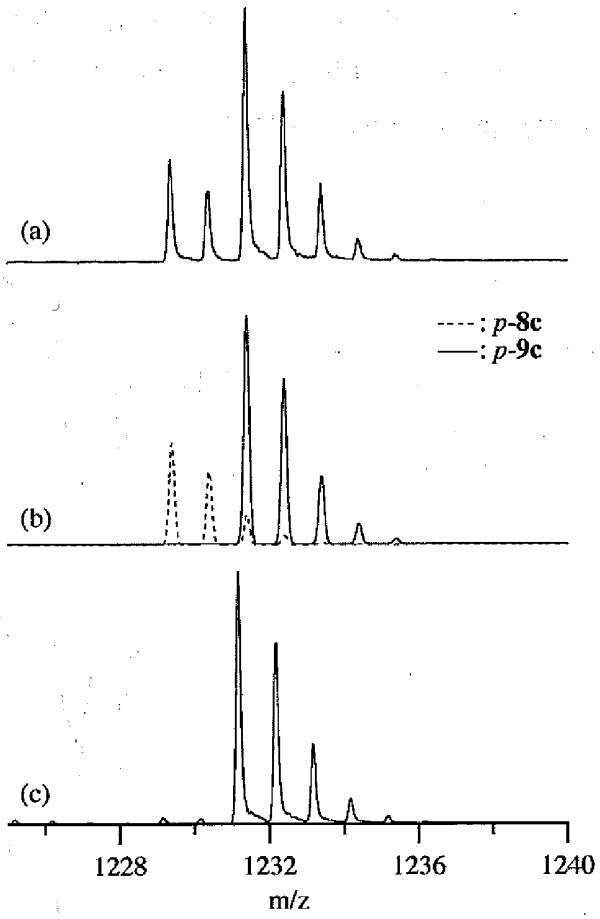

Figure 4-5 ESI-TOF mass spectral analysis of purification of *p*-**9c**. The ESI-TOF mass of *p*-**9c** before purification (a) and after RP-TLC purification (c). The crude product can be divided into two contributions of *p*-**8c** and *p*-**8c** (b). All peaks was found as $[M+Na]^+$.

4-2-5. IR spectra of deacetylated glycoconjugated chlorins **9**

The infra-red absorption spectra of deacetylated glycoconjugated chlorins **9** were recorded using attenuated total reflection (ATR) method (Figure 4-6). The band assignments and wavenumbers (cm^{-1}) are listed in Table 4-3 and 4-4. All chlorins **9** showed absorptions in the regions from 3000 to 2900 cm^{-1} due to C-H stretch in the phenyl ring ($\nu_{C\text{-}H}$) and the pyrrole ring β-carbon ($\nu_{Cp\text{-}H}$) (Figure 4-6) [18-20]. In addition, the characteristic absorption for tetraphenylchlorin was found at 666.5 cm^{-1} due to out-of-plane C-H bending in the phenyl ring ($op\delta_{C\text{-}H}$) for all chlorins **9** [19-21]. All porphyrins *p*-**8** showed one peak around 1600 cm^{-1} due to C=C stretch ($\nu_{C=C}$) and C=N stretch ($\nu_{C=N}$) in the porphyrin ring (Figure 4-6a) [19-21]. On the other hand, top of this peak splitted in all chlorins *p*-**9** (Figure 4-6b). This may be

reflected from asymmetric structure of chlorin ring. While all porphyrins *m*-**8** showed splitted peak around 1600 cm^{-1} due to C=C stretch ($\nu_{C=C}$) and C=N stretch ($\nu_{C=N}$) in the porphyrin ring, these peaks of all chlorins *m*-**9** broaded (Figure 4-6c and 4-6d). All chlorins **9** showed the peak at 3380 cm^{-1} due to O-H stretch (ν_{OH}) of hydroxyl groups. (Figure 4-6) [19-21].

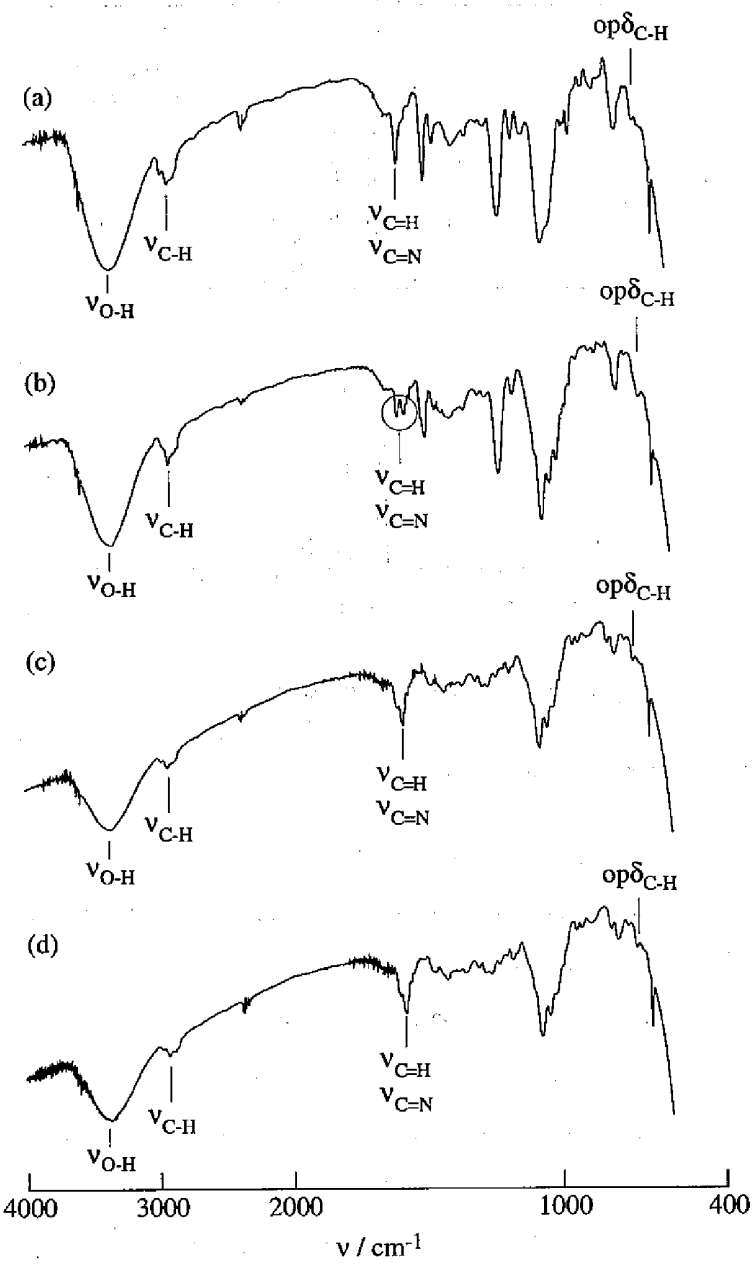

Figure 4-6 IR spectra of *p*-**8a** (a), *p*-**9a** (b), *m*-**8a** (c) and *m*-**9a** (d).

Table 4-3 IR spectral data of *p*-**9**[a]

assignment[b]	*p*-**9a**	*p*-**9b**	*p*-**9c**	*p*-**9d**	assignment[c]
ν_{OH}	3355.58	3354.62	3355.58	3367.16	ν_{OH}
$\nu_{a,C-H}$	2923.48	2918.65	2917.69	2920.58	ν_{C-H}
				2840.53	
$\nu_{s,C-H}$	2848.24	2846.31	2844.38		
	2354.41		2362.12	2355.37	
				1718.78	
$\nu_{C=C}$	1604.97	1604.01	1604.01	1602.08	$\nu_{C=C}$,$\nu_{C=N}$
	1578.93	1580.86			
δ_{N-H}	1503.70	1504.66	1503.70	1500.80	
δ_{N-H}			1468.01	1449.68	
$\nu_{C=C}$,$\nu_{C=N}$	1413.03	1406.28			$\nu_{C=N}$,δ_{CCN}
	1229.77	1230.73	1227.84	1225.91	
	1177.69	1177.69	1176.72		
ipδ_{CH}	1073.52	1074.48		1070.62	δ_{Cp-H},$\nu_{C=C}$
Ring deform.	1018.54		1038.79		ν_{C-C},ν_{C-C}
				947.16	
op$\delta_{CH(Aw)}$		878.68			πCH
	794.77	793.80	795.73		πCH
$\pi_{(ring)}$				769.69	
	666.49	666.49	666.49	666.49	
	429.21	429.21	421.50	421.50	
		409.92	413.78		
				409.92	
	402.21				

[a] ATR method. [b] Empirical assignment from Caughey et al [16]. The abbreviations are as follows: ip, in plane; op, out of plane; a, asymmetric; s, symmetric; p, pyrrole β-carbon (Cp). [c] Assignments are made from normal coordinate analysis of 18 E_u bands [16].

Table 4-4 IR spectral data of *m*-**9**[a]

assignment[b]	*m*-**9a**	*m*-**9b**	*m*-**9c**	*m*-**9d**	assignment[c]
ν_{OH}	3355.58	3356.55	3355.58	3342.08	ν_{OH}
$\nu_{a,C-H}$					ν_{C-H}
	2924.44	2918.65	2925.41	2923.48	
$\nu_{s,C-H}$		2851.14		2853.07	
	2353.44	2360.19	2363.09	2606.15	
				2498.12	
$\nu_{C=C}$				1655.13	$\nu_{C=C}$,$\nu_{C=N}$
			1582.79	1577.96	
$\nu_{C=N}$	1578.93	1577.96			
δ_{N-H}		1469.94	1468.97	1467.04	
$\nu_{C=C}$,$\nu_{C=N}$	1425.57	1425.57	1426.53		$\nu_{C=N}$,δ_{CCN}
			1308.86		δ_{Cp-H}
	1262.56	1262.56	1261.60	1257.74	
	1182.51	1181.54	1183.47		
ν_{C-O}		1142.96	1105.35		
ipδ_{CH}	1073.52	1071.59	1071.59	1070.62	
	1044.58		1038.79		δ_{Cp-H},$\nu_{C=C}$
Ring deform.					ν_{C-C},ν_{C-C}
	947.16	946.20	946.20	947.16	
		927.87	927.87		
op$\delta_{CH(Au)}$			818.88		πCH
					πCH
	792.84	790.91	782.23	774.51	
$\pi_{(ring)}$					
	666.49	666.49	666.49	666.49	
	425.36	429.21	425.36	425.36	
			413.78	406.07	
	413.78	402.21			

[a] ATR method. [b] Empirical assignment from Caughey et al [16]. The abbreviations are as follows: ip, in plane; op, out of plane; a, asymmetric; s, symmetric; p, pyrrole β-carbon (Cp). [c] Assignments are made from normal coordinate analysis of 18 E_u bands [16].

4-3. Summary

Eight deacetylated glycoconjugated chlorins **9** were synthesized by means of the Whitlock method with diimide reduction, and then this crude product by NaOMe in a mixture of MeOH and CH_2Cl_2. The crude deacetylated product was successfully purified by RP-TLC. The chlorins **9** were obtained in the yields of 14 ~ 49 % with the purities of >95 % after evaluation by HPLC using an octadecylsilyl-supported silica gel column. These photosensitizers were fully characterized was by ^{1}H NMR, ESI-TOF mass, IR and electronic absorption spectroscopy. The electronic absorption spectra of chlorins **9** were recorded in DMSO. The chlorins **9** have a strong Soret band at ca. 420 nm and four weak Q bands at ca. 520 (Q_{IV}), 550 (Q_{III}), 600 (Q_{II}), and 650 (Q_I) nm. In this result, the Q_I band of all chlorins **9** is greater than that of porphyrins **8**. The Q_I band of chlorin *p*-**9a** were about 3-fold greater than that of corresponding porphyrin *p*-**8a**. Because the Q_I band is usually used for PDT treatment, it is expected that that chlorins have higher photodynamic effect than that of porphyrins. In CD_3OD, the peak at 8.8 ppm in ^{1}H NMR spectra due to the β-pyrrole proton of porphyrins **8** disappeared completely in of chlorins **9** except for *m*-**9b** and *m*-**9d**. On the other hand, the peak at 8.6, 8.4, 8.2 and 4.2 ppm in ^{1}H NMR spectra due to the 8,17-β-pyrrole proton, 12,13-β-pyrrole proton, 7,18-β-pyrrole proton and 2,3-β-pyrrole proton of chlorins **9** appeared completely in of corresponding porphyrins **8**. The ESI-TOF mass spectroscopy, all porphyrins **8** and chlorins **9** were detected as a $[M + Na]^+$ species in the positive mode. The small difference in the molecular weight between chlorins **9** and corresponding porphyrins **8** was also clearly evidenced by ESI-TOF mass spectrometry.

4-4. Experimentals

Materials and Measurements

^{1}H NMR spectra were recorded on Bruker AVANCE 800 (800 MHz) (National Food Research Institute), Bruker DRX600 (600 MHz) (National Food Research Institute), JEOL JNM-AL400 (400 MHz) (Nara Women's University) and VARIAN GEMINI 2000 (300 MHz) (Nara Women's University) instruments. NMR assignment appears with following abbreviations; "P" is chlorin ring, "R" is saccharide residue, and "Ar" is aromatic group or bridging phenylene group between P and R. Electronic absorption spectra in dimethyl sulfoxide (DMSO) were recorded on a JASCO V-570 spectrophotometer (Nara Women's University) and HITACHI U-2000 spectrophotometer (Osaka Prefectural College of Technology). IR spectra were recorded on FT/IR-8900 JASCO (Osaka Prefectural College ofTechnology)

using an ATR-500/M instrument. Mass spectra in methanol were recorded on JMS T100LC JEOL (Nara Women's University), JEOL JMS-700 (Nara Institute of Science and Technology), and JMS-100LC (National Food Research Institute) instruments. The reversed phase thin layer chromatography (RP-TLC) was carried out using R-18 F_{254S} (Merck Japan Ltd.) eluted with mixture of methanol and water. The purity of the chlorins **9** was determined by high performance liquid chromatography (HPLC, HITACHI, L-6000) (Osaka Prefectural College of Technology) equipped with octadecylsilyl-bounded silica gel (HITACHI, HITACHI GEL 4 mmϕ × 150 mm) column and a diode array detector (HITACHI L-4000) using acetonitrile / water = 1 / 1 as an eluent.

4-4-1. 5,10,15,20-Tetrakis[4-(β-D-glucopyranosyloxy)phenyl]chlorin (p-9a)

p-**7a** (99 mg, 50 μmol), K_2CO_3 (0.59 g, 3.8 mmol), *p*-toluenesulfonylhydrazide (0.27 g, 1.4 mmol) and dry pyridine (20 mL) were stirred with N_2 flushing for 20 min. The mixture was heated at 110 ~ 120 °C for 6.5 h under N_2. *p*-Toluenesulfonylhydrazide (0.43 g, 2.3 mmol) dissolved in dry pyridine (2 mL) was added to the mixture twice at intervals of 2 h. The reaction mixture was added in benzene (100 mL) and distilled water (50 mL), and heated at 100 °C for 1 h to decompose remaining *p*-toluenesulfonylhydrazide. The organic layer was separated and washed with cold 2 M HCl (aq) (150 mL × 1), distilled water (150 mL × 1) and saturated $NaHCO_3$ (aq) (150 mL × 1), successively. To minimize the excess amount of tetrahydro-porphyrin (i.e., bacteriochlorin), *o*-chloranil (0.10 g, 0.41 mmol) was added slowly to the resulting mixture at room temperature until the absorption at 740 nm, that is due to tetrahydro-porphyrin, had just disappeared. The solution was washed with 5 % $NaHSO_3$ (aq) (150 mL × 2), distilled water (150 mL × 1), 5 % NaOH (aq) (150 mL × 1) and sat. $NaHCO_3$ (aq) (150 mL × 1). The solution was dried over Na_2SO_4, and the solvent was removed under reduced pressure. This crude powder was dissolved into the mixture of CH_2Cl_2 (10 mL) and methanol (10 mL). To the solution, sodium methoxide was added until pH 9. This mixture was stirred for 24 h at room temperature, then 25 % acetic acid (aq) was added to neutralize it. The solvent was evaporated, and the crude product was purified by gel filtration on a Sephadex LH-20® column eluted with methanol. The solvent was evaporated. In order to remove minor analogues, i.e., porphyrin and bacteriochlorin derivatives, the crude product was fully purified by reversed phase thin layer chromatography (RP-TLC, RP-18 F_{254S}, Merck Japan Ltd.) using an octadecylsilyl-bounded silica gel eluted with mixture of methanol and water (7/1, v/v). The extracted solution was neutralized by adding NH_3(aq), then evaporated. The precipitate was washed with water

and dried under *vacuo* to give *p*-**9a** as a dark red powder (31 mg, 47 %). R_f 0.53 (methanol/water, 20/1). Purity (HPLC): >99 %. ^{1}H NMR spectrum of *p*-**9a** was agreed with the literature [8].

4-4-2. 5,10,15,20-Tetrakis[4-(β-D-galactopyranosyloxy)phenyl]chlorin (p-9b)

The similar procedure for *p*-**9a** was applied to *p*-**7b** (226 mg, 113 μmol) to give *p*-**9b** as a dark red powder (48 mg, 32 %). R_f 0.25 (methanol/water, 7/1). Purity (HPLC): 98 %. ^{1}H NMR spectrum of *p*-**9b** was agreed with the literature [8].

4-4-3. 5,10,15,20-Tetrakis[4-(β-D-xylopyranosyloxy)phenyl]chlorin (p-9c)

The similar procedure for *p*-**9a** was applied to *p*-**7c** (189 mg, 110 μmol) to give *p*-**9c** as a dark red powder (40 mg, 30 %). R_f 0.45 (methanol/water, 7/1). Purity (HPLC): 97 %. ^{1}H NMR (CD_3OD, 800.03 MHz): δ (ppm) = 8.60 (2H, d, ^3J = 4.7 Hz, 8,17-β-P), 8.39 (2H, s, 12,13- β-P), 8.22 (2H, d, ^3J = 4.7 Hz, 7,18- β-P), 8.00 (2H, br, ^3J = 8.1 Hz, 10,15-(*o*-Ar)), 7.79 (2H, br, ^3J = 8.2 Hz, 5,20-(*o*-Ar)), 7.42 (2H, d, ^3J = 8.4 Hz, 10,15-(*m*-Ar)), 7.40 (2H, d, ^3J = 8.4 Hz, 5,20-(*m*-Ar)), 5.19 (2H, d, ^3J = 7.5 Hz, 10,15-(1-R)), 5.14 (2H, d, ^3J = 7.5 Hz, 5,20-(1-R)), 4.17 (4H, brs, 2,3-β-P), 4.06 (2H, dd, ^3J = 11.7 Hz, ^2J = 5.4 Hz, 10,15-(5-R)), 4.04 (2H, dd, ^3J = 11.7 Hz, ^2J = 5.4 Hz, 5,20-(5-R)), 3.69 (2H, ddd, ^3J = 10.3 Hz, ^3J = 8.6 Hz, ^2J = 5.4 Hz, 10,15-(4-R)), 3.62 (2H, ddd, ^3J = 10.2 Hz, ^3J = 8.6 Hz, ^2J = 5.2 Hz, 5,20-(4-R)), 3.62 (2H, dd, ^3J = 9.2 Hz, ^2J = 7.5 Hz, 10,15-(2-R)), 3.60 (2H, dd, ^3J = 9.2 Hz, ^2J = 7.5 Hz, 5,20-(2-R)), 3.55 (2H, dd, ^3J = 9.2 Hz, ^2J = 8.6 Hz, 10,15-(3-R)), 3.52 (2H, dd, ^3J = 9.2 Hz, ^2J = 8.6 Hz, 5,20-(3-R)), 3.52 (2H, dd, ^3J = 11.7 Hz, ^2J = 10.3 Hz, 10,15-(5-R)), 3.50 (2H, dd, ^3J = 11.7 Hz, ^2J = 10.2 Hz, 5,20-(5-R)). Fast atom bombardment high resolution mass spectrometry(FAB-HRMS) (m/z) = $[M+H]^+$ calcd for $C_{64}H_{65}N_4O_{20}$, 1209.41867; found, 1209.41837.

4-4-4. 5,10,15,20-Tetrakis[4-(β-D-arabinopyranosyloxy)phenyl]chlorin (p-9d)

The similar procedure for *p*-**9a** was applied to *p*-**7d** (408 mg, 239 μmol) to give *p*-**9d** as a dark red powder (49 mg, 17 %). R_f 0.75 (methanol/water, 10/1). Purity (HPLC): 96 %. ^{1}H NMR (CD_3OD, 800.03 MHz): δ (ppm) = 8.60 (2H, d, ^3J = 4.7 Hz, 8,17-β-P), 8.37 (2H, s, 12,13- β-P), 8.20 (2H, d, ^3J = 4.7 Hz, 7,18- β-P), 7.97 (2H, brd, ^3J = 6.8 Hz, 10,15-(*o*-Ar)), 7.72 (2H, brd, ^3J = 8.4 Hz, 5,20-(*o*-Ar)), 7.42 (2H, d, ^3J = 6.8 Hz, 10,15-(*m*-Ar)), 7.37 (2H, d, ^3J = 8.4 Hz, 5,20-(*m*-Ar)), 5.16 (2H, d, ^3J = 7.2 Hz, 10,15-(1-R)), 5.10 (2H, d, ^3J = 7.2 Hz, 5,20-(1-R)), 4.10 (4H, brs, 2,3- β-P), 4.06 (2H, dd, ^3J = 12.6 Hz,

^2J = 2.5 Hz, 10,15-(5-R)), 4.05 (2H, dd, ^3J = 12.5 Hz, ^2J = 2.4 Hz, 5,20-(5-R)), 3.99 (2H, dd, ^3J = 9.2 Hz, ^2J = 7.2 Hz, 10,15-(2-R)), 3.97 (2H, brs, 10,15-(4-R)), 3.96 (2H, dd, ^3J = 9.2 Hz, ^2J = 7.1 Hz, 5,20-(2-R)), 3.96 (2H, brs, 5,20-(4-R)), 3.85 (2H, brd, ^3J = 11.6 Hz, 10,15-(5-R)), 3.83 (2H, brd, ^3J = 11.6 Hz, 5,20-(5-R)), 3.76 (2H, dd, ^3J = 9.2 Hz, ^2J = 3.5 Hz, 10,15-(3-R)), 3.74 (2H, dd, ^3J = 9.2 Hz, ^2J = 3.4 Hz, 5,20-(3-R)). FAB-HRMS (m/z) = $[M+Na]^+$ calcd for $C_{64}H_{64}N_4O_{20}Na$, 1231.40061; found, 1231.40045.

*4-4-5. 5,10,15,20-Tetrakis[3-(β-D-glucopyranosyloxy)phenyl]chlorin (m-**9a**)*

The similar procedure for *p*-**9a** was applied to *m*-**7a** (419 mg, 210 μmol) to give *m*-**9a** as a dark red powder (103 mg, 37 %). R_f 0.54 (methanol/water, 8/1). Purity (HPLC): 96 %. ^{1}H NMR spectrum of *m*-**9a** was agreed with the literature [10].

*4-4-6. 5,10,15,20-Tetrakis[3-(β-D-galactopyranosyloxy)phenyl]chlorin (m-**9b**)*

The similar procedure for *p*-**9a** was applied to *m*-**7b** (669 mg, 335 μmol) to give *m*-**9b** as a dark red powder (218 mg, 49 %). R_f 0.77 (methanol/water, 20/1). Purity (HPLC): 99 %. ^{1}H NMR (CD_3OD, 300.07 MHz): δ (ppm) = 8.64 (2H, m, 8,17-β-P), 8.41 (2H, m, 12,13-β-P), 8.26 (2H, m, 7,18-β-P), 7.97 ~ 7.39 (8H, m, Ar), 5.17 ~ 5.08 (2H, m, 10,15-(1-R)), 5.08 ~ 5.05 (2H, m, 5,20-(1-R)), 4.20 (4H, m, 2,3-β-P), 3.93 ~ 3.83 (8H, m, 2,4-R), 3.67 ~ 3.53 (16H, m, 3,5,6-R). ESI-HRMS (m/z) = $[M+Na]^+$ calcd for $C_{68}H_{72}N_4O_{24}Na$, 1351.4434; found, 1351.44276.

*4-4-7. 5,10,15,20-Tetrakis[3-(β-D-xylopyranosyloxy)phenyl]chlorin (m-**9c**)*

The similar procedure for *p*-**9a** was applied to *m*-**7c** (121 mg, 70.9 μmol) to give *m*-**9c** as a dark red powder (30 mg, 35 %). R_f 0.76 (methanol/water, 10/1). Purity (HPLC): >99 %. ^{1}H NMR (DMSO-d_6, 300.07 MHz): δ (ppm) = 8.60 (2H, m, 8,17-β-P), 8.33 (2H, s, 12,13-β-P), 8.21 (2H, m, 7,18-β-P), 7.86 ~ 7.15 (8H, m, Ar), 5.45 (4H, m, 2-RO*H*), 5.20 ~ 5.03 (12H, m, 1-R, 3,4-RO*H*), 4.14 (4H, m, 2,3-β-P), 3.73 ~ 3.14 (20H, m, 2,3,4,5-R), -1.65 (2H, br, N*H*). ESI-HRMS (m/z) = $[M+Na]^+$ calcd for $C_{64}H_{64}N_4O_{20}Na$, 1231.4011; found, 1231.3962.

*4-4-8. 5,10,15,20-Tetrakis[3-(β-D-arabinopyranosyloxy)phenyl]chlorin (m-**9d**)*

The similar procedure for *p*-**9a** was applied to *m*-**7d** (192 mg, 112 μmol) to give *m*-**9d** as a dark red powder (19 mg, 14 %). R_f 0.38 (methanol/water, 10:1). Purity (HPLC): >99 %. UV-vis (DMSO): λ_{max}

(nm) ($\varepsilon \times 10^{-3}$ / $M^{-1} \cdot cm^{-1}$) = 421 (16.3), 516 (1.62), 547 (0.90), 602 (0.52), 651 (2.22). ^1H NMR (CD_3OD, 300.07 MHz): δ (ppm) = 8.53 (2H, m, 8,17-β-P), 8.31 (2H, s, 12,13-β-P), 8.15 (2H, m, 7,18-β-P), 7.81 ~ 7.21 (8H, m, Ar), 5.03 ~ 4.98 (2H, m, 10,15-(1-R)), 4.98 ~ 4.91 (2H, m, 5,20-(1-R)), 4.11 (4H, m, 2,3-β-P), 3.85 ~ 3.71 (8H, m, 2,5-R), 3.61 ~ 3.26 (12H, m, 3,4,5-R). ESI-HRMS (m/z) = $[M+Na]^+$ calcd for $C_{64}H_{64}N_4O_{20}Na$, 1231.401161; found, 1231.40061.

4-5. References

1. R. Bonnet, Chemical Aspects of Photodynamic Therapy., Taylor & Francis, UK, 2000.
2. I. Okura, Photosensitization of Porphyrins and Phthalocyanines., Kodansha, Tokyo, 2000.
3. M.H. Teiten, L. Bezdetnaya, J.L. Merlin, C. Bour-Dill, M.E. Pauly, M. Dicate, F. Guilleemim, Effect of meta-tetra(hydroxyphenyl)chlorin (m-THPC)-mediated photodynamic therapy on sensitive and multidrug-resistant human breast cancer cells. J. Photochem. Photobiol. B: Biol. 62 (2001) 146-152.
4. V. Melnikova, L. Bezdetnaya, I. Belitchenko, A. Potapenko, J. L. Merlin, F. Guillemin, Meta-tetra(hydroxyphenyl)chlorin-sensitized photodynamic damage of cultured and normal cells in the presence of high concentrations of α-tocopherol. Cancer Letters. 139 (1999) 89-95.
5. H.J. Hopkinson, D.I. Vernon, S.B. Brown, Identification and Partial Characterization of an Unusual Distribution of the Photosensitizer *meta*-Tetrahydroxyphenyl Chlorin (Temoporfin) in Human Plasma. Photochem. Photobiol. 69 (1999) 482-488.
6. H.W. Whitlock, R. Hanauer, M.Y. Oester, B.K. Bower, Diimide Reduction of Porphyrins. J. Am. Chem. Soc. 91 (1969) 7485-7489.
7. R. Bonnett, R, P. Charlesworth, B.D. Djelal, S. Foley, D.J. McGarvey, T.G. Truscott, Photophysical properties of *m*-THPP, *m*-THPC and *m*-THPBC: a comparative study. J. Chem. Soc., Perkin Trans. 2 (1999) 325-328.
8. Y. Mikata, Y. Onchi, M. Shibata, T. Kakuchi, H. Ono, S. Ogura, I. Okura, S. Yano, Synthesis and Phototoxic Property of Tetra- and Octa-Glycoconjugated Tetraphenylchlorins. Bioorg. Med. Chem. Lett. 8 (1998) 3543-3548.
9. G. Zheng, A. Graham, M. Shibata, J.R. Missert, A.R. Oseroff, T.J. Dougherty, R.K. Pandey, Synthesis of β-Galactose-Conjugated Chlorins Derived by Enyne Metathesis as Galactin-Specific Photosensitizers for Photodynamic Therapy. J. Org. Chem. 66 (2001) 8079-8716.

10. I. Laville, T. Figueiredo, B. Loock, S. Pigaglio, Ph. Maillard, D. S. Grierson, D. Carrez, A. Croisy, J. Blais, Synthesis, Cellular Internalization and Photodynamic Activity of Glycoconjugated Derivatives of Tri and Tetra (*meta*-hydroxyphenyl) chlorins. Bioorg. Med. Chem. 11 (2003) 1643-1652.

11. A.M.G. Silver, A.C. Tomé, M.G.P.M.S. Neves, A.M.S. Silva, J.A.S. Cavaleiro, D. Perrone, A. Dondoni, Porphyrins in 1,3-dipolar cycloaddition reactions with sugar nitrones. Synthesis of glycoconjugated isoxazolidine-fused chlorins and bacteriochlorins. Tetrahedron Lett. 43 (2002) 603-605.

12. R. Bonnett, B. D. Djelal, G. E. Hawkes, P. Haycock, F. Pont, Fine Structure of 5, 10, 15, 20-Tetrakis(*m*-hydroxyphenyl)chlorin (*m*-THPC): a ^{1}H, ^{13}C and ^{15}N NMR Study. J. Chem. Soc, Perkin Trans. 2. (1994) 1839-1843.

13. M. Momenteau, D. Oulmi, Ph. Maillard, A. Croisy, Photodynamic Therapy of cancer II. SPIE. 2325 (1994) 13-23.

14. K. Kohara, H. Higashio, Y. Yamaguchi, M. Koketsu, T. Odashima, Synthesis and Characterization of New Style of Water-Soluble Glycoconjugated Porphyrins as a Spectrophotometric Reagent for Metal Ions. Bull. Chem. Soc. Jpn. 67 (1994) 668-679.

15. P. Mailippe, J.-L. Guerquin-Kern, C. Hiel, M. Momenteau, Glycoconjugated Porphyrins. 2. Synthesis of Sterically Constrained Polyglycosylated Compounds Derived from Tetraphenylporphyrins. J. Org. Chem. 58 (1993) 2774-2780.

16. Y. Mikata, Y. Onchi, K. Tabata, S. Ogura, I. Okura, H. Ono, S. Yano, Sugar-dependent photocytotoxic property of tetra- and octa- glycoconjugated tetraphenylporphyrins. Tetrahedron Lett. 39 (1998) 4505-4508.

17. A. Kasselouri, O. Bourdon, D. Demore, J.C. Blais, P. Prognon, G. Bourg-Heckly, J. Blais, Fluorescence and Mass Spectrometry Studies of Meta-tetra(hydroxyphenyl)chlorin Photoproducts, Photochem. Photobiol. 70 (1999) 275-279.

19. R. Bonnett, Chemical Aspects of Photodynamic Therapy. Taylor & Francis, London. (2000) 149-156.

20. K. M. Smith, PORPHYRINS AND METALOPORPHYRINS. ELSEVIER SCIENTIFIC PUBLISHING COMPANY. New York. (1975) 526-535.

21. J.O. Alben, Infrared Spectroscopy of Porphyrins. *The Porphyrins*, 3; D. Dolphine., Academic Press. New York. 3 (1978) 323-332.

Chapter 5

In Vitro Study of Glyconjugated Chlorins

5-1. Introduction

Photodynamic therapy (PDT) is a kind of anti-cancer therapy which uses photosensitizers and light to generate cytotoxic singlet oxygen molecule ($^1O_2$) in tumor cells [1-6]. In the foregoing statements (chapter 3), the cellular uptake and photocytotoxicity of the glycoconjugated porphyrins **8** were examined using HeLa cells *in vitro*. The sugar-dependent cellular uptake and the photocytotoxicity were observed. And the results indicated that the photocytotoxicity is not related simply to cellular uptake. The photochemical properties of aggregates and/or the quantity of remaining monomeric species are different between glycoconjugated porphyrins having sugar units behavior in aqueous media such as cytoplasm. It may make difference in photodynamic effect in HeLa cells between glycoconjugated porphyrins having sugar units behavior.

In chapter 4, the author designed and synthesized deacetylated glycoconjugated chlorins **9** (Chart 5-1). In this chapter, the chemical properties of chlorins **9** estimated by Shake-Flask method and reversed phase high performance liquid chromatography (RP-HPLC). These chlorins **9** were subjected to test *in vitro* the cellular uptake by HeLa cells and the photocytotoxicity. These cellular uptake behavior and photocytotoxicity were discussed on the basis of hydrophobicity, and photochemical study in cytoplasm and aqueous media for these photosensitizers.

5-2. Results and discussion

5-2-1. Hydrophobicity parameters of deacetylated glycoconjugated chlorins p-9

It was reported that the cellular uptake amount of some porphyrin derivatives is closely related to their hydrophobicity parameters [7,8]. At first, the partition coefficients (Log *P* value) of monomiric form of deacetylated glycoconjugated chlorins *p*-**9** (c = 0.00695 μM) between phosphate buffered saline (PBS) and *n*-octanol were determined by conventional Shake-Flask method which reported in Chapter 3. The average Log *P* values of six replicate experiments ranged from -0.68 to -0.72, hence all photosensitizers are hydrophilic (Table 5-1). Because of the large standard deviations as same as case in porphyrins *p*-**8**, however, the Shake-Flask method could not clarify the differences in Log *P* values between chlorins *p*-**9**. The hydorophobicity of chlorins *p*-**9** was also determined by the RP-HPLC method reported in chapter 3. However, the *meta*-substituted chlorins *m*-**9** could not be determined by RP-HPLC because of their atropisomeric mixture. The chromatograms of chlorins *p*-**9** were independent of sample concentration in the range from 0.1 to 0.01 μmol·L^{-1} under the RP-HPLC condition used. The retention time t_R reflects the

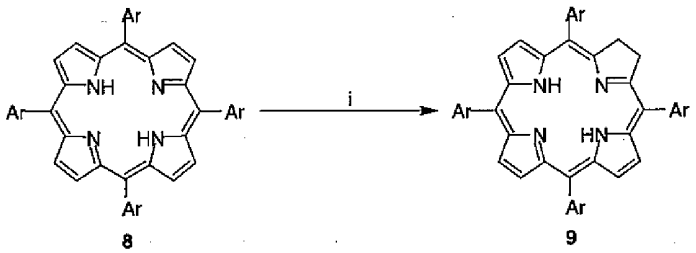

Types of Glycopyranosyl Groups	Substitution Position	
	para-Substituted (denoted as *p*-)	*meta*-Substituted (denoted as *m*-)
a: D-glucose	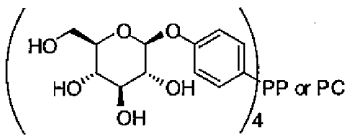	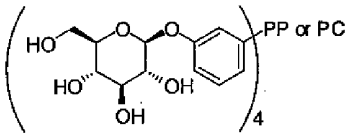
b: D-galactose	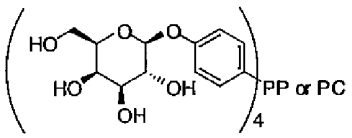	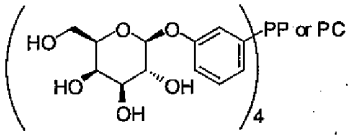
c: D-xylose	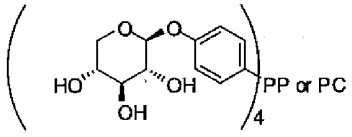	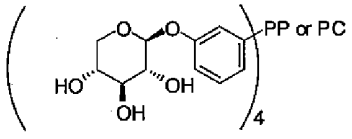
d: D-arabinose	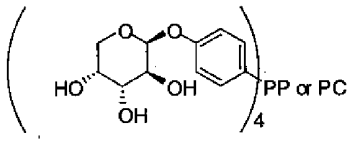	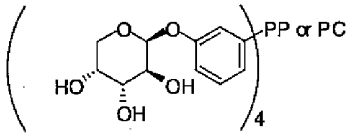

Chart 5-1

Table 5-1 Log *P* values and RP-HPLC retaintion time (t_R) of *p*-**9**

	Shake Flask method	RP-HPLC
compounds	Log *P* [a]	t_R / min
p-**9a**	-0.69 ± 0.03	6.18
p-**9b**	-0.69 ± 0.04	6.18
p-**9c**	-0.68 ± 0.05	6.73
p-**9d**	-0.72 ± 0.03	6.58

[a] The Log *P* value was determined after 18 h. The values represent the means ± s.d. of six replicate experiments.

nature of the monomeric form of these photosensitizers. The t_R value varies ranged from 6.18 to 6.73 min and reflects the hydrophobicity (lipophilicity) of chlorins *p*-**9**. As with the porphyrin derivatives, chlorins *p*-**9a** and *p*-**9b** have shorter retention time than chlorins *p*-**9c** and *p*-**9d**.

5-2-2. The $^1O_2$ producing ability of deacetylated glycoconjugated chlorins m-9

The $^1O_2$ producing ability of deacetylated glycoconjugated chlorins *m*-**9** was examined using degradation of 1,3-diphenylisobenzofuran (DPBF) by $^1O_2$ [9-13]. The maximum absorption wavelength of DPBF in DMSO (418 nm) was used to detect the photolysis of DPBF under O_2 saturated conditions. The plot of $\ln([Abs_{418}]/[Abs_{418}]_0)$ versus time shows linearity, indicating the degradation is pseudo 1st order reaction (Figure 5-1). The slope of the plot is proportional with the quantum yield of $^1O_2$. Table 5-2 lists the relative quantum yield of $^1O_2$ (Φ_Δ) to tetraphenylporphyrin tetrasulfonic acid (TPPS) as a standard. The Φ_Δ values slightly depended on sugar units attached in DMSO (i.e., monomeric form), and varied from 1.3 to 0.6.

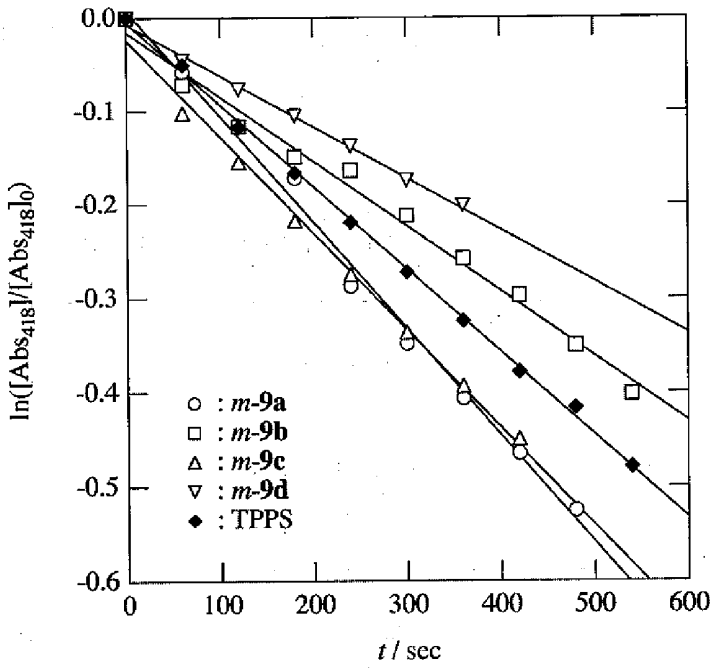

Figure 5-1 Degradation of DPBF by *m*-**9** and TPPS under O_2 saturated condition at 37 °C. [Photosensitizer] = 0.08 μM. [DPBF] = 36.7 μM. The light intensity applied was 40 mW/cm^2 using a 100 W halogen lamp ($\lambda > 500$ nm).

Table 5-2 Relative quantum yield (Φ_Δ) of $^1O_2$ in DMSO (c = 0.08 μM)

	Φ_Δ
TPPS	1
m-**9a**	1.29
m-**9b**	0.79
m-**9c**	1.17
m-**9d**	0.62

5-2-3. Cellular uptake of deacetylated glycoconjugated chlorins **9**

The cellular uptake of deacetylated glycoconjugated chlorins **9** by HeLa cells were determined using the same protocol reported in chapter 3. The uptake amount of photosensitizer was estimated on the basis of calibration data for each photosensitizer in DMSO (Figure 5-2). Figure 5-3 shows the relative cellular uptake of chlorins **9** as well as corresponding porphyrins **8** (chapter 3) in comparison with that of TPPS as a reference. All chlorins **9** show higher uptake than TPPS. The chlorins **9** show cellular uptake equal to or greater than those of the corresponding porphyrins **8**. The order of the cellular uptake amount was *m*-**9c** > *p*-**9d** > *m*-**9d** > *p*-**9a** > *p*-**9b** > *p*-**9c** > *m*-**9a** > *m*-**9b** > TPPS. Note that chlorin *m*-**9c** showed an uptake 50-fold greater than that of TPPS. At first, the lipophilicity of chlorins **9** and TPPS is roughly evaluated by the R_f values on RP-TLC (Table 5-3). Increase in lipophilicity of the photosensitiser decreases the R_f value on RP-TLC because of the octadecylsilyl-modified surface. All chlorins **9** showed much higher lipophilicity than that of TPPS. The R_f values of chlorins **9c** and **9d** (i.e.,

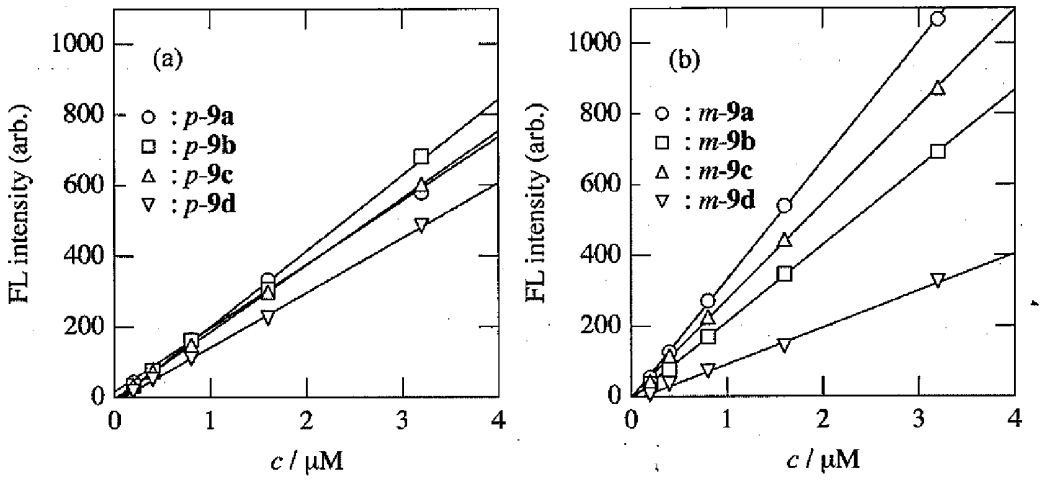

Figure 5-2 Calibration curve of the fluorescence intensity versus the concentration of photosensitizer

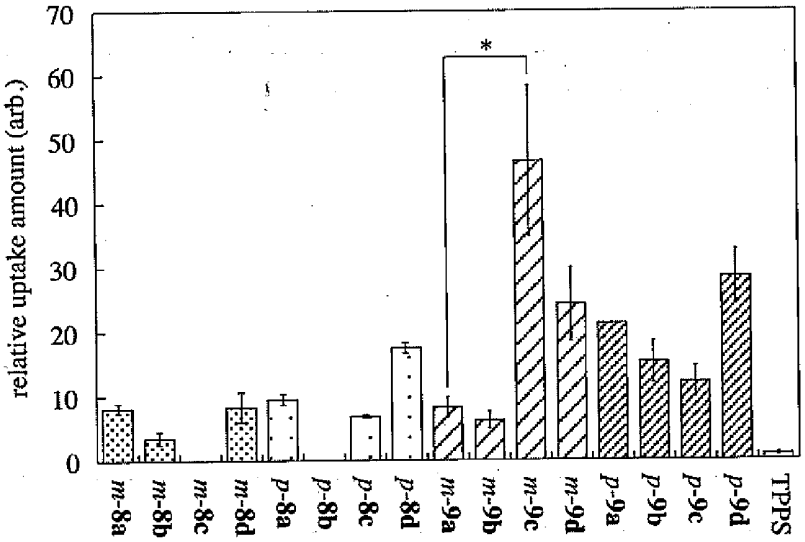

Figure 5-3 The cellular uptake of porphyrins **8** and chlorins **9** by HeLa cells after incubation for 24 h. The values represent the mean ± s.d. of three replicate experiments. The values for *m*-**8c** and *p*-**8b** could not be quantified because of precipitation. ***The value of *m*-**9c** was statistically significantly ($p < 0.001$) different from that of *m*-**9a**.

Table 5-3 Electronic absorption and fluorescence spectral data of *p*-**8a** and *m*-**9** in DMSO (c = 4.97 μM, 37 °C)

	Electronic absorption spectra					Fluorescence spcetra[b]	
	λ_{max} (nm)					λ_{max} (nm)	
	Soret[a]	IV	III	II	I	(0,0)	(0,1)
p-**8a**	422 (407)	518.5	554	595	649.5	658	722
m-**9a**	421 (408.5)	519.5	545	598	652.5	657	721
m-**9b**	420 (408.5)	516.5	545	596.5	652.5	657	719
m-**9c**	420.5 (408)	519	545	598	652	657	720
m-**9d**	420 (408.5)	516	545	595.5	651	656.5	718

[a] The value in parenthesis is a shoulder peak by Soret band. [b] λ_{ex} = 430 nm.

pentose groups) are smaller than those of chlorins **9a** and **9b** (i.e., hexose groups) regardless of the substituent position, indicating enhanced lipophilic character of **9c** and **9d** (i.e., pentose groups). In general, a significant lipophilicity is required for a drug to interact with the hydrophobic cell membrane and pass through it, i.e., to show effective cellular uptake [14,15]. Except for chlorin *p*-**9c**, xylopyranosyl (**c**) and arabinopyranosyl (**d**) groups (i.e., pentose groups) are much more effective to improve the cellular uptake than glucopyranosyl (**a**) and galactopyranosyl (**b**) groups (i.e., hexose groups). This may reflect the lack of one hydroxymethyl group.

Figures 5-4 shows the plot of cellular uptake amount of porphyrins *p*-**6**, porphyrins *p*-**8** and chlorins *p*-**9** as a function of retention time t_R on RP-HPLC. For same sugar conjugated phtosensitizers, the cellular uptake amount increased with an increase of t_R value, i.e., in the order of *p*-**6** < *p*-**8** < (or =) *p*-**9**. (Figure 5-4a). This indicates the porphyrin ring affects the hydrophobicity and results in variation of the cellular uptake. On the other hand, Figure 5-4b shows the sugar unit effects on cellular uptake and t_R values for each porphyrinoids. The hydrophobicity change due to the sugar unit is not simply connected to the cellular uptake. Hence, the sugar unit affects the nature of cellular uptake by another fashion besides of hydrophobic interaction.

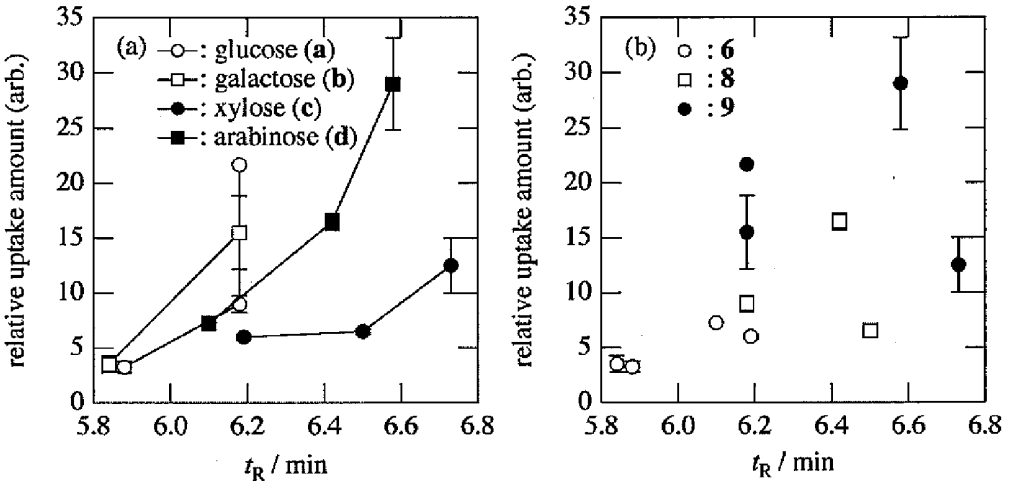

Figure 5-4 The plots of cellular uptake as a function of RP-HPLC retention time t_R showing the effect of porphyrin ring (a) and sugar unit (b).

5-2-4. Drug dose-dependence in the photodynamic effect of m-9a

The above results indicate a unique effect of sugar units on the interaction with HeLa cells. Among the deacetylated glycoconjugated chlorin *m*-**9c** shows the highest uptake by HeLa cells. Hence, *m*-**9c** and its related ß, *m*-**9a**, were investigated for photocytotoxicity in comparison with TPPS. The *in vitro* assessment of photocytotoxicity was carried out under the same protocol reported in chapter 3. HeLa cells were almost completely killed by chlorin *m*-**9a** at the concentration of 1 μM. The cell survival was 33.6 % when the drug concentration was 0.2 μM. From these results, the photosensitizer dose inducing a 50 % death rate (LD_{50}) was estimated as around 0.2 μM. In chapter 3, the LD_{50} value of porphyrin *p*-**8a** is determined to be 5 μM under the same conditions. Thus, the photocytotoxicity of chlorin *m*-**9a** is

almost 25-fold greater than that of porphyrin *p*-**8a**. This is impressive, because the cellular uptake of chlorin *m*-**9a** is almost the same as that of porphyrin *p*-**8a**. It is well known that there is no difference in the quantum yield of $^1O_2$ between porphyrin and chlorin derivatives [5]. Bonnett reported the photophysical properties and photocytotoxicity of 5,10,15,20-tetrakis(*m*-hydroxyphenyl)porphyrin (*m*-THPP) and 5,10,15,20-tetrakis(*m*-hydroxyphenyl)chlorin (*m*-THPC) [5], and noted that the photocytotoxicity of *m*-THPC is almost 10-fold higher than that of *m*-THPP, although the $^1O_2$ quantum yield for *m*-THPC is almost the same as that for *m*-THPP in methanol. In this case, the photocytotoxicity was almost proportional to the absorbance at the Q_1 band [5]. A difference in the transition probability may account for the difference in photocytotoxicity between the chlorin and porphyrin rings. For *m*-**9a** and *p*-**8a**, however, the difference in the molar extinction coefficient at the Q_1 band is too small to explain the difference in the photocytotoxicity (3.22×10^4 $M^{-1} \cdot cm^{-1}$ for *m*-**9a** and 0.64×10^4 $M^{-1} \cdot cm^{-1}$ for *p*-**8a** in DMSO) (Figure 5-5). Hence, there is no doubt that the glycopyranosyl group influences not only cellular uptake, but also the photodynamic effect, although the reason for this remains to be established.

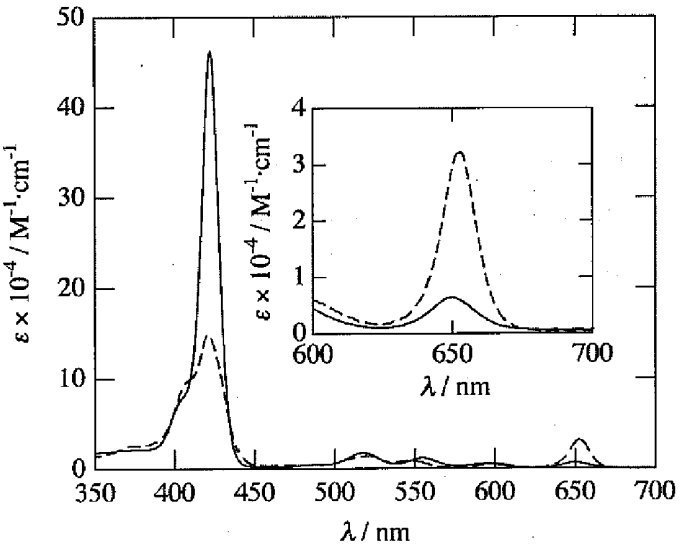

Figure 5-5 Electronic absorption spectra of *p*-**8a** (c = 4.97 μM, solid line) and *m*-**9a** (c = 4.97 μM, broken line) in DMSO at 20 °C.

5-2-5. In vitro study of the relationship between cellular uptake and photocytotoxicity

The photocytotoxicity of glycoconjugated chlorins *m*-**9a**, *m*-**9c** and TPPS was evaluated by irradiation of cells with a 100 W halogen lamp ($\lambda > 500$ nm, 24 mW/cm^2) at a light dose of 16 J/cm^2 after incubation with photosensitizer for 24 h. Figure 5-6a shows the percentage cell survival after 24 h incubation without light irradiation. These photosensitizers showed no cytotoxicity in the dark. Figure 5-6b shows the percentage cell survival after 24 h incubation. The photocytotoxicity of *m*-**9a** (27.8 %) is significantly higher than that of *m*-**9c** (96.5 %) or TPPS (110.8 %). Surprisingly, *m*-**9a** exerted higher photocytotoxicity than *m*-**9c**, although the cellular uptake of *m*-**9a** was only about 5-fold of that of *m*-**9c**. This result clearly shows that the amount of cellular uptake is not related simply to the photodynamic effect. The absorbance at the Q_1 band of *m*-**9a** (3.22×10^4 M^{-1}·cm^{-1}) is almost the same to that of *m*-**9c** (3.28×10^4 M^{-1}·cm^{-1}) in DMSO. As reported previously, in general, the sugar unit does not affect the $^1O_2$-producing ability of glycoconjugated chlorins in an organic solvent [5]. Hence, the physical properties of *m*-**9a** and *m*-**9c** in organic solvents can not explain the difference in *in vitro* photocytotoxicity. In organic solvents such as DMSO, *m*-**9a** and *m*-**9c** are in monomeric form, so these physical properties reflect those of the monomeric state. One possible explanation of the results is that the photosensitizers aggregate inside or on the surface of the cells. The stacking interaction of porphyrins reduces the fluorescence life time and $^1O_2$ quantum yield [16]. Because *p*-**9c** is much hydrophobic than *p*-**9a**, the hydrophobic interaction may facilitate aggregate formation of *p*-**9c**, leading to quenching of the $^1O_2$ production. Another possibility is

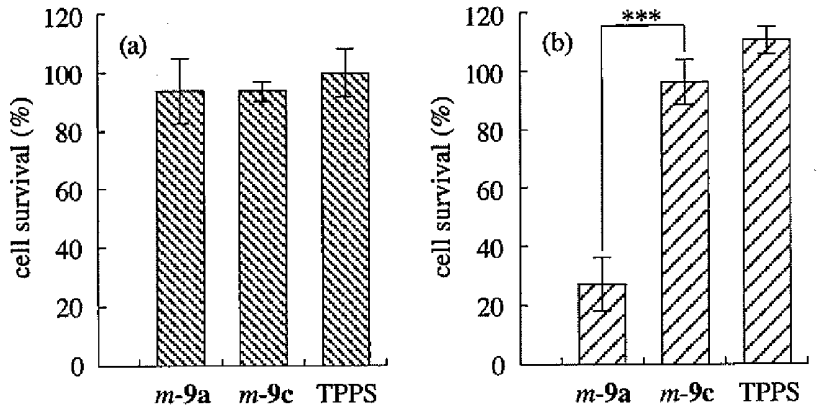

Figure 5-6 Cytotoxicity in the dark (a) and photocytotoxicity (b) of *m*-**9a**, *m*-**9c** and TPPS in HeLa cells. [Photosensitizer] = 0.2 μM. The light intensity applied was 25 mW/cm^2 using a 100 W halogen lamp ($\lambda > 500$ nm). The percentage cell survival was determined by Cell Titer-Glo™ Luminescent assay after 48 h incubation. The values represent the means ± s.d. of six replicate experiments. ***Significant difference, $p < 0.001$.

a difference of subcellular localization between the photosensitizers.

5-2-6. Confocal fluorescence images of glycoconjugated porphyrin p-8a, p-8d and chlorins m-9

The above result clearly shows that the amount of cellular uptake is not related simply to the photodynamic effect on HeLa cells. In order to explore the subcellular localization of photosensitizers, hence, deacetylated glycoconjugated chlorins *m*-**9** as well as porphyrins *p*-**8a** and *p*-**8d** were investigated by confocal laser scan microscope (CLSM) in comparison with TPPS. Figure 5-7 shows the confocal fluorescence images of photosensitizers uptaken by HeLa cells without glutaraldehyde. These photosensitizers were diffusively distributed throughout the cytoplasm except for *m*-**9b**. No fluorescence was detected in nuclear area, this is agreed with the results reported previously [17]. The chlorins *m*-**9** excited the stronger fluorescence than porphyrins and TPPS. The fluorescence of *m*-**9a** was the strongest in all photosensitizers. In the case of *m*-**9a**, it should be noted that the apoptosis was induced immediately by the laser of the microscope (Figure 5-8). Figure 5-9 shows the confocal fluorescence images of *m*-**9** with glutaraldehyde to fix HeLa cells. Interestingly, the fluorescence increased by addition of glutaraldehyde, especially for *m*-**9c** and *m*-**9d**. Hence the *m*-**9c** and *m*-**9d** were fairly uptaken by HeLa cells. However, the excited *m*-**9c** and *m*-**9d** could be quenched efficiently in the cytoplasm environment to reduce the photocytotoxicity. Hence, sugar moieties of glycoconjugated photosensitizers influenced not only cellular uptake by HeLa cells but also photochemical behavior in cytoplasm.

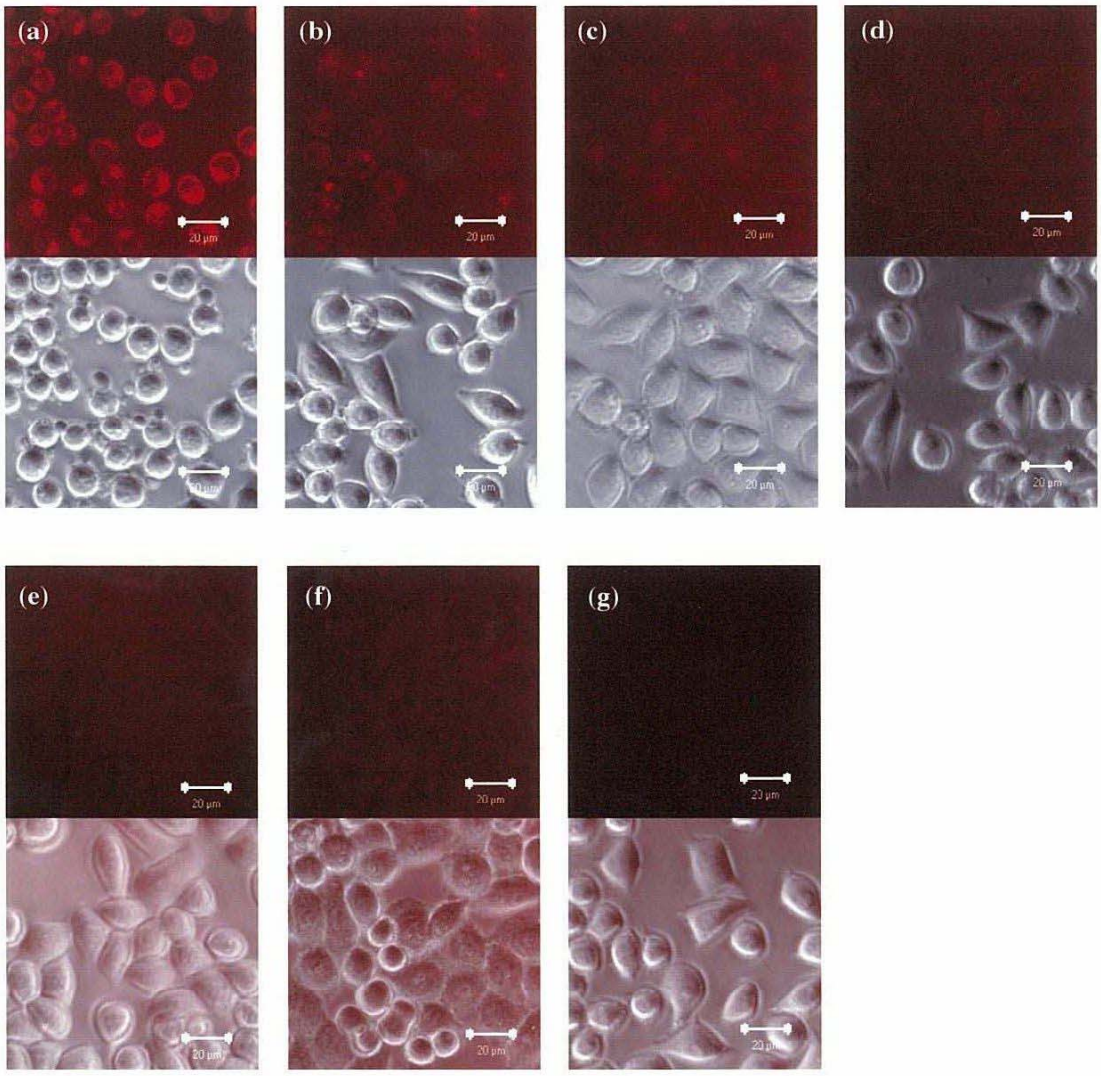

Figure 5-7 Confocal laser scanning microscope images of fluorescence from chlorins *m*-**9a** (a), *m*-**9b** (b), *m*-**9c** (c), *m*-**9d** (d), *p*-**8a** (e), *p*-**8d** (f) and TPPS (g) uptaken by HeLa cell.

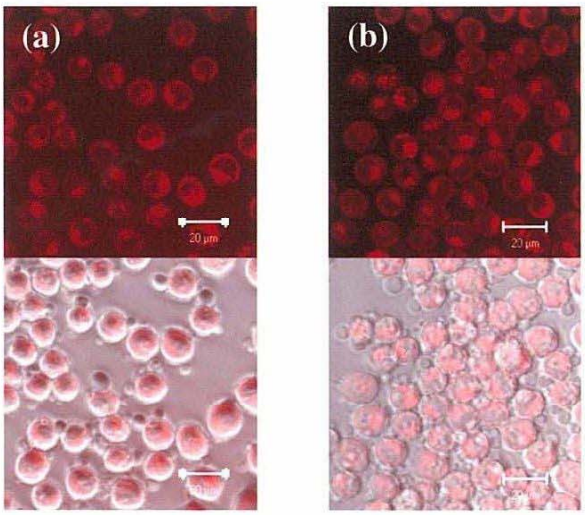

Figure 5-8 Confocal laser scanning microscope images of fluorescence from chlorin *m*-**9a** uptaken by HeLa cell at the early stage (a) and after 10 min (b) of observation.

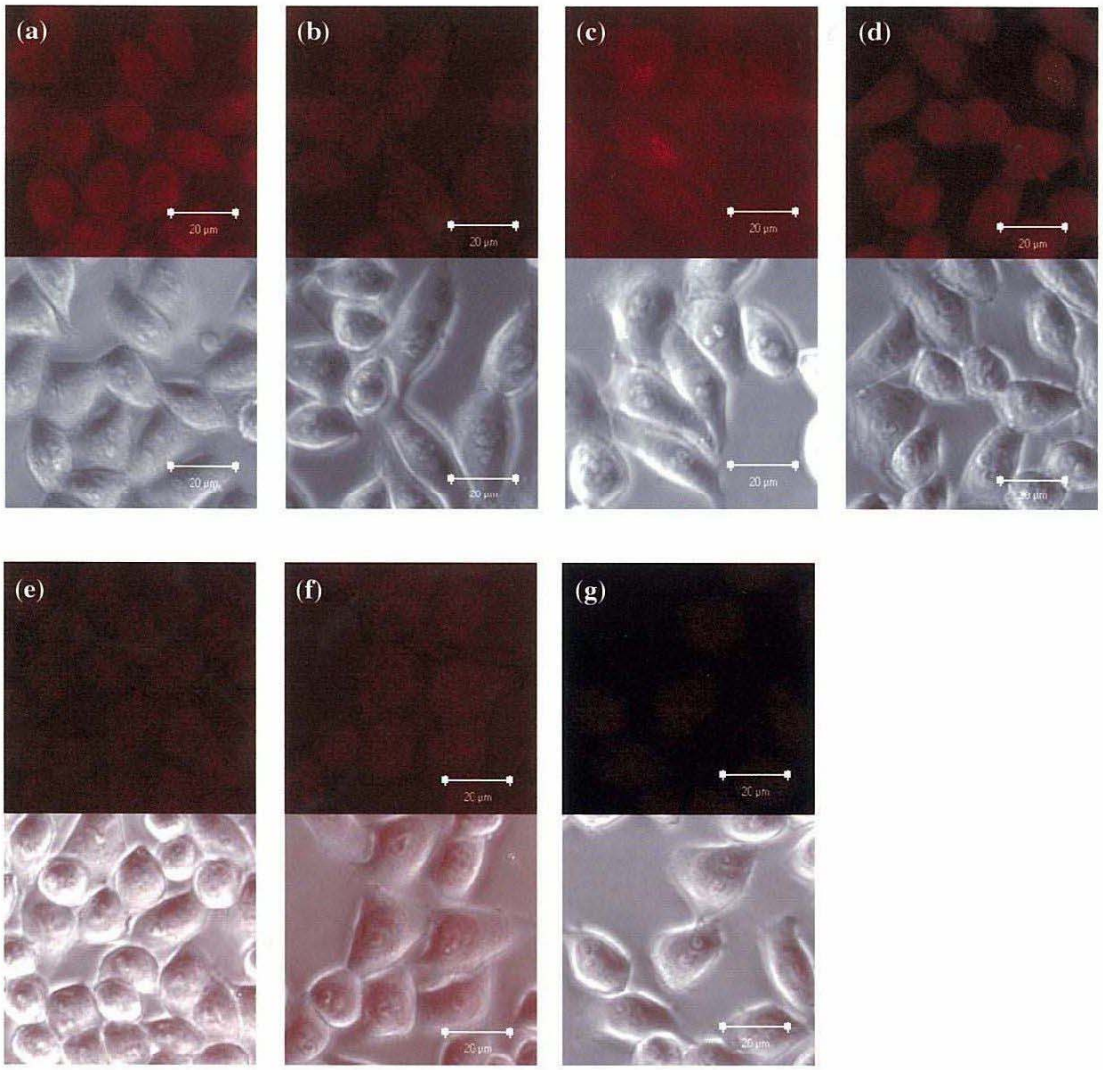

Figure 5-9 Confocal laser scanning microscope images of fluorescence from chlorins *m*-**9a** (a), *m*-**9b** (b), *m*-**9c** (c), *m*-**9d** (d), *p*-**8a** (e), *p*-**8d** (f) and TPPS (g) uptaken by HeLa cell fixed by glutaraldehyde.

5-2-7. Spectroscopic properties of deacetylated glycoconjugated chlorins m-9 in aqueous solution

In chapter 3, it is reported that the photochemical properties of aggregates and/or the quantity of remaining monomeric species are different between porphyrins having sugar unit attached in aqueous media such as cytoplasm. The electronic absorption and fluorescence spectra of deacetylated glycoconjugated chlorins *m*-**9** (c = 5 μM) were measured in various composition of DMSO and PBS to investigate the effect of aggregation state on photochemical properties. The electronic absorption spectra of *m*-**9** in DMSO are resemble to each other as same as porphyrin *p*-**8a** (Figure 5-10a). On the other hand, the Soret band decreased significantly in PBS (Figure 5-10b). The Soret band widths of *m*-**9c** and *m*-**9d** (i.e., pentose groups) are broader than those of *m*-**9a** and *m*-**9b** (i.e., hexose groups). And the Soret bands of *m*-**9a** and *m*-**9b** (i.e., hexose groups) shifted toward shorter wavelength, while the Soret band of *m*-**9c** and *m*-**9d** (i.e., pentose groups) shows a bathochloromic shift. These results suggest the aggregation form of *m*-**9** depends on sugar unit attached, especially hexose or pentose. The aggregation form of chlorins having hexose is H-type structure, i.e. face-to-face π-stacked aggregates, while the chlorins having pentose forms J-type aggregation state, i.e. side-by-side aggregates [18,19].

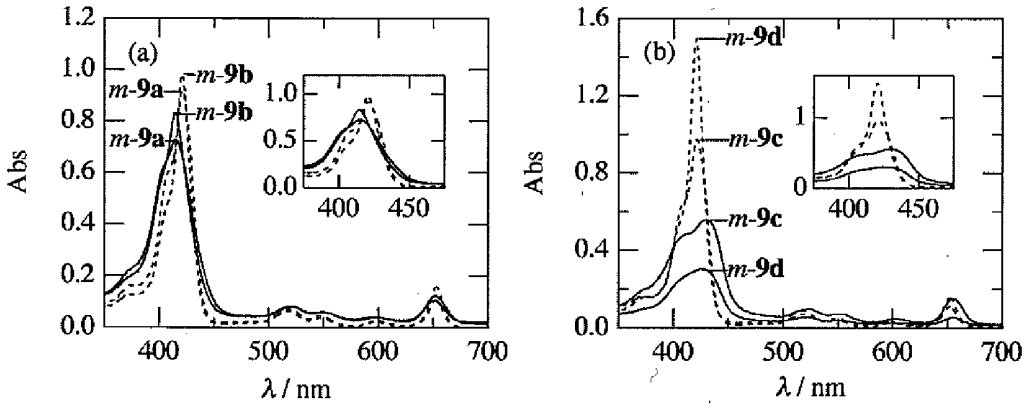

Figure 5-10 Electronic absorption spectra of *m*-**9a** and *m*-**9b** (a) and *m*-**9c** and *m*-**9d** (b) in DMSO (broken line) and PBS (solid line) (c = 4.97 μM) at 37 °C.

Figure 5-11 shows fluorescence spectra of chlorins *m*-**9** and porhyrin *p*-**8a** in DMSO using an excitation wavelengths of 430 nm at 37 °C. The spectral data are listed in Table 5-4. In DMSO, the fluorescence intensities of *m*-**9** were about 4-fold greater than that of *p*-**8a**. There are no differences in fluorescence intensities between chlorins *m*-**9** in DMSO (i.e., monomeric form). However the fluorescence intensities of *m*-**9a** and *m*-**9b** (i.e., chlorins having hexose groups) were about 20-fold greater than those of *m*-**9c** and *m*-**9d** (i.e., chlorins bearing pentose groups) in PBS (Figures 5-12 and Table 5-5). This suggests that the photochemical properties of aggregates and/or the quantity of remaining monomeric species are different between chlorins having hexose and pentose groups.

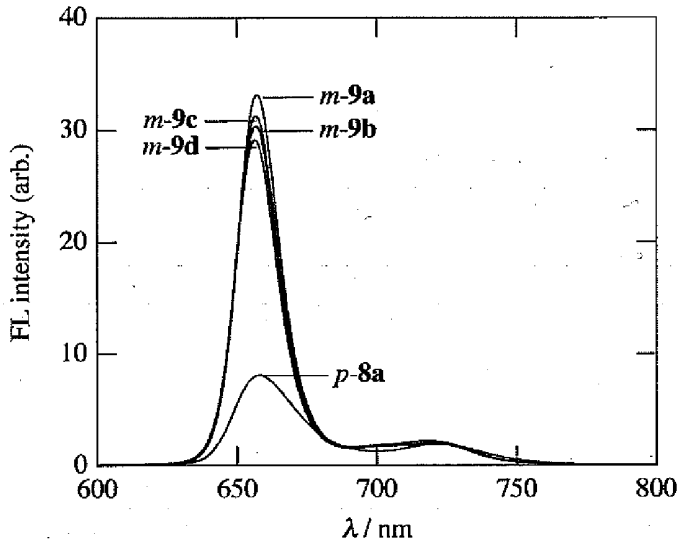

Figure 5-11 Fluorescence spectra of porphyrin *p*-**8a** and chlorins *m*-**9** in DMSO (c = 4.97 μM) at 37 °C. λ_{ex} = 430 nm.

Table 5-4 Electronic absorption and fluorescence spectral data of *p*-**8a** and chlorins *m*-**9** in PBS (c = 4.97 μM, 37 °C).

	Electronic absorption spectra					Fluorescence spcetra[b]	
	λ_{max} (nm)					λ_{max} (nm)	
	Soret[a]	IV	III	II	I	(0,0)	(0,1)
p-**8a**	415.5	521	561.5	608	652	663	714
m-**9a**	414.5 (401.5)	519.5	551.5	599	651.5	653.5	714
m-**9b**	415 (401.5)	519.5	549	598.5	650.5	653.5	715.5
m-**9c**	429.5 (405.5)	524	549	602	655	661.5	730
m-**9d**	428 (403.5)	524	552.5	600	655	656.5	731.5

[a] The value in parenthesis is a shoulder peak by Soret band. [b] λ_{ex} = 430 nm.

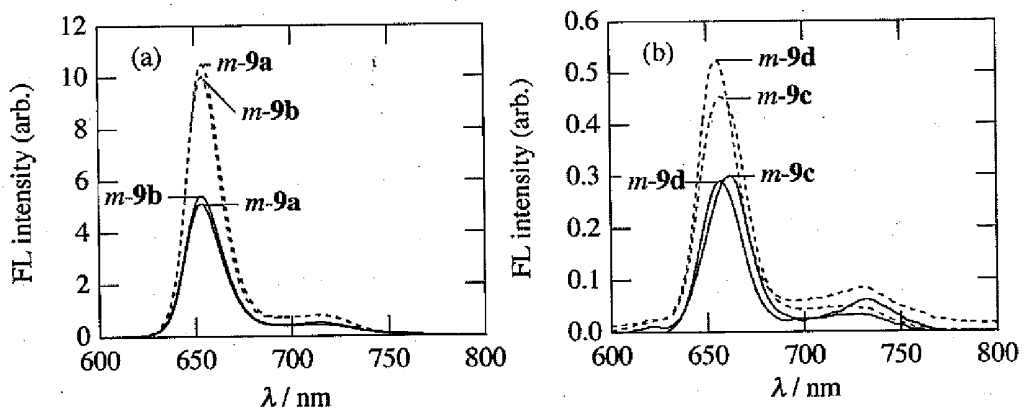

Figure 5-12 Fluorescence spectra of *m*-**9a** and *m*-**9b** (a) and chlorins *m*-**9c** and *m*-**9d** (b) in PBS ($c = 4.97$ μM) at 37 °C. $\lambda_{ex} = 430$ nm.

Table 5-5 Electronic absorption and fluorescence spectral data of *p*-**8a** and *m*-**9** in PBS containing 1 % glutaraldehyde ($c = 4.97$ μM, 37 °C)

	Electronic absorption spectra					Fluorescence spcetra[b]	
	λ_{max} (nm)					λ_{max} (nm)	
	Soret[a]	IV	III	II	I	(0,0)	(0,1)
p-**8a**	416	518.5	560	589	647.5	659	720
m-**9a**	415.5 (398.5)	521	549	594	649.5	654	714
m-**9b**	415	520.5	547.5	594	648	653.5	712
m-**9c**	429.5 (413.5)	522	552	601.5	656	656.5	723
m-**9d**	417.5	521.5	552	603	654	654.5	723.5

[a] The value in parenthesis is a shoulder peak by Soret band. [b] $\lambda_{ex} = 430$ nm.

5-2-8. Concentration dependence in the fluorescence of the deacetylated glycoconjugated chlorins

The results in the previous section suggest the aggregation behavior of *m*-**9c** deteriorate the $^1O_2$ production. In order to control the aggregation behavior, the fluorescence intensities of *m*-**9a** and *m*-**9c** were measured in the lower concentration region. Figure 5-13 shows the plots of the fluorescence intensities in the concentration range from 5 to 0.008 μM in PBS using excitation wavelengths of 430 nm at 37 °C. The fluorescence intensities were increase with an increase of the drug concentration until 3 μM for *m*-**9a** and 0.2 μM for *m*-**9c**, respectively, and reached a plateau level. In order to break an aggregate up, *m*-**9c** requires lower concentration (i.e., < 0.2 μM) than *m*-**9a**. The fluorescence intensity difference between *m*-**9a** and *m*-**9c** decreased with a decrease of concentration in this region.

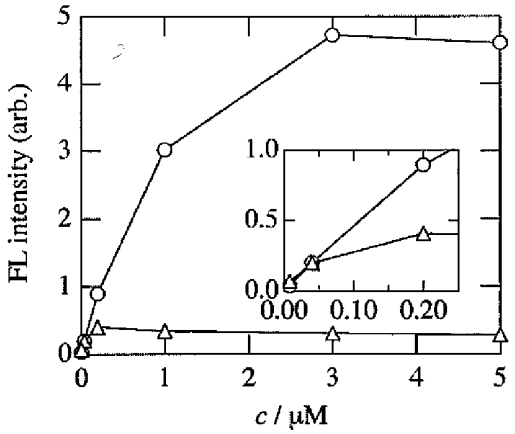

Figure 5-13 Fluorescence intensity of *m*-**9a** and *m*-**9c** in PBS as a function of the concentration at 37 °C. λ_{ex} = 430 nm. λ_{em} = 657 nm.

5-2-9. Drug dose-dependence of the photodynamic effect of m-9a and m-9c

The photocytotoxicty of *m*-**9a**, *m*-**9c**, and TPPS was examined against HeLa cells in the concentration range from 0.2 to 0.04 μM. The cytotoxicity of these photosensitizers to HeLa cells were carried out under the same protocol reported in chapter 3. As reported previously, these photosensitizers showed no dark cytotoxicity. Figure 5-14 shows the plot of cell survivals as a function of drug concentration. The photocytotoxicity of *m*-**9a** decreased with a decrease of drug concentration from 0.2 to 0.04 μM. In the case of *m*-**9c**, on the other hand, the cell survival slightly decreased from 96.5 to 85.6 % with a decrease of the drug concentration from 0.2 to 0.16 μM. The cell survival was around 100 % within the drug concentration less than 0.16 μM.

In above results, the cellular uptake of *m*-**9c** was about 5-fold greater than that of *m*-**9a** [3,16]. The uptake amount of *m*-**9a** at the concentration of 0.2 μM, in which the cell survival was 27.8 %, can be equal to that of *m*-**9c** at the concentration of 0.04 μM. However, the cell survival in the case of *m*-**9c** at the concentration of 0.04 μM was 99.8 %. This indicates the situation of *m*-**9c** in HeLa cells was totally different from that of *m*-**9a**. Interestingly, it seems that the photocytotoxicity of *m*-**9c** slightly increased with decrease of drug concentration from 0.2 to 0.16 μM. The $^1O_2$ generation from photosensitizers should decreases with a decrease of the drug concentration. At the same time, however, the monomeric form of photosensitizers, which is more active to form $^1O_2$, increases with the decrease of the drug concentration. These two contributions should make the photocytotoxicity complicated. These finding suggest the sugar moieties of chlorins affects not only cellular uptake behavior but also subcellular

photochemical behavior.

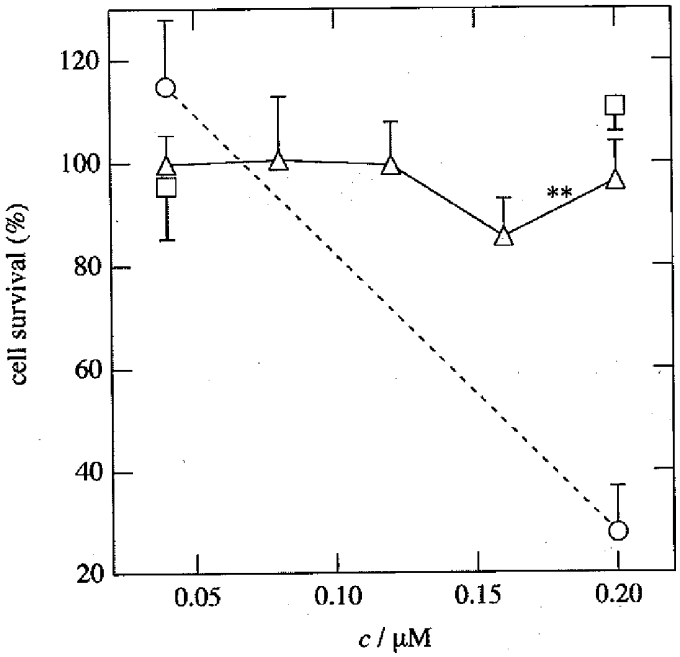

Figure 5-14 Photocytotoxicity of *m*-**9a**, *m*-**9c** and TPPS in HeLa cells as a function of the drug concentration. The dose applied was 16 J/cm^2 using a 100 W halogen lamp ($\lambda > 500$ nm). The percentage cell survival was determined by Cell Titer-Glo™ Luminescent assay after 48 h incubation. The values represent the means ± s.d. of of six replicate experiments. **Significant difference, $p < 0.01$.

5-3. Summary

The hydrophobicity parameter (Log *P*) of deacetylated glycoconjugated chlorins *p*-**9** was evaluated by the Shake-Flask and the RP-HPLC methods. The Log *P* values of chlorins *p*-**9** were ranged from -0.68 to -0.72, hence all photosensitizers are hydrophilic. The $^1O_2$ producing ability of chlorins *m*-**9** was examined using degradation of DPBF by $^1O_2$. The relative quantum yield of $^1O_2$ (Φ_Δ) slightly depended on sugar units attached in DMSO (i.e., monomeric form), and varied from 1.3 to 0.6 toTPPS as a standard. The cellular uptake of chlorins **9** was evaluated in HeLa cells. All chlorins **9** showed higher cellular uptake than TPPS, and corresponding porphyrins **8**. The order of the cellular uptake amount was *m*-**9c** > *p*-**9d** > *m*-**9d** > *p*-**9a** > *p*-**9b** > *p*-**9c** > *m*-**9a** > *m*-**9b** > TPPS. *m*-**9c** showed an uptake 50-fold greater than that of TPPS. The plot of cellular uptake amount of porphyrins *p*-**6**, *p*-**8** and chlorins *p*-**9** as a function of retention time t_R on RP-HPLC. For same sugar conjugated photosensitizers, the cellular uptake amount

increased with an increase of t_R value, i.e., in the order of *p*-**6** < *p*-**8** < (or =) *p*-**9**. This indicates the porphyrin ring affects the hydrophobicity and results in variation of the cellular uptake. On the other hand, the sugar unit effects on cellular uptake and t_R values for each porphyrinoids. The hydrophobicity change due to the sugar unit is not simply connected to the cellular uptake. The photocytotoxicity of towards HeLa cells was examined at the concentration of 0.2 μM. The photocytotoxicity of the chlorin *m*-**9a** is almost 25-fold greater than that of porphyrin *p*-**8a**. These photosensitizers had no cytotoxicity in the dark, but their photocytotoxicity increased in the order of TPPS < *m*-**9c** < *m*-**9a**. However these result clearly shows that the amount of cellular uptake is not related simply to the photodynamic effect on HeLa cells. Hence, *p*-**8a**, *m*-**9**, and TPPS were investigated by CLSM with and without glutaraldehyde. These photosensitizers were diffusively distributed throughout the cytoplasm except for *m*-**9b**. No fluorescence was detected in nuclear area. The chlorins *m*-**9** exerted the stronger fluorescence than the corresponding porphyrin *p*-**8a** and TPPS without glutaraldehyde. The fluorescence of chlorin *m*-**9a** was the strongest in all photosensitizers. In addition, the electronic absorption and fluorescence spectra of the chlorins *m*-**9** and corresponding porphyrin *p*-**8a** were measured in DMSO and PBS to explore the photochemical behavior of glycoconjugated photosensitizers in aqueous media such as cytoplasm. In DMSO, the fluorescence intensities of chlorins *m*-**9** were about 4-fold greater than that of porphyrin *p*-**8a**. There is no difference in fluorescence intensities between chlorins *m*-**9** in DMSO (i.e., monomeric form). However the fluorescence intensities of *m*-**9a** and *m*-**9b** (i.e., chlorins having hexose groups) were about 20-fold greater than those of *m*-**9c** and *m*-**9d** (i.e., chlorins bearing pentose groups) in PBS. This suggests that the photochemical properties of aggregates and/or the quantity of remaining monomeric species are different between chlorins having hexose and pentose groups. It may make difference in photodynamic effect in HeLa cells between *m*-**9a** and *m*-**9c**. In addition, the photocytotoxycity of *m*-**9c**, the cell survival slightly decreased from 96.5 to 85.6 % with a decrease of the drug concentration from 0.2 to 0.16 μM. These finding suggest the sugar moieties of chlorins affects not only cellular uptake behavior but also subcellular photochemical behavior.

5-4. Experimental

Materials and Measurements

Measurements

Electronic absorption spectra were recorded on a JASCO V-570 spectrophotometer (Nara Women's University). Fluorescence spectra were recorded on a JASCO FP-6300 spectro fluorometer (Nara Women's University). Fluorescence intensity and luminescence intensity were determined by a plate reader (SPECTRA Fluor Plus, TECAN) (Nara Institute of Science and Technology). Image analysis was accomplished with the confocal laser scanning microscope (CLSM) (Model LSM 510, Zeiss) (Nara Institute of Science and Technology). The deacetylated chlorins **9** was estimated by liquid chromatography (HITACHI, L-6000) (Osaka Prefectural College of Technology) equipped with silica gel-ODS (HITACHI, HITACHI GEL 4 mmϕ × 150 mm) column and a diode array detector (HITACHI L-4000) using acetonitrile / water = 1 / 1 as an eluent.

Photosensitizers

Stock solutions of photosensitizers (TPPS, glycoconjugated chlorins **9**, porphyrin *p*-**8a** and *p*-**8d**) were prepared by weighing the dried photosensitizers and dissolving them in dimethyl sulfoxide (DMSO, Wako Pure Chemical Industries, Ltd.). The stock solutions were kept in the freezer (-30 °C).

Materials

1,3-Diphenylisobenzofuran (DPBF) and tetraphenylporphyrin tetrasulfonic acid (TPPS) were purchased from Sigma Aldrich Japan Corporation. All other reagents were of analytical grade.

5-4-1. Partition coeffient between phosphate buffered saline (PBS) and n-octanol

The measurement was carried out under the same protocol reported in chapter 3.

5-4-2. Hydrophobicity parameter determined by RP-HPLC method

The measurement was carried out under the same protocol reported in chapter 3.

5-4-3. $^1O_2$ Producing Ability

The singlet oxygen ($^1O_2$) producing ability of deacetylated glycoconjugated chlorins *m*-**9** for the formation of $^1O_2$ studied using 1,3-diphenylisobenzofuran (DPBF) as $^1O_2$ quencher [9-13]. Photosensitizers (c = 0.08 μM) and DPBF (c = 36.7 μM) were dissolved in DMSO. All measurements were carried out in

a square quartz cell (1 cm) at 37 °C. Solution of photosensitizers and DPBF were freshly prepared and kept in the dark before measurement. Prior to irradiation, oxygen gas was bubbled through the solution in a square quartz cell for 1 min. The solution were then exposed to light from a 100 W halogen lamp (USHIO, KBEX-102A) equipped with a Y-50 cut-off filter ($\lambda > 500$ nm, Toshiba). The light intensity was determined to be 40 mW/cm^2 by using an UV-vis power meter (OPHIR, ORION/TH). The solution was stirred during photolysis. The DPBF concentration was determined by the absorption of DPBF at 418 nm. TPPS was used as calibrating standard.

5-4-4. Cellular uptake by HeLa cells

The cellular uptake measurement of deacetylated glycoconjugated chlorins **9** by HeLa cells were carried out under the same protocol reported in chapter 3.

5-4-5. In vitoro photocytotoxicity test against HeLa cells

The *in vitro* assessment of photocytotoxicity was carried out under the same protocol reported in chapter 3. For all experiments, the drug concentration was varied from 5 to 0.2 μM in DMEM containing 10% FCS (1 % DMSO)).

5-4-6. Confocal fluorescence images

HeLa cells were grown in Dulbecco's modified Eagle's medium (DMEM) with phenol red and 10 % fetal calf serum (FCS) (Hyclone Laboratories, Inc.). Confocal fluorescence images of TPPS, *m*-**9**, *p*-**8a** and *p*-**8d** were taken as follows: HeLa cells (5×10^4 cells/well) were plated in a 24-well plate (Nalge Nunc International K.K.) in 500 μL per well of DMEM with phenol red and 10 % FCS, and the plates were incubated for 24 h (37 °C, 5 % CO_2). To each well was added 500 μL of 10 μM (2 % DMSO) photosensitizers in DMEM with phenol red and 10 % FCS (hence the concentration of photosensitzers was 5 μM (1 % DMSO)). The medium was removed and the cells were then washed twice with Dulbecco's PBS (13.7 mM NaCl, 2.7 mM KCl, 8.1 mM $Na_2HPO_4 \cdot 12H_2O$, and 1.5 mM KH_2PO_4 pH 7.4) (Wako Pure Chemical Industries, Ltd.), and 100 μL of PBS or PBS containing 1 % glutaraldehyde (fixation agent) was added. Image analysis were accomplished the confocal laser scanning microscope (CLSM) (Model LSM 510, Zeiss). The excitation wavelength was set at 543 nm, and the fluorescence image was then scanned and recorded.

5-4-7. Statistical analysis

All statistical evaluations were performed using Student's *t*-test. All values for cellular uptake and cytotoxicity are expressed as mean ± standard deviation.

5-5. References

1. R. Bonnett, Photosensitizers of the Porphyrin and Phthalocyanine Series for Photodynamic Therapy. Chem. Soc. Rev. 24 (1995) 19-33.
2. Y.N. Konan, R. Gurny, E. Allémann, State of art in the delivery of photosensitizers for photodynamic therapy. J. Photochem. Photobiol. B: Biol. 66 (2002) 89-106.
3. M. Momenteau, D. Oulmi, Ph. Maillard, A. Croisy, Photodynamic Therapy of cancer II. SPIE. 2325 (1994) 13-23.
4. D.M. Tarak, Pharmaceutical development and medical applications of Porphyrin-type macrocycles. J. Porphyrins Phthalocyanines. 4 (2000) 362-367.
5. R. Bonnet, Chemical Aspects of Photodynamic Therapy., Taylor & Francis, UK, 2000.
6. I. Okura, Photosensitization of Porphyrins and Phthalocyanines., Kodansha, Tokyo, 2000.
7. T.T. Tominaga, V.E. Yusbmanov, I.E. Borissevitcb, H. Imasato, Aggregation Phenomena in the Complexes of Iron Tetraphenylporphine Sulfonate with Bovine Serum Albumin, J. Inorga. Chem. 65 (1997) 235-244.
8. P. Kubát, K. Lang, P. Anzenbacher, Jr., Modulation of porphyrin binding to serum albumin by pH, Biochem. Biophys. Acta. 1670 (2004) 40-48.
9. Y. Mikata, Y. Onchi, K. Tabata, S. Ogura, I. Okura, H. Ono, S. Yano, Sugar-dependent photocytotoxic property of tetra- and octa- glycoconjugated tetraphenylporphyrins. Tetrahedron Lett. 39 (1998) 4505-4508.
10. Y. Mikata, Y. Onchi, M. Shibata, T. Kakuchi, H. Ono, S. Ogura, I. Okura, S. Yano, Synthesis and Phototoxic Property of Tetra- and Octa-Glycoconjugated Tetraphenylchlorins. Bioorg. Med. Chem. Lett. 8 (1998) 3543-3548.
11. K. Oda, S. Ogura, I. Okura, Preparation of a water-soluble fluorinated zinc phthalocyanine and effect for photodynamic therapy. J. Photochem. Photobiol. B: Biol. 59 (2000) 20-25.
12. E. Gandin, Y. Lion, A. VandeVorst, QUANTUM YIELD OF SINGLET OXYGEN PRODUCTION BY XANTHENE DERIVATIVES. Photochem. Photobiol. 37 (1983) 271-278.

13. D. Wöhrle, M. Shopova, S. Müller, A.D. Milev, V.N. Mantareva, K.K. Krastev, Liposome-delivered Zn(II)-2,3-naphthalocyanines as potential sensitizers for PDT: synthesis, photochemical, pharmacokinetic and phototherapeutic studies. J. Photochem. Photobiol. B: Biol. 21 (1993) 155-165.
14. K.K. Yee, K.C. Soo, B.H. Bay, M. Olivo A Comparison of Protoporphyrin IX Dimethyl Ester as a Photosensitizer in Poorly Differentiated Human Nasopharyngeal Carcinoma Cells. Photochem. Photbiol. 2002 (76) 678-682.
15. K. Oda, S. Ogura, I. Okura, Preparation of a water-soluble fluorinated zinc phthalocyanine and effect for photodynamic therapy. J. Photochem. Photobiol. B: Biol. 59 (2000) 20-25.
16. K. Lang, J. Mosinger, D.M. Wagnerová, Photophysical properties porphyrinoid sensitizers non-covalently bound to host molecules; models for photodynamic therapy. Coordination Chemistry Reviews. 248 (2004) 321-350.
17. I. Laville, T. Figueiredo, B. Loock, S. Pigaglio, Ph. Maillard, D. S. Grierson, D. Carrez, A. Croisy, J. Blais, Synthesis, Cellular Internalization and Photodynamic Activity of Glycoconjugated Derivatives of Tri and Tetra (*meta*-hydroxyphenyl) chlorins. Bioorg. Med. Chem. 11 (2003) 1643-1652.
18. H. García-Ortega, J.L. Bourdelande, J. Crusats, Z. El-Hachemi, J.M. Ribó, Excitred Triplet States in Aggregates and Monomers of Water Soluble Meso-Aryl Substituted Porphyrins. J. Phys. Chem. B. 108 (2004) 4631-4639.
19. R. Bonnett, B. D. Djelal, A. Nguyen, Physical and chemical studies related to the development of *m*-THPC (FOSCAN®) for the photodynamic therapy (PDT) of tumours. J. Porphyrins Phthalocyanines. 5 (2001) 652-661.

Chapter 6

Concluding Remarks

In this study, glycoconjugated tetraphenylporphyrins (TPPs) and tetraphenylchlorins (TPCs) were synthesized, and the sugar unit effect on pharmaceutical nature and photocytotoxicity by HeLa cells were investigated systematically for these photosensitizers.

Thirty-two glycoconjugated porphyrins were synthesized by a modification of Lindsey method in the presence of $Zn(OAc)_2 \cdot 2H_2O$ as a template. Yields of acetylated zinc porphyrins were given in 53 ~ 93 %. The Zn^{2+} ion in these photosensitizers was easily removed by washing with 4 M HCl to give free-base porphyrins in 36 ~ 86 % yield. The Zn^{2+} ion template strategy improved the yield about 3-fold in the case of 5,10,15,20-tetrakis[3-(β-D-glucopyranosyloxy)phenyl]porphyrin. This provides an efficient means to prepare wide variety of glycoconjugated porphyrins, which can be used as a precursor for glycoconjugated chlorins having similar structures to Foscan®. Deprotection of these acetylated photosensitizers was carried out using NaOMe in THF or in a mixture of MeOH and CH_2Cl_2. Eventually, sixteen deacetylated glycoconjugated porphyrins were obtained in moderate yield. In addition, eight deacetylated glycoconjugated chlorins were synthesized by means of the Whitlock method with diimide reduction, and then this crude product by NaOMe in a mixture of MeOH and CH_2Cl_2. The crude deacetylated product was successfully purified by RP-TLC. The deacetylated chlorins were obtained in the yields of 14 ~ 49 %. All glycoconjugated porphyrins and chlorins were obtained in the purities of >95 % after evaluation by HPLC using an octadecylsilyl-supported silica gel column. These photosensitizers were fully characterized by ^1H NMR, ESI-TOF mass, IR, and electronic absorption spectroscopy. In the electronic absorption spectra, these photosensitizers have a strong Soret band at ca. 420 nm and four weak Q bands at ca. 520 (Q_{IV}), 550 (Q_{III}), 600 (Q_{II}), and 650 (Q_I) nm in DMSO. The Q_I bands of all chlorins were about 4-fold greater than those of corresponding porphyrins.

The hydrophobicity parameter (Log *P*) of glycoconjugated porphyrins was evaluated by the Shake-Flask and the reversed phase hight performance liquid chromatography (RP-HPLC) methods. The RP-HPLC method is very useful to estimate the order of hydrophobicity. The Log *P* values of acetylated porphyrins were ranged from +4.8 to +7.8, so that most of the photosensitizers are less hydrophobic. On the other hand, the Log *P* values of *p*-substituted deacetylated porphyrins and chlorins were ranged from -0.68 to -0.74, hence all photosensitizer are hydrophilic. Zinc porphyrins exerts higher hydrophilicity regardless of the sugar unit attached. These photosensitizers having hexose groups are more hydrophilic than those having pentose groups. The each sugar unit attached has unique effect on the hydrophobicity.

The binding equilibrium of the *p*-substituted deacetylated porphyrins with bovine serum albumin

(BSA) was investigated by means of fluorometric titration. The n and K values varied from 0.41 ± 0.04 to 1.57 ± 0.11 and from (0.25 ± 0.02) × 10^6 to (1.57 ± 0.11) × 10^6 M^{-1} owing to sugar unit attached. The number of binding porphyrin to BSA (n) increases monotonically with an increase of retention time t_R on RP-HPLC. Hence the formation of porphyrins - BSA complex is simply driven by hydrophobic interaction.

The $^1O_2$ producing ability of *m*-substituted chlorins was examined using degradation of DPBF by $^1O_2$. The relative quantum yield of $^1O_2$ (Φ_Δ) slightly depended on sugar units attached in DMSO (i.e., monomeric form), and varied from 1.3 to 0.6 to TPPS as a standard.

Except for 5,10,15,20-tetrakis[3-(β-D-xylopyranosyloxy)phenyl]porphyrin and 5,10,15,20-tetrakis[4-(β-D-galactopyranosyloxy)phenyl]porphyrin, the cellular uptake of deacetylated porphyrins and chlorins was evaluated in HeLa cells. All these photosensitizers showed higher cellular uptake than TPPS. The uptake amount of 5,10,15,20-tetrakis[4-(β-D-arabinopyranosyloxy)phenyl]porphyrin (*p*-**8d**) showed about 2-fold higher cellular uptake than that of 5,10,15,20-tetrakis[4-(β-D-glucopyranosyloxy)phenyl]porphyrin (*p*-**8a**). And, the uptake amount of 5,10,15,20-tetrakis[3-(β-D-xylopyranosyloxy)phenyl]chlorin (*m*-**9c**) showed about 5-fold higher cellular uptake than that of 5,10,15,20-tetrakis[3-(β-D-glucopyranosyloxy)-phenyl]chlorin (*m*-**9a**). The cellular uptake amount of *p*-substituted porphyrins and chlorins by HeLa cells increased with an increase of t_R value on RP-HPLC method, i.e., in the order of zinc porphyrins < free-base porphyrins < (or =) chlorins regardless of the sugar unit attached. This indicates the porphyrin ring affects the hydrophobicity and results in variation of the cellular uptake. On the other hand, the sugar unit effects on cellular uptake and t_R values for each porphyrinoids. The hydrophobicity change due to the sugar unit is not simply connected to the cellular uptake.

In porphyrins, the photocytotoxicity of *p*-**8a**, *p*-**8d** and TPPS was examined with HeLa cells, using a light dose of 16 J/cm^2 and the drug concentration of 5 μM. These photosensitizers had no cytotoxicity in the dark. Their photocytotoxicity increased in the order of TPPS < *p*-**8a** < *p*-**8d**. However the difference in photocytotoxicity between *p*-**8d** and *p*-**8a** was small in contrast with the cellular uptake difference. In chlorins, on the other hand, the photocytotoxicity of *m*-**9a**, *m*-**9c** and TPPS was examined with HeLa cells, using a light dose of 16 J/cm^2 and the drug concentration of 0.2 μM. Hence, the photocytotoxicity of *m*-**9a** is almost 25-fold greater than that of porphyrin *p*-**8a** (i.e., chlorin is lower drug dose than porphyrin). These photosensitizers had no cytotoxicity in the dark, but their photocytotoxicity increased in the order of TPPS < *m*-**9c** < *m*-**9a**. However, these results of glycocnjugated porphyrins and chlorins clearly shows that the amount of cellular uptake is not related simply to the photodynamic effect on HeLa

cells. Hence, the confocal fluorescence images of *p*-**8a** *p*-**8d** and *m*-substituted chlorins and TPPS with and without glutaraldehyde. The all glycoconjugated photosensitizers were diffusively distributed throughout the cytoplasm except for 5,10,15,20-tetrakis[3-(β-D-galactopyranosyloxy)phenyl]chlorin (*m*-**9b**), and no fluorescence was detected in nuclear area. The *m*-substituted chlorins exerted the stronger fluorescence than *p*-**8a** and TPPS without glutaraldehyde. The fluorescence of *m*-**9a** was the strongest in all photosensitizers.

In addition, the electronic absorption and fluorescence spectra of the chlorins and corresponding porphyrin *p*-**8a** and *p*-**8d** were measured in DMSO and PBS to explore the photochemical behavior of glycoconjugated photosensitizers in aqueous media such as cytoplasm. In DMSO, the fluorescence intensities of *m*-substituted chlorins were about 4-fold greater than that of *p*-**8a**. There is no difference in fluorescence intensities between each chlorins or each porphyrins in DMSO (i.e., monomeric form). In porphyrins, the fluorescence intensities of *p*-**8a** (i.e., hexose group) were about 5-fold greater than those of *p*-**8d** (pentose group) in PBS. And the fluorescence intensities of chlorins having hexose groups were about 20-fold greater than those of chlorins bearing pentose groups in PBS. These glycoconjugated photosensitizers (i.e., porphyrins and chlorins) suggests that the photochemical properties of aggregates and/or the quantity of remaining monomeric species are different between photosensitizers having hexose and pentose groups. It may make difference in photodynamic effect in HeLa cells between photosensitizers having hexose and pentose groups. In addition, the photocytotoxycity of *m*-**9c**, the cell survival slightly decreased from 96.5 to 85.6 % with a decrease of the drug concentration from 0.2 to 0.16 μM. These finding suggest the sugar moieties of photosensitizers affects not only cellular uptake behavior but also subcellular photochemical behavior.

Finally, the author clarified that sugar unit on the porphyrinoids effects on the hydrophobicity, cellular uptake, serum albumin binding and photocytotoxicity. These pharmaceutical properties can affect on the photodynamic effect on PDT treatment. Hence the vast diversity of sugar chamistry may afford us mean to control the nature of photosensitizers.

Publication

Chapter 2

a) S. Hirohara, M. Obata, S. Ogura, I. Okura, S. Higashida, C. Ohtsuki, S. Ogata, Y. Nishikawa, M. Takenaka, H. Ono, Y. Mikata, S. Yano, "Log *P* Values of Glycoconjugated Porphyrins for Photodynamic Therapy Evaluated by Reverse-Phase HPLC", *J. Porphyrins Phthalocyanines. in press.*

b) S. Hirohara, M. Obata, A. Saito, S. Ogata, C. Ohtsuki, S. Higashida, S. Ogura, I. Okura, Y. Sugai, Y. Mikata, M. Tanihara, S. Yano, "Cellular Uptake and Photocytotoxicity of Glycoconjugated Porphyrins in HeLa Cells", *Photochem. Photobiol.* 80 (2004) 301-308.

Chapter 3

a) S. Hirohara, M. Obata, S. Ogura, I. Okura, S. Higashida, C. Ohtsuki, S. Ogata, Y. Nishikawa, M. Takenaka, H. Ono, Y. Mikata, S. Yano, "Log *P* Values of Glycoconjugated Porphyrins for Photodynamic Therapy Evaluated by Reverse-Phase HPLC", *J. Porphyrins Phthalocyanines. in press.*

b) S. Hirohara, M. Obata, A. Saito, S. Ogata, C. Ohtsuki, S. Higashida, S. Ogura, I. Okura, Y. Sugai, Y. Mikata, M. Tanihara, S. Yano, "Cellular Uptake and Photocytotoxicity of Glycoconjugated Porphyrins in HeLa Cells", *Photochem. Photobiol.* 80 (2004) 301-308.

c) S. Hirohara, M. Obata, S. Higashida, S. Ogata, C. Ohtsuki, M. Tanihara, S. Yano, "Sugar-dependent hydrophobic effect of glycoconjugated porphyrins and chlorins on the cellular uptake to HeLa cells and interaction with bovine serum albumin (BSA)". *Biochem. Biophys. Acta. submitted for publication.*

Chapter 4

S. Hirohara, M. Obata, A. Saito, S. Ogata, C. Ohtsuki, S. Higashida, S. Ogura, I. Okura, Y. Sugai, Y. Mikata, M. Tanihara, S. Yano, "Cellular Uptake and Photocytotoxicity of Glycoconjugated Chlorins in HeLa Cells", *J. Photochem. Photobiol. B: Biol.* 78 (2005) 7-15.

Chapter 5

a) S. Hirohara, M. Obata, A. Saito, S. Ogata, C. Ohtsuki, S. Higashida, S. Ogura, I. Okura, Y. Sugai, Y. Mikata, M. Tanihara, S. Yano, "Cellular Uptake and Photocytotoxicity of Glycoconjugated Chlorins in HeLa Cells", *J. Photochem. Photobiol. B: Biol.* 78 (2005) 7-15.

b) S. Hirohara, Makoto Obata, K. Kajiwara, S. Ogata, Chikara Ohtsuki, Masao Tanihara, Shigenobu Yano, "Subcellular Photochemical Properties of Glycoconjugated Chlorins", *J. Photochem. Photobiol. B: Biol. submitted for publication.*

Other Contribution

a) A. Hamazawa, I. Kinoshita, B. Breedlove, K. Isobe, M. Shibata, T. Kakuchi, S. Hirohara, M. Obata, Y. Mikata, S. Yano, "*meso*-Tetraphenylporphyrin Having Hexa-maltosyl and Decyl Chain as an Amphiphilic Photosensitizer toward Photodynamic Therapy", *Chem. Lett.* 3 (2002) 388-389.

b) Y. Arima, S. Akimoto, T. Yamazaki, M. Shibata, S. Hirohara, S. Yano, T. Kakuchi, I. Yamazaki, "Excitation relaxation dynamics and molecular dispersion of malto hexaose-linked tetra phenyl porphyrins in aqueous solution", *Chem. Phys. Lett.* 361 (2002) 152-158.

Acknowledgments

The author would like to express her gratitude to Professor Shigenobu Yano (Nara Women's University) for his help in the preparation of this thesis. The author is deeply grateful to Dr. Makoto Obata (Nara Women's University) for his helpful advice and valuable suggestions with continuous encouragement throughout this thesis. The author wishes to express deeply appreciation to Professor Yuji Mikata (Nara Women's University), Dr. Shin-ichi Ogata, Professor Chikara Ohtsuki and Professor Masao Tanihara (Nara Institute of Science and Technology), Professor Suguru Higashida (Osaka Prefectural College of Technology), Dr. Shun-ichiro Ogura, Professor Ichiro Okura (Tokyo Institute of Technology), Professor Toyoji Kakuchi (Hokkaido University), Professor Masako Kato (Nara Women's University) , Professor Shosuke Kojo (Nara Women's University) for their great helpful discussions and valuable suggestions with continuous encouragement throughout this work.

The author would like to acknowledge Dr. Atsuhiro Saito and Dr. Kazumi Kajiwara (Nara Institute of Science and Technology), Professor Isamu Kinoshita and Professor Akio Ichimura (Osaka City University), Professor Ken'ichi Kitano (Osaka Prefectural College of Technology), Professor Mikio Hoshino (Institute of Physical and Chemical Research), Professor Michio Matsumura (Osaka University) and Professor Toru Fujinaga (Hokkaido University) for their kind help. The author also thanks Dr. Yoshiteru Mizukoshi, Professor Keiji Ito and President Yoshisada Murotsu (Osaka Prefectural College of Technology) for their kind help.

The author enjoyed working with her colleagues because the friendship and good humor of the members in the laboratory created a pleasant and stimulating environment in which to work. In particular, the author is very thankful to Mr Takanori Iwasaki (Osaka University), Mr Tsuyoshi Higashiwada (Okayama University), my laboratory members and laboratory members of Professor Higashida.

The author is indebted to Ms Yoshiko Nishikawa (Nara Institute of Science and Technology), Dr. Makiko Takenaka and Dr. Hiroshi Ono (National Food Research Institute) for mass and NMR measurements.

January, 2005

Shiho Hirohara

謝辞

本研究をまとめるにあたり、矢野重信教授にご指導とご鞭撻を賜りました。ここに心から感謝の意を表し厚く御礼申し上げます。この研究をまとめるにあたり、多くの助言並びに直接の御指導いただきました小幡誠助手に心より御礼申し上げます。本研究を行うに当たり、直接ご指導頂きました三方裕司助教授に心より御礼申し上げます。化合物の *in vitro* 評価を行うにあたり、多くの助言並びに御指導いただきました奈良先端大学院大学物質創成科学研究科 谷原正夫教授、大槻主税助教授、尾形信一助手に心から感謝の意を表し厚く御礼申し上げます。研究を行うにあたり、合成などの適切な助言並びに直接の御指導いただきました大阪府立工業高等専門学校工業化学科 東田卓助教授に心から感謝の意を表し厚く御礼申し上げます。化合物の光毒性評価を行って頂きました、東京工業大学大学院生命理工学研究科 大倉一郎教授、小倉俊一郎助手に厚く御礼申し上げます。また副査としてお世話になりました小城勝相教授、加藤昌子助教授に感謝いたします。

細胞の継代などを行って頂きました、奈良先端大学院大学物質創成科学研究科 齋藤充弘博士、梶原一美博士に心から感謝いたします。研究を行うにあたり、御指導並びに種々測定をして頂きました北海道大学大学院工学研究科 覚知豊次教授、大阪市立大学大学院物質科学研究科 木下勇教授、大阪市立大学大学院理学部化学科 市村彰男教授、大阪府立工業高等専門学校一般教養化学科 北野健一助教授、理化学研究所 星野幹雄主任研究員、大阪大学太陽エネルギー化学研究センター 松村道雄教授、北海道大学大学院獣医学研究科 藤永徹教授に厚く御礼申し上げます。

本研究の機会を与えていただいた大阪府立工業高等専門学校第８代 室津義定校長に感謝いたします。筆者の大阪府立工業高等専門学校での仕事をサポートしていただいた伊藤詣二教授、水越克彰講師及び工業化学科教職員に感謝いたします。

また様々な面でご支援頂きました、矢野研究室の現役及び卒業生の皆さん、大阪大学大学院基礎工学研究科 岩崎孝紀氏と岡山大学大学院自然科学学科 東和田剛司氏と大阪府立工業高等専門学校 東田研究室の皆さんにに心から感謝いたします。

化合物のNMR及びマススペクトルの綿密な解析を行って頂きました、農林水産省食品総合研究所の小野裕嗣博士、ならびに竹中真紀子博士に厚く御礼申し上げます。化合物のマススペクトルの綿密な解析を行って頂きました、奈良先端大学大学院物質創成科学研究科 西川嘉子技官に厚く御礼申し上げます。

2005年1月　　廣原志保